**MARYLAND DEPARTMENT OF TRANPORTATION
STATE HIGHWAY ADMINISTRATION**

RESEARCH REPORT

**INTEGRATION OF RAMP METERING AND OFF-RAMP
PROGRESSION**

**GANG-LEN CHANG, YAO CHENG, YEN-YU CHEN,
AND YEN-HSIANG CHEN**

**THE UNIVERSITY OF MARYLAND,
COLLEGE PARK**

FINAL REPORT

June 2020

TECHNICAL REPORT DOCUMENTATION PAGE

1. Report No. MD-20-SHA/UM/5-14	2. Government Accession No.	3. Recipient's Catalog No.	
4. Title and Subtitle Integration of ramp metering and off-ramp progression		5. Report Date June 2020	
		6. Performing Organization Code .	
7. Author(s) Gang-Len Chang, Yao Cheng, Yen-Yu Chen, and Yen-Hsiang Chen		8. Performing Organization Report No. .	
9. Performing Organization Name and Address The University of Maryland, College Park College Park, MD 20742		10. Work Unit No.	
		11. Contract or Grant No. SP910B4B	
12. Sponsoring Agency Name and Address Maryland Department of Transportation (SPR) State Highway Administration Office of Policy & Research 707 North Calvert Street Baltimore MD 21202		13. Type of Report and Period Covered SPR-B Final Report (January 2019 –April 2020)	
		14. Sponsoring Agency Code (7120) STMD - MDOT/SHA	
15. Supplementary Notes			

16. Abstract

The primary objective of this project was to develop an integrated freeway control system that can effectively guide the timely activation of key operation components either concurrently or sequentially in contending with daily recurrent congestion. This project produced four traffic models for highway agencies to overcome various constraints existing in practice. Depending on the congestion patterns and their spatial evolution over the target freeway segment, responsible traffic control centers can apply these models individually or collectively, ranging from local ramp metering to coordinated freeway control or eventual integrated corridor management. Such applications can be in either a time-of-day mode or real time responsive mode if traffic detection is available at the required level of accuracy.

17. Key Words Ramp metering, off-ramp control, coordinated freeway control, off-ramp signal control		18. Distribution Statement This document is available from the Research Division upon request.		
19. Security Classif. (of this report) None		20. Security Classif. (of this page) None	21. No. of Pages 93	22. Price

Form DOT F 1700.7 (8-72)   Reproduction of completed page authorized

Table of Contents

List of Figures

List of Tables

Chapter 1 Introduction of the Project

1.1 Research background

Dealing with daily traffic congestion is a challenge not only for commuters, but also for the entire community, who must contend with aggressive driving behaviors and the ever-increasing incidents in highway corridors during congested peak hours. Therefore, effectively managing highway congestion is a priority to highway agencies. Intelligent Transportation Systems (ITS) have been promoted as solutions to these challenges since the late 1980s. Since them a large body of studies from traffic monitoring to advanced traffic management have been conducted. However, except for very limited implementation of the time-of-day local ramp metering, nearly all advanced strategies/systems reported in the literature have been mainly at the project demonstration level. The perceived technical challenges, from the perspective of congestion nature and characteristics, can be classified as follows:

- lacking coordination between freeway ramps and surrounding local arterial signal controls;
- not evaluating the impact of the off-ramp queue spillback on freeway mainline operations; and
- insufficient modeling work to mitigate the mainline congestion due mainly to the behavioral variations of the driving populations, such as lane-changing maneuvers in response to the lane reduction on the mainline, or speed variance on the non-weaving mainline segments.

Figure 1-1 shows the defined zones on a freeway segment that often experience congestion and traffic queues. Congestion in any of these three zones will eventually spread to the entire system. For example, most ramp control strategies for Zone-1 congestion are embedded with a mechanism to deactivate the "metering control" if the ramp queue is detected to reach a preset threshold or spill back to the neighboring arterial. Such deactivation mechanisms often cause the weaving area on the mainline to exceed its capacity and propagate the queue upstream. Without such a deactivation function, the ramp queue would spill back to the local arterial, making the ramp metering control politically and socially unacceptable to the general public. This is the reason that both local and coordinated metering strategies are not widely used.

To alleviate both the public concerns of queue spillback and the impacts of weaving congestion on freeway flows, detouring excessive on-ramp flow to downstream ramps should be included in the design of coordinated ramp metering controls. Each subnetwork for local

coordinated control shall include both the freeway and arterial segments between two neighboring ramps, and have the objective functions of minimizing the total system's travel time and balancing the congestion level between the respective freeway and arterial segments.

Progressing off-ramp flows to prevent queue spillback to the freeway mainline (see Zone-3 in Figure 1-1) is another recent focus. Failing to account for both the impacts of off-ramp queues on mainline traffic delays and the conflicts between the arterial and off-ramp flows' progression needs will inevitably result in insufficient signal timings for the off-ramp flows and consequentially contribute to freeway congestion, especially at the interchange areas.

Speed variance and lane-changing maneuvers in response to a permanent lane-drop or a long-term work zone are also contributing factors to recurrent congestion on a freeway mainline (see Zone-2 in Figure 1-1). Well-calibrated variable speed limit (VSL) control, coupled with the display of estimated travel times, has proved its potential to significantly mitigate such congestion patterns in the field demonstration.

Note that even with the recent technological advancements in these areas, there are some missing links between those developments for integrated operations. Examples of such links include the consistency in data quality, the communications between key devices/hardware for different control purposes, activation/deactivation sequences in response to various traffic conditions, and the mechanism to coordinate freeway and arterial control strategies to balance the traffic conditions in the same commuting corridor.

Zone 2 (Mainline)

Mainline congestion

VMS #3 VMS #2 VMS #1 Lane drop

Possible Solutions

- Variable Speed Limit (VSL)
- Dynamic Lane Merge

Zone 1 (On-ramp) **Zone 2 (Mainline)** **Zone 3 (Off-ramp)**

ON-RAMP OFF-RAMP

Zone 1 (On-ramp)

Merge / weaving

ON-RAMP

Spillback

Possible Solutions

- Ramp metering
- Detour to downstream on-ramps with signal coordination
- Spillback control

Zone 3 (Off-ramp)

Queue Spillback

Off-RAMP

Possible Solutions

- Off-ramp multi-path progression
- Detour to upstream off-ramps

Figure 1-1: Primary congestion contributing areas in a freeway corridor

1.2 Research objectives

The primary objective of this project was to develop an integrated freeway control system that can effectively guide the timely activation of key operation components either concurrently or sequentially in contending with daily recurrent congestion. The system has the following key features:

- integration of state-of-the-art developments in freeway traffic controls, including but not limited to coordinated dynamic ramp metering, variable speed limits, off-ramp signal progression, and on-line detection of congestion patterns;
- identification of missing links that prevent existing freeway control models from effective use in practice, and development of essential algorithms to integrate such models/strategies to function reliably and effectively under inevitable operational constraints in practice;
- a real-time congestion detection module that enables the responsible highway agencies to reliably estimate the duration of a detected congestion pattern—from its formation to dissipation—and select proper control strategies in time to prevent or mitigate the resulting impacts; and
- a user-friendly advisory module to assist responsible agencies in selecting proper traffic control strategies and deploying them in proper sequences during real-time operations, such as: the right times to activate and deactivate ramp metering; information/messages to freeway users prior to implementing mainline VSL control; essential coordinating tasks in operating the off-ramp progression control; and criteria to justify the detouring operations during ramp queue spillback or freeway incidents.

1.3 Report organization

The next chapter presents the core model for freeway control, a local ramp metering system that features effective coordination with arterial traffic flows in optimizing the total throughput for the target control area, including both the freeway and arterial segments. To prevent a potential ramp queue spillback to its neighboring arterial, the developed arterial-friendly ramp metering model (named AF-ramp model) includes the formulations that capture the complex time-varying interrelations between ramp-arriving flows controlled by the arterial turning-green ratios and the impacts of ramp merging flows on the freeway's traffic condition. Because of concerns that traffic gridlock at the local arterial may also impede a ramp's arriving and exiting flows, and consequently its efficiency, the AF-ramp model is also embedded with the function to concurrently optimize both the cycle length, green ratio, and progression offsets for all signals in the vicinity of the freeway ramp.

Chapter 3 details an on-ramp merging model that computes the impacts of vehicles changing from the on-ramp auxiliary lane to the mainline segment on the receiving freeway segment's speed, flow rate, and density. A reliable estimate of such impacts will serve as the basis for estimating the available freeway capacity downstream of the on-ramp to accommodate the arriving flows from both the upstream freeway segment and the on-ramp. Since a good estimate of such on-ramp merging impacts may vary with the behaviors of location-specific driving populations, this chapter will also illustrate the model calibration process with field data in addition to a detailed discussion of the formulations and all involved critical traffic flow variables.

Chapter 4 contains the model and formulations for estimating the impacts of off-ramp queue spillback on the freeway segment's traffic conditions and also in design of the arterial intersection signal designated to receive the off-ramp flows. Both mandatory lane-changing maneuvers to exit the ramp and discretionary choice maneuvers to avoid off-ramp queues have been captured from the macroscopic traffic flow perspective and calibrated with field data for potential applications. To show the necessity of incorporating such off-ramp queue impacts in the off-ramp signal design, this chapter also presents the results of a case study and sensitivity analyses.

Chapter 5 highlights an innovative multi-path progression model (MP-progression) for congested arterials, especially those serving as commuting corridors to accommodate large on- and off-ramp flows from the neighboring freeway. Such a MP-progression model allows traffic engineers to produce a set of optimized cycle length, green ratios, phase sequence, and offsets for the entire arterial to facilitate not only the large off-ramp volume that travels through multiple intersections, but also non-through path flows (e.g., right-turn after traveling through several links) to minimize the likelihood of forming turning queues with designated progression bands.

Chapter 6 summarizes the operational flows and implementation criteria for responsible traffic agencies to sequentially expand available traffic management strategies—from local ramp metering to integrated corridor control—in contending with recurrent congestion. Starting from mitigating local freeway bottlenecks due to on- and off-ramp weaving flows, this chapter will first highlight the criteria for activating/deactivating a local metering control, followed by a discussion on the need to deploy some supplemental control modules that can ensure the achievement of mutual benefits between the freeway and its neighboring arterials under the local ramp control environment.

Chapter 2
An Arterial-Friendly Local Ramp Metering Control

2.1 Research background

Despite the abundance of literature in freeway ramp metering, such control, either at the local or coordinated level, is generally viewed as favoring the freeway at the cost of local traffic. Therefore, it has not been well received by highway agencies in practice yet since its emergence in the 1970s. The excessive ramp waiting time and the resulting queue spillback to the connected surface streets are the two primary concerns frequently raised by both the users of local arterials and the agencies responsible for traffic control and management. A standard practice to circumvent the queue spillback issue is to deactivate the metering control (i.e., max. metering rate) when the ramp queues exceed the deployed queue detectors. However, since ramp metering control is primarily deployed at those interchanges experiencing high on-ramp volume, the resulting on-ramp queue length is likely to trigger frequent overriding calls by the queue detectors, thus rendering it difficult to achieve the desired level of performance.

Any traffic control strategy intended for a congested corridor shall conceivably have the functions to benefit both its freeway and arterial users, and evolve both traffic systems to concurrently achieve the same optimal state under the given volume and available roadway capacity. As such, for the local ramp metering design, its control objective of optimizing the selected measure of effectiveness (MOE) ought to cover not only the freeway and ramp, but also all arterial intersections feeding traffic to the ramp that are likely to suffer from excessive ramp queues that often cause a gridlock. More specifically, a control system, intending to yield the target metering rate to best the freeway conditions but not spill ramp queues back to the surface street, should concurrently optimize the signal plans, including phase sequence and offsets for those intersections sending turning flows to the ramp. Such an arterial-friendly ramp control system will more likely ease the concerns of local commuters and offer the best prospect for comprehensive field implementation at freeway local bottlenecks caused mainly by heavy on-ramp weaving flows.

With such a control objective in mind, this study presents an arterial-friendly local ramp metering system (named AF-ramp) for time-of-day control. The proposed system can also serve as the base module for extending to real-time on-line control, or multi-ramp coordinated operations under a reliable traffic surveillance environment. Figure 2-1 shows the principal modules and their interrelations within the proposed AF-ramp system, including the control objectives and model output. Its key system features, as illustrated in the figure, include:

- Maximizing the total throughput for both the freeway and arterial links within the control area;
- Preventing ramp queues from spilling back to neighboring local streets by coordinating intersection signal plans with ramp metering control;
- Minimizing the impacts of an intersection's turning-to-ramp flows on the arterial's other traffic flow movements with local progression, a set of specially designed offsets to provide progression for all path-flows within the control area of the local arterial; and
- Optimizing the signal plan, including the phase sequence, for each intersection to ensure that its turning queues heading to the on-ramp will not exceed the available bay length.

A detailed discussion of mathematical formulations to model those key system features and operational constraints is presented in sequence below, followed by performance evaluation with extensive numerical analyses and simulation experiments.
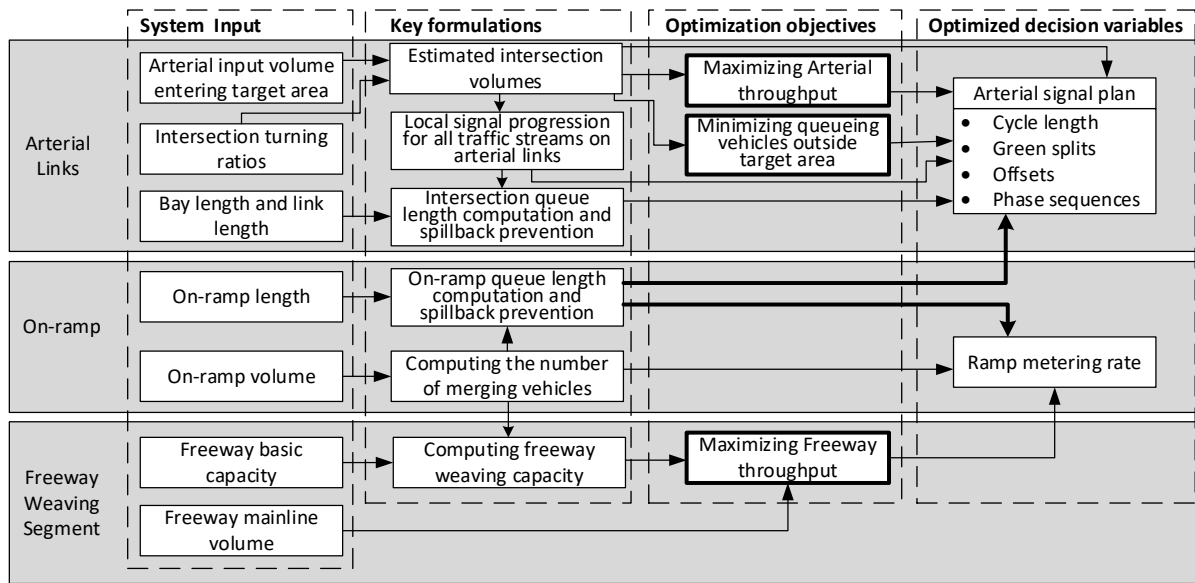
Figure 2-1: Model structure for the arterial-friendly local ramp metering control system

2.2 Model formulations

To facilitate the presentation of the proposed system's embedded formulations, Table 2-1 lists the key notations of all variables and parameters used in this study.

Table 2-1: List of key notations

Sets	
Ω	Set of intersection movements heading to the on-ramp
Δ	Set of movements exiting the target network
Φ	Set of movements entering the target network
Parameters	
v_i	Average vehicle speed on Lane i of the freeway (fps)
a	Deceleration rate of the rear vehicle for cooperative lane change (ft/s^2)
k_i	Average density on Lane n of the freeway (veh/mile)
C_w	Capacity in the weaving section (veh/hr)
C_b	Freeway basic capacity (veh/hr)
l	Average vehicle spatial headway (ft)
L_o	On-ramp length (veh)
s_o	Saturation flow rate at the ramp metering point (veh/hr)
$d(m), u(m)$	Downstream and upstream movements of traffic path m between two adjacent intersections
t_i	Travel time from intersection i to $i+1$ (in cycle);
$V_{\mu,i}$	Volume demand for movement μ at intersection i (veh/hr)
V_{fm}	Freeway mainline demand (veh/hr);
$f_{\mu,i}$	Lane use factor based on the number of lanes for movement μ at intersection i
$r_{\mu,i}$	Volume ratio of movement μ from arterial at intersection i
$L_{b,i}, L_{l,i}$	Bay length and the link length at intersection i (veh)
t_l	Lost time for each signal phase(sec)
T	Time duration of study (hr)
C_{max}, C_{min}	Upper bound and lower bound for the cycle length (sec)
δ_1, δ_2	Parameters for estimating the weaving section capacity
γ	Robustness factor that represents the sensitivity of volume fluctuation to the occurrence of queue spillback
α, β	Weighting factors in the objective function
Variables	
r_o	On-ramp metering green ratio
C_{r1}	Capacity reduction in the weaving section due to cooperative deceleration of the mainline vehicle behind the merging vehicle (veh/hr)
C_{r2}	Capacity reduction in the weaving section due to pre-allocation lane change (veh/hr)
V_o^a	Number of on-ramp vehicles merging into the freeway mainline (veh)
$V_{\mu,i}^a$	Actual volume for movement μ at intersection i (veh/hr)
V_f^a	Freeway throughput (veh/hr)
V_r^a	Arterial throughput (veh/hr)
R_i	Number of queueing vehicles outside the target area due to the limited green time (veh/hr)
L_{rv}	The length of the rear void created by cooperative deceleration of the freeway mainline vehicle behind the on-ramp merging vehicle (ft)
l_p	Queue length caused by excessive demand at the end of the study period (veh)
l_c	Queue length caused by arrivals from the upstream intersection in every cycle (veh)
ξ	Reciprocal of the cycle length at the arterial intersections (/sec)
$b_{m,i}$	Local progression bands, i.e., the duration within which vehicles from traffic path m can traverse

	intersections i-1 and i without stop (in cycle)
$t_{\mu,i}^a, t_{\mu,i}^b$	Start and end of the green phase for downstream movement μ at intersection i
$\tau_{d(m),i}$	Queue clearance time of movement $d(m)$ at intersection i (in cycle)
$l_{\mu,i}$	Queue length for movement μ at intersection i (veh)
$g_{\mu,i}$	Green ratio, including the lost time (in cycle)
$g_{t,i}\left(\overline{g}_{t,i}\right)$	Through green ratio for outbound (inbound) direction along the arterial (in cycle)
$g_{l,i}\left(\overline{g}_{l,i}\right)$	Left-turn green ratio for outbound (inbound) direction from the arterial (in cycle)
$g_{ml,i}\left(\overline{g}_{ml,i}\right)$	Green ratio for side street left-turn that would join outbound (inbound) direction along the arterial (in cycle)
$g_{mt,i}\left(\overline{g}_{mt,i}\right)$	Through green ratio for side street where corresponding left-turn would join outbound (inbound) direction along the arterial (in cycle)

Available capacity to accommodate the on-ramp flows

The optimal on-ramp metering rate, irrespective of the control strategy, depends primarily on the receiving freeway segment's available capacity. The capacity, however, is not a constant, but varies with the following two variables: arriving flow rates from the ramp's upstream mainline and from the connected local intersections. Because of the need to exercise corporative deceleration with on-ramp flows, traffic streams—especially in the rightmost lane—often comprise a series of voids between a leading on-ramp and following mainline vehicles. Such voids, as noted by Lertworawanich and Elefteriadou (2003), inevitably contribute to a reduction in the freeway segment's available capacity to accommodate the on-ramp traffic.

Conceivably, depending on the purpose of having such capacity reduction information (e.g., service quality evaluation or adaptive on-line control) and its required accuracy, one can perform such estimation from either the macroscopic or microscopic perspective, based on some or all of the following data: geometric features of freeway and ramps, traffic flow characteristics, volume distributions across lanes, behavioral patterns of the driving populations, and percentage of heavy vehicles (Roess and Ulerio, 2009; Rakha and Zhang, 2006; Lertworawanich and Elefteriadou, 2003). Hence, this study for the design of time-of-day local ramp control employs the following equation to approximate the capacity reduction due to the total loss time incurred by those voids between mainline and ramp vehicles:

$$L_{rv} = \frac{v_1^2 - v_0^2}{2a} \tag{2-1}$$

$$C_{r1} = \delta_1 V_o^a \frac{v_1^2 - v_0^2}{2al} \tag{2-2}$$

Note that L_{rv} is the length of the rear void (ft); v_1 and v_0 refer to the vehicle speed on

the rightmost and acceleration lanes (ft/s), respectively; and a denotes the deceleration rate of the rear vehicles following the on-ramp flows (ft/s^2). Hence, L_{rv} divided by the vehicle length, offers the base for approximating the impact of per void created by on-ramp vehicles. One can then approximate the resulting reduction in freeway capacity due to such on-ramp volume, V_o^a, as C_{r1}, where δ_1 is a parameter.

Eq. (2-3) shows that the allowable on-ramp volume can be determined by the actual flow rate for movement μ at intersection i, the set of movements heading to the on-ramp (Ω); the on-ramp metering green ratio (r_o); and the saturation flow rate (s_o) for the metered on-ramp.

$$V_o^a = \min\left(s_o r_o, \sum_{\mu \in \Omega} V_{\mu,i}^a\right) \tag{2-3}$$

Note that the collective manifestation of ramp-upstream drivers' discretionary lane-changing maneuvers to avoid the speed impedance by ramp flows, as noted by Kwon (1999), may also contribute significantly to the capacity reduction of the downstream freeway segment. Methodologies for a precise estimate of such a lane-changing frequency and the resulting impacts on the capacity from a behavioral perspective are available elsewhere (Beinum *et al.*, 2018; Zheng *et al.*, 2013; Zheng *et al.*, 2011), but for the purpose of this application it is assumed to be a function of the density ratio between the rightmost lane (i.e., lane 1) and its neighboring lane (lane 2), as expressed below:

$$C_{r2} = \delta_2 V_o^a \frac{k_2}{k_1 + k_2} \tag{2-4}$$

Where, k_1 and k_2 denote, respectively, the density for lane 1 and lane 2 prior to receiving the on-ramp merging vehicles (veh/mile), and where δ_2 is a parameter.

Note that Eq. (2-4) is grounded in the assumption that the density ratio between lane 1 and lane 2 before and after receiving the merging flows will be approximately unchanged, because traffic flows, when perceiving the impacts from on-ramp flows, tend to evolve to the same state by exercising discretionary lane changes. Hence, to achieve such a state after accommodating on-ramp volumes, if without those upstream lane changes, it is expected that the $k_2/(k_1+k_2)$ ratio of total on-ramp volume should be distributed to lane 2. However, most such on-ramp vehicles, as shown in most field observations, tend to stay in lane 1 over certain time intervals, thus often triggering a series of lane changes by those upstream lane-1 vehicles so that the lane density ratio between these two neighboring lanes can evolve back to the same level. Each of such lane-

changing maneuvers, approximated with the number of on-ramp vehicles to be distributed to lane 2 to maintain the before-merge density ratio, will occupy the spaces on both lane 1 and lane 2 when taking place, and thus inevitably cause impedance to the traffic flows and consequently contribute to the capacity reduction, denoted as C_{r2}, on the downstream segment.

As such, the available freeway capacity for local ramp control, accounting for the aforementioned two primary impacts, can be expressed as follows:

$$C_w = C_b - C_{r1} - C_{r2} = C_b - \delta_1 V_o^a \frac{v_1^2 - v_0^2}{2al} - \delta_2 V_o^a \frac{k_2}{k_1 + k_2} \tag{2-5}$$

Constraints for ramp queues

The on-ramp queue length typically consists of the residual queues after the whole control period and the arriving vehicles discharged per cycle from connected intersections. For the former, one can formulate Eq. (2-6) to compute the resulting queue length (in the unit of vehicles), whereas the latter can be approximated with Eq. (2-7). During the target control period, the total queue length is constrained to be within the ramp length, as specified by Eq. (2-8).

$$l_p = \max\left(\sum_{\mu \in \Omega} V_{\mu,i}^a - s_o r_o, 0\right) \times T \tag{2-6}$$

$$l_c = \sum_{\mu \in \Omega} V_\mu^a / 3600\xi \tag{2-7}$$

$$l_p + l_c \leq L_o \tag{2-8}$$

Where, l_p represents the queue length (veh) due to the excessive demand at the end of each control period; and l_c reflects the queue length (veh) by arriving vehicles per cycle from connected intersections.

Formulations of intersection queue constraints

To ensure that ramp control will not cause queue spillback at those intersections feeding flows to the freeway, the proposed system has adopted the local band notion (Chen *et al.*, 2020) to estimate the number of vehicles to stop at the intersections within the ramp's impacted area. Figure 2-2 illustrates the local band for one traffic path between two adjacent intersections in the time-space relation, where a special-designed signal plan, coordinated with ramp control, is

included in the proposal system to offer a progression band for each of those nine possible path flows over the arterial link between two intersections in the vicinity of an interchange. Note that each of those nine possible path flows consists of one upstream movement *u(m)* and one downstream movement *d(m),* as shown in Figure 2-2. Only vehicles not within their local progression bands must stop at the downstream intersection and contribute to the queues.

m: traffic paths between two adjacent intersections

$u(m) \in \{$through, left-turn from side street, right-turn from side street$\}$

$d(m) \in \{$through, left-turn, right-turn$\}$
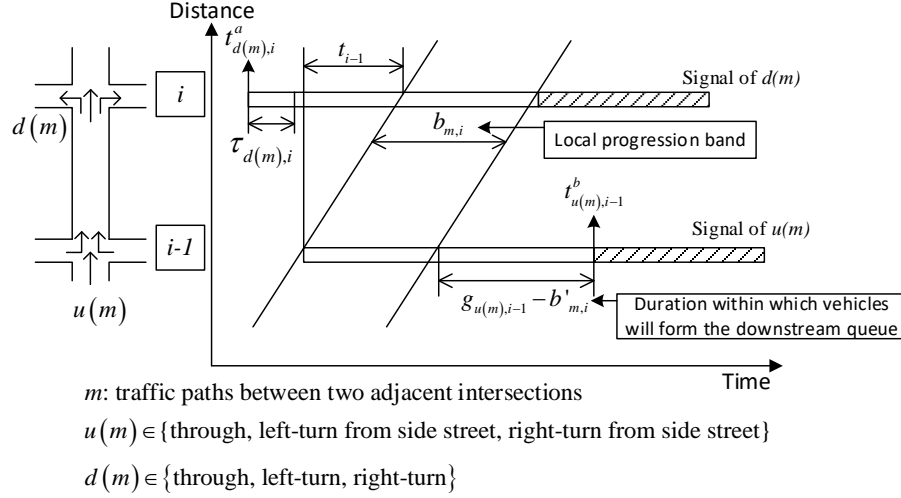
Figure 2-2: Example of a local progression band for one traffic path between two adjacent intersections

A mathematical expression for such local progression bands for the outbound direction is shown with Eq. (2-9):

$$b_{m,i} = \min\left(t^b_{d(m),i}, t^b_{u(m),i-1} + t_{i-1}\right) - \max\left(t^a_{d(m),i} + \tau_{d(m),i}, t^a_{u(m),i-1} + t_{i-1}\right) \tag{2-9}$$

Where,

$b_{m,i}$ is progression band for vehicles from path-flows *m* to move from intersections *i*-1 to *i*;

$d(m)$ and $u(m)$ are the downstream and upstream movements for traffic path-flow *m*;

$\tau_{d(m),i}$ is the queue clearance time of movement $d(m)$ at intersection *i* (in cycle);

t_i is the travel time from intersection *i* to *i*+1 (in cycle);

$t^a_{d(m),i}$ and $t^b_{d(m),i}$ are the start and end of the green phase for downstream movement *m* at intersection *i*, respectively; and

$t^a_{u(m),i}$ and $t^b_{u(m),i}$ are the start and end of the green phase for upstream movements *m* at intersection *i*, respectively.

Note that the second term in the right-hand side, $\max\left(t^a_{d(m),i} + \tau_{d(m),i}, t^a_{u(m),i-1} + t_{i-1}\right)$, shows the

starting time of the local progression band, which is to be determined by the arrival time of the first vehicle from traffic path m to the downstream intersection and the queue clearance time of the downstream movement associated with traffic path m. By the same token, the ending time of the local progression band, denoted by $\min\left(t^{b}_{d(m),i}, t^{b}_{u(m),i-1} + t_{i-1}\right)$, depends on the earlier time between the end of the downstream green phase and the last vehicle arrival from the same traffic path to the downstream intersection.

From the local bands associated with left-turn and through movements at the downstream intersection, one can formulate their resulting queues at the downstream intersection based on their volumes and turning ratios, as follows:

$$l_{\mu,i} = \sum_{d(m)=\mu} V^{a}_{u(m),i-1} r_{d(m),i}\left(g_{u(m),i-1} - b_{m,i-1}\right) f_{d(m),i} / 3600\xi, \ \mu=\text{through or left-turn} \tag{2-10}$$

Where, $l_{\mu,i}$ denotes the queue length for movement μ at intersection i (veh); $f_{d(m),i}$ refers to the lane-use factor based on the number of lanes for movement $d(m)$ at intersection i; and $r_{d(m),i}$ is the volume ratio of movement $d(m)$ from arterial at intersection i.

To prevent the queue spillback from the left-turn bay and the through lanes, one can present the following equations:

$$l_{\mu,i} \frac{s}{s - V_{\mu,i} f_{\mu,i}} \times \gamma \le L_{b,i} \tag{2-11}$$

$$l_{\mu,i} \frac{s}{s - V_{u,i} f_{u,i}} \times \gamma \le L_{l,i} \tag{2-12}$$

Where, s is the saturation flow rate (veh/hr); $L_{b,i}$ and $L_{l,i}$ are the bay length and the link length at intersection i, respectively (veh); and γ is a robustness factor greater than 1 that represents the sensitivity of volume fluctuation to the occurrence of queue spillback. The left-hand side represents the estimated maximum queue length during a cycle. The queue discharging time in Eq. (2-9) can then be estimated with the obtained queue length as follows:

$$\tau_{\mu,i} = l_{\mu,i} \frac{3600\xi}{s - V_{u,i} f_{u,i}} \tag{2-13}$$

Following the same logic, one can develop similar constraints as Eqs. (2-9) - (2-13) for the inbound direction.

Constraints for intersection flows and signal parameters

Note that the actual number of vehicles arriving at a downstream intersection can be derived from the flows moving out from its upstream intersection, as with Eq. (2-14).

$$V_{\mu,i}^a = r_{\mu,i} \sum_{d(m)=\mu} V_{u(m),i-1}^a \tag{2-14}$$

If any internal link within the target area experiences overflow, the queues would rapidly spill back to the upstream intersection and cause a local bottleneck. Therefore, such a situation should be avoided by providing sufficient green time to discharge all vehicles on the links within the target control area, as shown with Eq. (2-15).

$$V_{\mu,i}^a f_{\mu,i} \leq \left(g_{\mu,i} - t_l \xi \right) s \tag{2-15}$$

Where, $g_{\mu,i}$ represents the green ratio, including the lost time (in cycle), and t_l denotes the lost time (sec). The green ratios at the intersections should satisfy the following constraints to be practical:

$$g_{t,i} + \overline{g}_{l,i} = g_{l,i} + \overline{g}_{t,i} = g_{major,i} \tag{2-16}$$

$$g_{mt,i} + \overline{g}_{ml,i} = g_{ml,i} + \overline{g}_{mt,i} = g_{minor,i} \tag{2-17}$$

$$g_{major,i} + g_{minor,i} = 1 \tag{2-18}$$

The cycle length will be constrained with its lower and upper bounds using Eq. (2-19).

$$1/C_{max} \leq \xi \leq 1/C_{min} \tag{2-19}$$

Objective function

As previously stated, this study focuses on maximizing the total throughput for the freeway and the local arterial. Furthermore, queueing vehicles are not able to enter the control area due to the lower cycle length and green ratio, and should cause a penalty in the objective function since these vehicles would incur excessive delay if not properly discharged. Therefore, the objective function of the proposed model can be expressed with,

$$\max V_f^a + \alpha V_r^a - \beta R_i \tag{2-20}$$

$$V_f^a = \min\left(V_{fm} + V_o, C_w\right) \tag{2-21}$$

$$V_r^a = \sum_i \sum_{\mu \in \Delta} V_{\mu,i}^a \tag{2-22}$$

$$R_i = \sum_{\mu = \Phi} \left(V_{\mu,i} - V_{\mu,i}^a\right) \tag{2-23}$$

Where, V_f^a denotes freeway throughput (veh/hr), which is determined by freeway mainline demand, on-ramp volume, and weaving section capacity, as expressed in Eq. (2-21); V_r^a represents the arterial throughput (veh/hr), which counts all vehicles exiting the target area, as expressed in Eq. (2-22); R_i is the number of queueing vehicles outside the target area due to the limited green time (veh/hr); α and β are weighting factors; V_{fm} denotes the freeway mainline demand (veh/hr); $V_{\mu,i}$ is the volume demand for movement μ at intersection i (veh/hr); Δ is the set of movements exiting the target network; and Φ is the set of movements entering the target network.

In brief, the proposed model can be summarized as follows:

Max $V_f^a + \alpha V_r^a - \beta R_i$

s.t.

    Eqs. (2-21)-(2-23)
    Freeway capacity constraints: Eqs. (2-2)-(2-5)
    On-ramp queue constraints: Eqs. (2-6)-(2-8)
    Intersection queue constraints: Eqs. (2-9)-(2-13)
    Constraints for intersection flows and signal parameters: Eqs. (2-14)-(2-19)

2.3 Case study

To verify the unique capability of the developed AF-ramp model and evaluate its effectiveness, this case study included both numerical investigations and simulation experiments within a real-world network. The numerical results are presented to show the model's functions in response to the volume surge and geometric constraints such as the ramp length, while the resulting measures of effectiveness (MOEs) and the impacts on the local arterial under such control are assessed with microscopic traffic simulation. All analysis results from this case study constitute the basis to confirm the AF-ramp model's capability of concurrently improving traffic conditions on the freeway and local arterials, and not causing queues to overflow from the on-ramp.

Study site

Figure 2-3 shows the key geometric information and the input volume associated with the study site at I-270 @ MD 187 in Maryland. The freeway mainline volume and hourly demand for all movements entering the target control area are shown in the figure, along with the number of lanes on the arterial links and the freeway segment. The eastbound on-ramp for metering control is colored in grey and the turning ratios onto the on-ramp are also shown in the figure. The maximum and minimum cycle lengths are 90 and 180 seconds, respectively. Table 2-2 show the AF-ramp model's key output for the area-wide ramp control under the following scenarios:

- **Scenario 1**: the base-level volume as shown in Figure 2-3**;**
- **Scenario 2**: same as Scenario 1 but with an increase of 10% to all arterial volumes;
- **Scenario 3**: same as Scenario 1 but with an increase of 20% to all arterial volumes; and
- **Scenario 4**: same as Scenario 3 but with a shorter ramp length (from 792 ft to 500 ft).
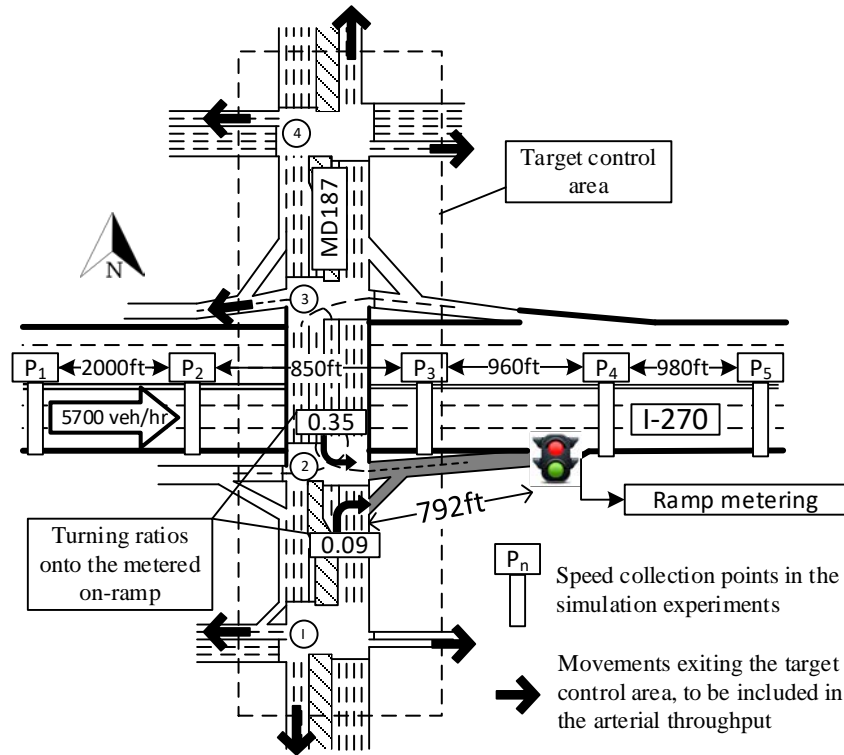
Intersection	Northbound			Southbound			Eastbound			Westbound		
	LT	TH	RT	LT	TH	RT	LT	TH	RT	LT	TH	RT
1	173	1867	2	-	-	-	515	29	182	7	17	49
2	-	-	-	-	-	-	579	-	130	-	-	-
3	-	-	-	-	-	-	-	-	-	63	-	172
4	-	-	-	81	1270	278	301	263	100	336	380	96

* Volumes are in unit of vph. LT: left-turn, TH: through, RT: right-turn.
* "-" indicates non-boundary movements inside the target control area

Figure 2-3: The key geometric and volume information associated with the study site

Table 2-2: Optimization results from the proposed model under four designed scenarios

	Scenario 1	Scenario 2	Scenario 3	Scenario 4
Ramp metering green ratio	0.38	0.42	0.47	0.45
Arterial cycle length (sec)	90	90	150	100
SB LT green ratio at Intersection 2	0.36	0.40	0.42	0.41
Intersection offsets (sec)				
Intersection 1	0	12	135	0
Intersection 2	83	70	101	59
Intersection 3	84	0	3	35
Intersection 4	58	5	0	96

* SB: Southbound

Note that the optimal on-ramp metering green ratio, as expected, increases with the arterial's volume (i.e., from 0.38 for Scenario 1 to 0.47 for Scenario 3), confirming the AF-ramp model's unique feature to adjust the ramp metering rate, based not only on the available freeway capacity, but also on the on-ramp volume from its neighboring intersections. Also note that the model will concurrently increase the ramp green ratio (from 0.38 to 0.47) and intersection's cycle length (90 to 150 seconds) to accommodate the 20% volume surge as in Scenario 3.

To prevent queue spillback on a short ramp as in Scenario 4, the model with its embedded functions to capture the interrelations between ramp and arterial flows can concurrently generate a shorter cycle length and less green ratio to constrain the on-ramp's arriving flows. For instance, compared with Scenario 3, the cycle length in Scenario 4 is reduced from 150 seconds to 100 seconds, along with a slightly adjusted green ratio (from 0.42 to 0.41) for the left-turn movement to get onto the ramp.

Simulation experiments

To evaluate the model's effectiveness with MOEs, simulation experiments with Scenarios 1 and 2 were conducted using VISSIM. The model performance was compared with the following two controls:

- _no-RM_ control: no metering control and the arterial signal timing is calculated with Critical Lane Volume (CLV) and the coordination offsets are optimized with MAXBAND (Little *et al.*, 1981); and

- *RM-only* control: the ramp metering rate is set only to maximize the freeway throughput based on Eq. (2-21), and the arterial signal timing plan is optimized independently as with the *No-RM* control.

The set of MOEs generated from the simulation includes: 1) average vehicle speed for all lanes and on the rightmost lane, collected at five locations (denoted as P_1 to P_5) shown in Figure 2-3); 2) completed trips on the freeway mainline over the one-hour control period; 3) average freeway mainline delay; 4) arterial's total throughput from the target control area (including all movements leaving the target control area shown in Figure 2-3); 5) average arterial through-movement delay; 6) network average delay; and 7) queue lengths on the on-ramp and arterial links. The results are obtained from 10 simulation runs with different random seeds.

Figure 2-4 shows the time-dependent on-ramp queue length with the AF-ramp model and the RM-only control. As expected, the RM-only control, without accounting for the arterial traffic, would rapidly increase the on-ramp queues and further overflow those vehicles to the upstream intersection about 1600 ft away. In contrast, such on-ramp queuing vehicles under the AF-ramp control are all contained within the ramp, due mainly to the higher metering rate designed to avoid on-ramp queue spillback and the coordinated operation of the arterial signals.

(a) Scenario 1

On-ramp queue length with the proposed model and RM-only control under Scenario 2

(b) Scenario 2

* Due to the design features of VISSIM, the spillback queue from the ramp will be counted only up to the upstream intersection only, i.e., 1600 ft in the case study site.
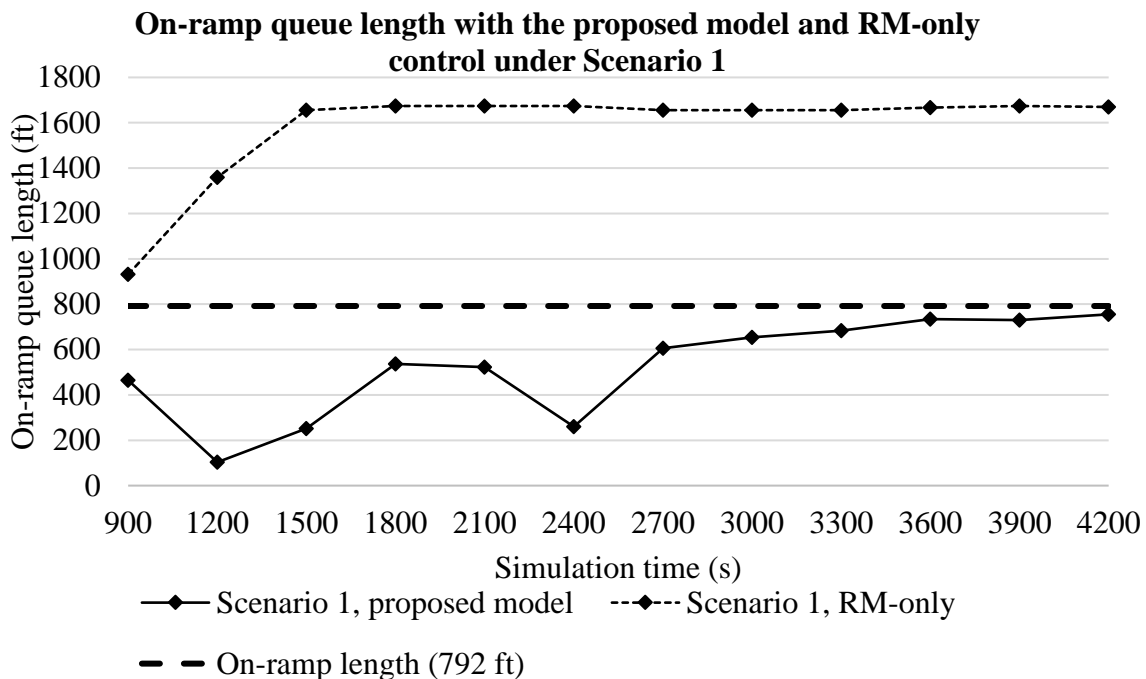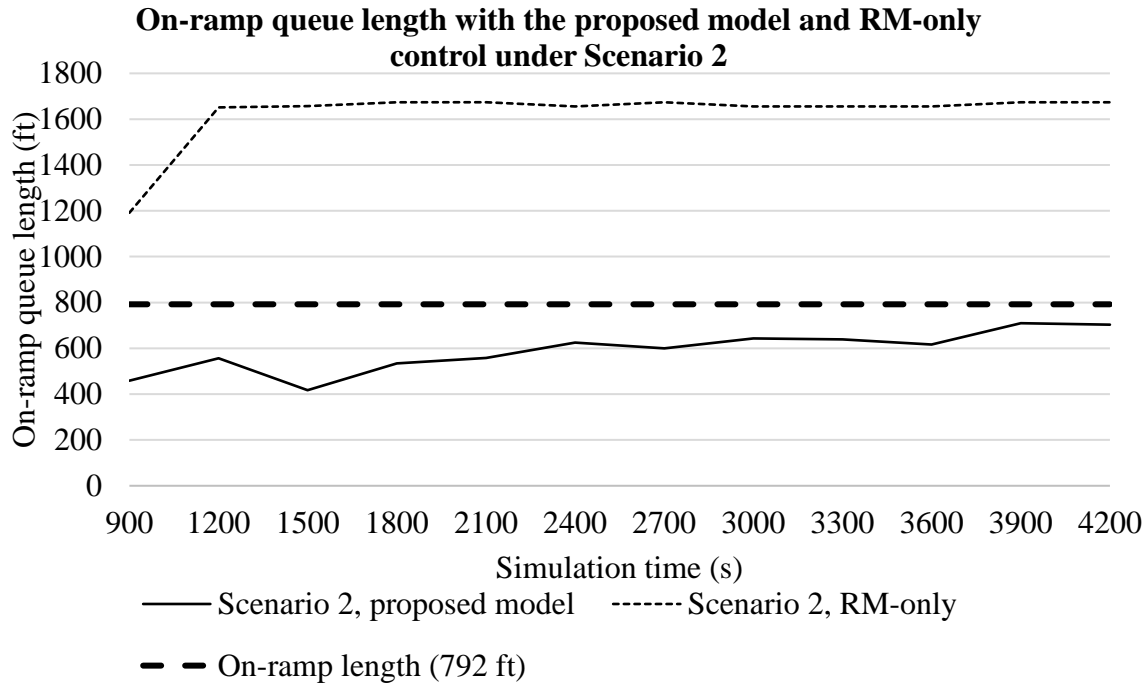
Figure 2-4: Evolution of on-ramp queue length with the proposed model and RM-only control

Note that since RM-only control will yield undesirable long queues to the arterial, the benefits analysis presented hereafter for the developed AF-ramp model will focus on its resulting benefits, using the No-RM control as the baseline for comparison. Table 2-3 and Table 2-4 show the average speed of all lanes and on the rightmost lane, along with all other MOEs with these two control strategies under Scenarios 1 and 2. Figure 2-5 further shows the results from the same comparison but focuses on the time-dependent queue length on the arterial link, which is often plagued by the excessive queues in the vicinity of the freeway ramp.

As shown in Table 2-3, the freeway segment upstream of the on-ramp, without ramp metering control, exhibits a significant speed drop, but the traffic flows recover once passing the ramp and entering the downstream segment. For example, under Scenario 1, the average speed progressively drops from its initial speed of 54.7 mph at the most upstream detection point to 38.3 mph right at the on-ramp merging area, and then back to 50.1 mph at the P_5 detection point. One can also detect the same spatial evolution pattern of the average speed for Scenario 2, but with a more pronounced drop due to the impact of higher ramp flows (i.e., from 49.2 mph to 33.9, and back to 50.1 mph). In both scenarios, its rightmost lane, as shown in the Table, suffers the most impact from the ramp flows, reducing its speed from 54.5 mph to 34.2 mph in Scenario

20

1, and likewise from 48.9 mph to 28.6 mph in Scenario 2. Such significant speed drop phenomenon clearly justifies the need to implement ramp metering.

Table 2-3: Average speed with two control strategies under Scenarios 1 and 2

Location	P_1	P_2	P_3	P_4	P_5
Scenario 1 Three-lane average speed (mph)					
No-RM	54.7	45.2	38.3	44.7	50.1
Proposed	56.6 (3.5%)	51.1 (13.1%)	46.6 (21.5%)	45.2 (1.1%)	50.2 (0.2%)
Scenario 1 Rightmost lane average speed (mph)					
No-RM	54.5	42.4	34.2	42.6	50.0
Proposed	56.6 (3.7%)	48.5 (14.4%)	42.8 (25.0%)	44.0 (3.3%)	50.2 (0.4%)
Scenario 2 Three-lane average speed (mph)					
No-RM	49.2	38.0	33.9	44.5	50.1
Proposed	53.3 (8.4%)	47.9 (26.1%)	40.4 (19.5%)	44.5 (0.1%)	50.1 (-0.1%)
Scenario 2 Rightmost lane average speed (mph)					
No-RM	48.9	35.0	28.6	42.0	50.0
Proposed	53.1 (8.4%)	45.2 (29.0%)	36.0 (25.7%)	43.2 (2.7%)	50.0 (-0.1%)

* Percentages in the brackets indicate the improvement over the No-RM strategy.

Table 2-4: Related MOEs with two control strategies under Scenarios 1 and 2

	Freeway mainline avg delay (s)	Freeway mainline completed trips	Average arterial through delay (s)	Arterial throughput (vph)	Network average delay (s)
Scenario 1					
No-RM	32.17	5592	100.14	6180	70.29
Proposed	17.62 (45.2%)	5621 (0.5%)	76.63 (23.5%)	6193 (0.2%)	53.92 (23.3%)
Scenario 2					
No-RM	51.90	5522	105.54	6777	82.92
Proposed	29.15 (43.8%)	5591 (1.2%)	86.83 (17.7%)	6800 (0.3%)	61.97 (25.3%)

* Percentages in the brackets indicate the improvement over the No-RM strategy.

In contrast, under the proposed AF-ramp control, the average speed on the bottleneck segment increases from 45.2 mph to 51.1 mph at P_2, and 38.3 mph to 46.6 mph at P_3 in Scenario 1, an average of 17.3% (i.e., 13.1% and 21.5%) improvement. As expected, the rightmost lane, generally benefiting more from an effective ramp metering control, exhibits the speed improvement of 14.4% and 25.0% respectively in Scenario 1 over the same detection points in the bottleneck area. In general, the magnitude of such improvement may increase with the ramp

volume, as evidenced by the 29.0% and 25.7% speed improvement for the rightmost lane under Scenario 2 at the same data collection points.

Table 2-4 summarizes various MOEs for both the freeway and arterial with the AF-ramp model and under No-RM control, where the delay on the freeway mainline improves by 45.2% and 43.8%, respectively under these two scenarios, attributed mainly to the AF-ramp control's function to prevent the formation of a local bottleneck by the on-ramp flows. The results in Table 2-4 clearly show that the arterial's traffic conditions can concurrently benefit from such control. For example, the through movement's average delay exhibits a reduction of 23.5% and 17.7%, respectively, in Scenario 1 and Scenario 2, due to the AF-ramp model's embedded progression design and its coordinated function between metering rate and intersection signal plans. In addition, the same arterial throughput under these two controls further supports the fact that the AF-ramp control does not have undesirable impacts on the local traffic flows.

To ensure that the coordination between intersection signals and ramp metering control does not result in excessive queues on the arterial links, especially those accommodating vehicles turning to the ramp, this study further analyzed the queue length evolution at all intersection approaches and confirmed that no links or turning bays have experienced traffic overflows under the AF-ramp control. For example, the queue evolution patterns for the northbound through movement and southbound left-turn traffic, shown in Figure 2-5, clearly demonstrate that those arterial links connecting to the freeway ramp are likely to experience a traffic gridlock and extend their queues to their upstream intersections. However, under the local progression and coordination with ramp metering control, both arterial links under AF-ramp can well constrain the resulting queues in a relatively stable pattern, and also within their designated space.

Northbound through queue length at Intersection 3

(a) Northbound through queue length at Intersection 3
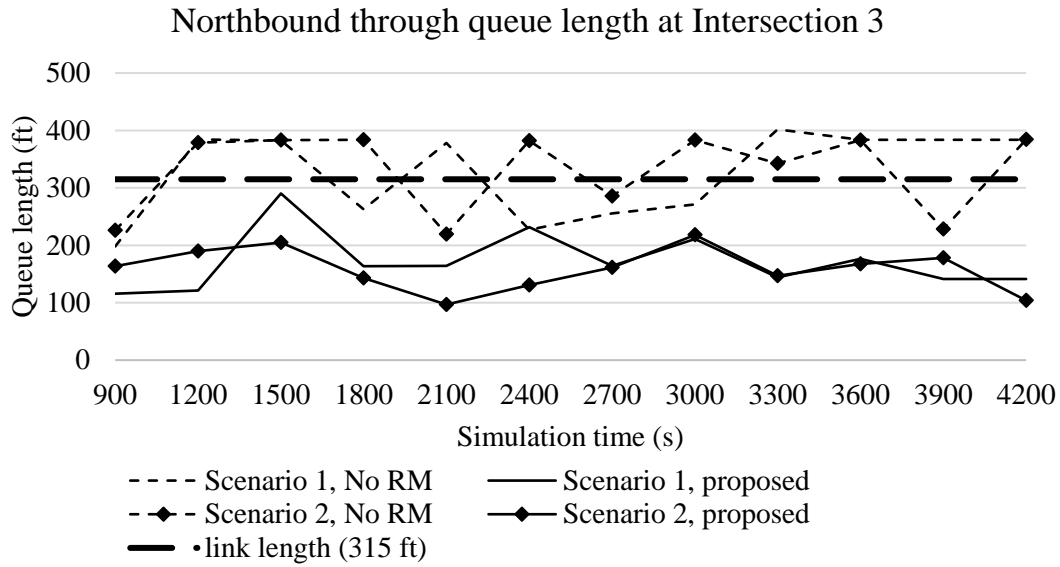
Southbound left-turn queue length at Intersection 2
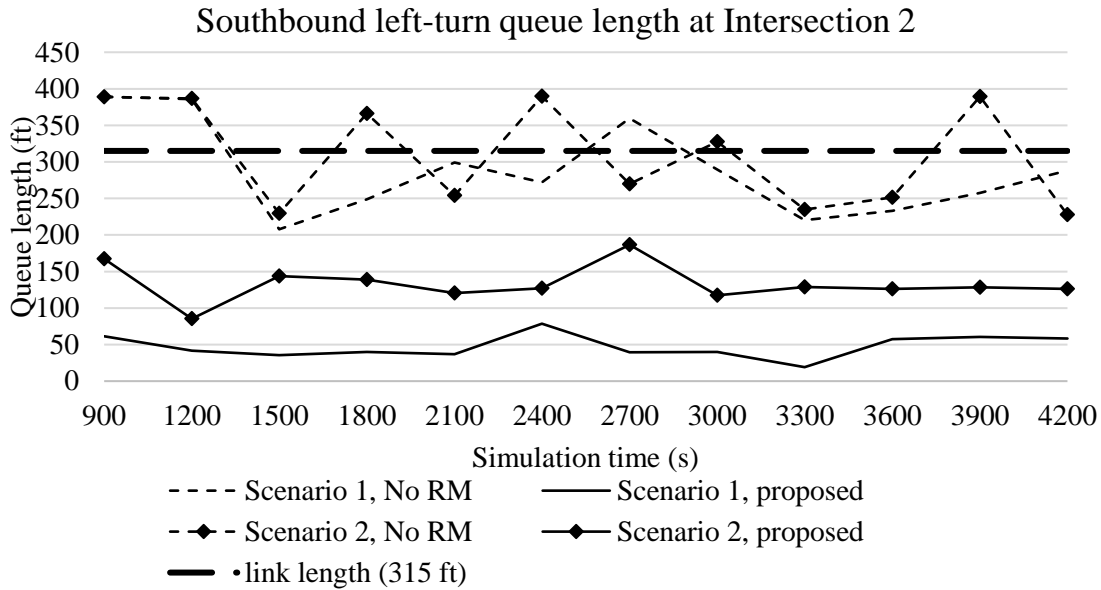
(b) Southbound left-turn queue length at Intersection 2

Figure 2-5: Time-dependent queue length on the arterial link with the proposed model and No-RM control under the two scenarios

In brief, the above analysis results from both the numerical investigation and simulation evaluation have confirmed the developed AF-ramp model's effectiveness in terms of concurrently improving traffic conditions on both the freeway and its neighboring arterial links, and most importantly, yielding no queue spillback on either the ramp or arterial links.

2.4 Extension to real-time control

For extension of the AF-ramp model from the time-of-day control to real-time mode, one effective way to circumvent the demanding on-line computing requirements is to best divide the control period into a sufficient number of small time periods based on the day-to-day detected traffic patterns, and then monitor such time-of-day control with the information from real-time available traffic data.

As shown in Figure 2-6, traffic operators, in practice, can first execute the optimal control plan, off-line computed with AF-ramp, for each time period, and then proceed the operations with real-time available traffic data and queue information. If the detected traffic information for either freeway or local arterials differs significantly and sustainably from the traffic data classified for that control period, one can then switch to a new control plan from the database that contains the set of off-line optimized control plans for all observed day-to-day historical traffic patterns.

Conceivably, a real-time operating system extended from time-of-day off-line control does not require its controller to have high computing power, and is sufficiently flexible for accommodating fluctuating traffic conditions and non-recurrent congestion due to special events or incidents. Note that to optimize such a system's performance in real time operations, ideally it shall also have one supplemental module that functions to inform the system with respect to the optimal timing to change the current control plan if justified to do so, and also the selection of new plans from the database to best respond to the newly detected traffic conditions.
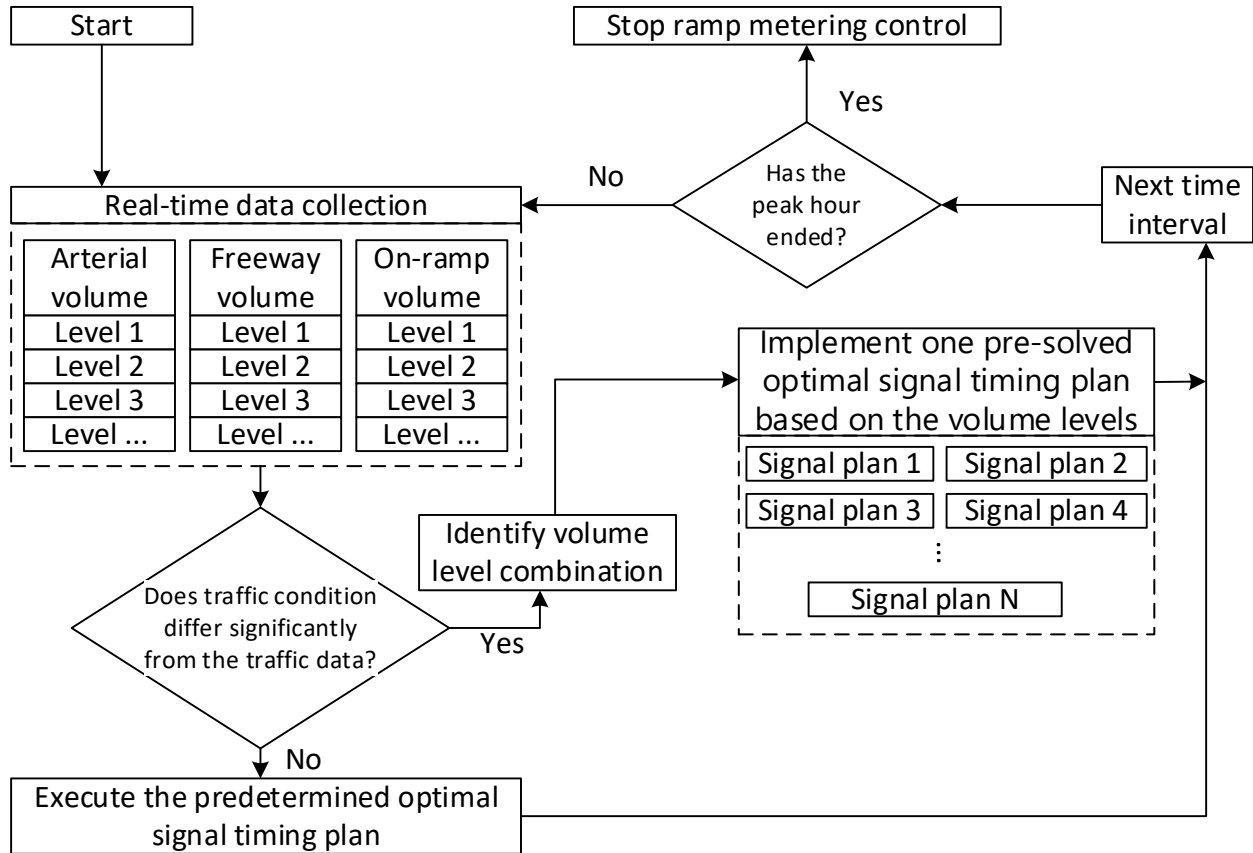
Figure 2-6: Real-time operation of arterial-friendly local ramp metering system

Chapter 3
A Lane-Group-Based Traffic Model for Assessing On-Ramp Traffic Impact and Coordinated Ramp Control

3.1 Research background

Coordinated ramp metering has long been viewed as one potentially effective control strategy for most highway agencies to contend with recurrent congestion on a freeway corridor, especially when the impacts from ramp merging flows propagate sustainably to their upstream mainline segments. One of the most popular practices for exercising such coordinated control is to integrate local ramp metering operations with a macroscopic freeway traffic model that functions to project the spatial and temporal evolution of the mainline traffic conditions under various ramp-merging volumes. With such integrated freeway mainline-ramp traffic flow relations, one can then best set the metering rate for each ramp based on the upstream ramp metering rate and projected arriving flow rate from the freeway mainline.

One of the most commonly-used tools by traffic professionals for operating freeway coordinated ramp metering or various dynamic control is the METANET model (Messener and Papageorgiou, 1990), a macroscopic traffic flow model that first views the target highway under control as a series of interconnected spatial segments (see Figure 3-1), and then employs the fundamental relations between flow rate, density, and speed within each segment to project its outgoing flow rate during each time interval. With the assumption of spatial uniformity for vehicles within the same segment and the flow conservation during each time interval, it can update the temporal and spatial evolution of traffic state for the target freeway with the following core equations.
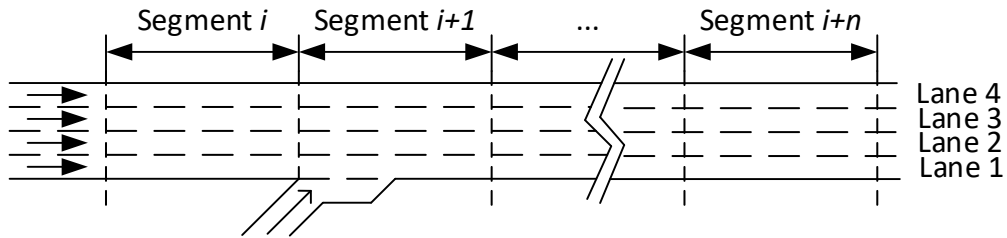
Figure 3-1: A macroscopic view of the freeway under the METANET model

$$\rho_i(k + 1) = \rho_i(k) + \frac{T}{L_i \lambda_i}[q_{i-1}(k) - q_i(k)] \tag{3-1}$$

$$v_i(k+1) = \min\{v^m, v_i(k) + \frac{T}{\tau}\big[V_i\big(\rho_i(k)\big) - v_i(k)\big]$$

    Relaxation term

$$+ \frac{T}{L_i} v_i(k)[v_{i-1}(k) - v_i(k)] - \frac{\upsilon T}{\tau L_i} \frac{[\rho_{i+1,}(k) - \rho_i(k)]}{\rho_i(k) + \kappa}\}$$

    Convection term   Anticipation term

(3-2)

$$V_i\big(\rho_i(k)\big) = v_i^f * \exp[-\frac{1}{a_i}(\frac{\rho_i(k)}{\rho_i^C})^{a_i}]$$

(3-3)

$$q_i(k) = \lambda_i \rho_i(k) v_i(k)$$

(3-4)

Where,

$\rho_i(k)$ and $q_i(k)$ are the density and flow rate of segment i at time k;

λ_i and L_i denote the number lanes and the length, respectively, on segment i;

v^m is minimum speed;

$v_i(k)$ is the speed of segment i at time k;

$V_i(.)$, v_i^f, and ρ_i^C denote the function for speed-density relation, the free-flow speed, and critical density, respectively, for segment i;

τ, υ, κ and a_i are the location-specific parameters to be calibrated with field data; and

T stands for the time interval for updating the traffic state in each segment.

Note that the convection term in Eq. (3-2) is to reflect the continuity of traffic conditions between two consecutive freeway segments that are divided for convenience of model computation. Likewise, the anticipation term is proposed to capture the perceivable impacts of the downstream segment's traffic conditions—such as congestion—on the speed of drivers in the current segment.

For those freeway segments having either lane reduction or on-ramps, traffic researchers have suggested to include the following additional terms to reflect their impacts on their traffic flow speeds:

$$-\phi v_i(k) \frac{v_i(k) T \rho_i(k) \Delta\lambda_i}{L_i \lambda_i \rho_i^C}$$

(3-5)

$$-v_i(k) \frac{\delta T r_i(k)}{L_i \lambda_i(k)(\rho_i(k) + \kappa)}$$

(3-6)

Where,

$\Delta\lambda_i$ denotes the number of dropped lanes;

$r_i(k)$ indicates the on-ramp flow rate at time k; and

ϕ, δ, κ are parameters to be calibrated with field data.

Conceivably, Eq. (3-5) is to show that the speed reduction due to lane drops varies with the ratio between the number of vehicles on such lanes (i.e., $v_i(k)T\rho_i(k)\Delta\lambda_i$) and the number of vehicles segment i can accommodate under critical density condition (i.e., $L_i\lambda_i\rho_i^C$). Eq. (3-6) functions to approximate the speed impact by on-ramp merge flows, based on the ratio between the number of on-ramp vehicles, $Tr_i(k)$, and the number of vehicles in the segment, $L_i\lambda_i(k)\rho_i(k)$.

3.2 A lane-group-based macroscopic freeway traffic model

As is noticeable from the above description, the METANET model, despite its effectiveness in projecting the segment-based traffic conditions, does not distinguish the speed differences between different travel lanes, and thus may yield insufficient information for implementing advanced traffic management strategies, such as lane-based variable speed control or coordinated adaptive ramp metering operations that may need precise lane-by-lane speed and concentration data. Note that the speed variation between travel lanes is especially pronounced on the highway segments upstream and downstream of a ramp, where on-ramp weaving flows may impede the rightmost-lane traffic speed with their mandatory lane changes, which will in turn trigger the discretionary lane changes by drivers on the neighboring lanes to avoid the speed reduction. A graphical illustration of such impacts is shown in Figure 3-2.
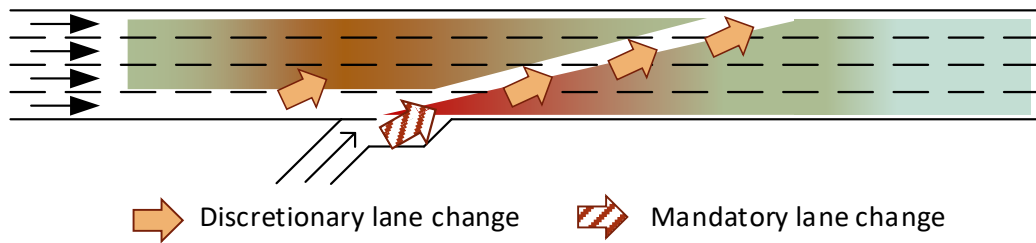
Figure 3-2: Graphical illustration of the impacts by the on-ramp merging flows

Depending on the aggressiveness of the driving population and the congestion level, the resulting speed variance between travel lanes due to lane changes, shown in Figure 3-2, may be so significant as to affect the optimal metering rate or the strategy of variable speed control. Hence, a freeway traffic model that fails to address the between-lane discrepancies of traffic conditions within the same segment due to ramp merging flows may not project the spatial and temporal evolution of downstream traffic conditions at the desirable level of accuracy for various

control operations.

Hence, grounded on the core notion of the METANET model, this study has proposed the following lane-group-based traffic flow model to address such concerns. Figure 3-3 shows the key inputs and principal components of the proposed model, including the relations between its key components and primary model outputs.
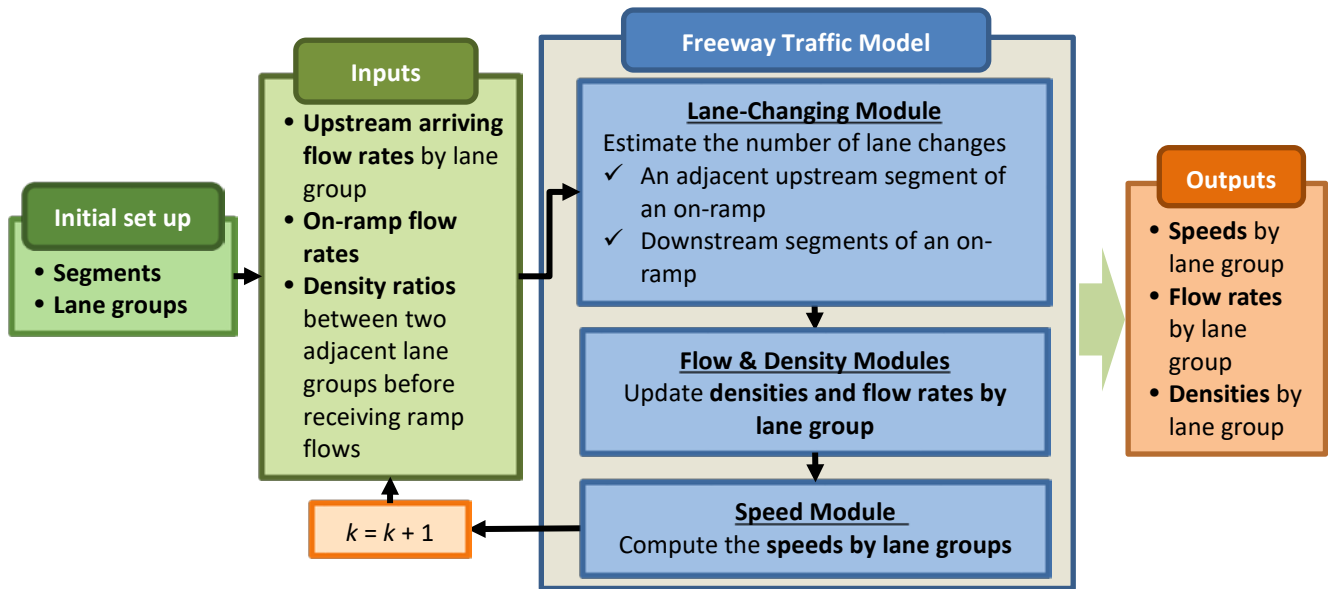
Figure 3-3: Key inputs, outputs, and primary components of the proposed lane-group-based model

Principal modules of the lane-group-based traffic model, along with their embedded logic relations, are detailed in sequence below; all notations for variables used hereafter are shown in Table 3-1.

Table 3-1: List of key variables used in the lane-group-based freeway traffic flow model

|	
$N_{i,j,j+1}(k)$	Number of vehicles changing from lane groups j to $j+1$ in segment i at time k. ($j = 1,.., G_i - 1$; G_i is the number of lane groups in segment i)
L_i	Length of segment i (mile)
$\rho_{i,j}(k)$	Density of lane group j in segment i at time k (prior to experience the lane changes by vehicles) (veh/mile)
$\rho_{i,j}^*(k)$	Density of lane group j of segment i at time k (after accommodating lane-changing vehicles) (veh/mile)
$\lambda_{i,j}$	Number of lanes in lane group j in segment i
ρ^{jam}	Jam density (veh/mile)
$\alpha_{j,j+1}$	Target density ratio between lane groups j and $j+1$
$S_{i,j}$	The set of lane groups in the adjacent upstream segment connected to lane group j in segment i ($|S_{i,j}|$ is the number of lane groups in $S_{i,j}$)
$D_{i,j}$	The set of lane groups in the adjacent downstream segment connected to lane group j in segment i ($|D_{i,j}|$ is the number of lane groups in $D_{i,j}$)
$q_{i,j}(k)$	Flow rate of lane group j in segment i at time k (vph)
T	Time interval for updating the traffic state (hour)
$v_{i,j}(k)$	Speed of lane group j in segment i at time k (mph)
v^m	Minimum speed (mph)
$V_i(.)$	Speed-density relation for segment i
ρ_i^C	Critical density of segment i (veh/mile)
$\eta, \tau, \upsilon, \kappa, \phi$	Parameters

Initial system setup module

To replicate the complex interactions between freeway ramp and mainline flows from the lane-group view, one needs to first divide the freeway within the control area into several segments, and then classify their travel lanes into a number of lane groups, based on both the geometric features and speed variance within each segment. Conceivably, one can formulate each lane as one group if the traffic flow speeds vary significantly across lanes.

Note that for convenience of presentation but without loss of the generality, all travel lanes in each freeway segment within the on-ramp control area are classified into three lane groups, with the rightmost and leftmost lanes being defined as lane group 1 and lane group 3, respectively. All middle lanes are denoted as lane group 2, as shown in Figure 3-4.
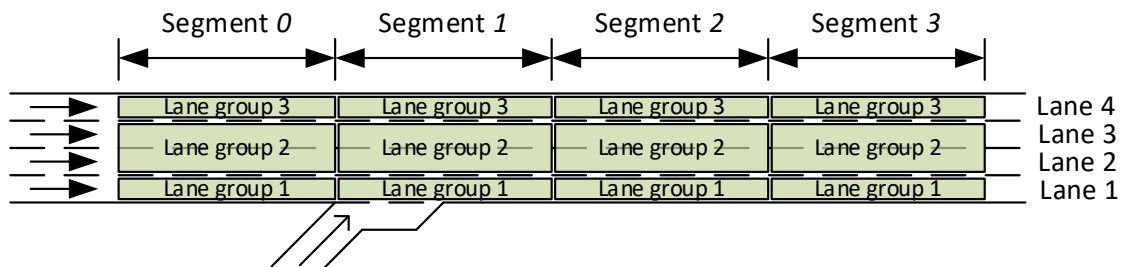
Figure 3-4: Freeway segments under the lane-group-based traffic flow model

Lane-changing module

This module serves to estimate the number of lane changes, based on lane change purposes and the current densities in lane groups. Eq. (3-7) shows such dynamics resulted from the number of vehicles performing lane changes in responding to the perceived interference by ramp flows.

$$N_{i,j,j+1}(k)$$

$$= \begin{cases} \min(L_i\rho_{i,j}(k), \; \eta \, \lambda_{i+1,j}\lambda_{i+1,j+1}L_{i+1}\dfrac{\rho_{i+1,j}(k) - \rho_{i+1,j+1}(k)}{\lambda_{i+1,j} + \lambda_{i+1,j+1}}, \; (\rho^{jam} - \rho_{i,j+1}(k))L_i), \; if \, \rho_{i+1,j}(k) > \rho_{i+1,j+1}(k) \\ \qquad\qquad 0, \; otherwise \end{cases} \quad (3\text{-}7)$$

Where,

$N_{i,j,j+1}(k)$ is the number of vehicles changing from lane groups j to $j+1$ in segment i at time k; and

η is the parameter to reflect the characteristics of driving populations and their reactions to the perceived on-ramp volume.

Note that by setting i and j to 0 and 1, respectively, the second term, $\lambda_{i+1,j}\lambda_{i+1,j+1}L_{i+1}\dfrac{\rho_{i+1,j}(k)-\rho_{i+1,j+1}(k)}{\lambda_{i+1,j}+\lambda_{i+1,j+1}}$, is to approximate the number of vehicles in lane group 1 that must perform the lane changes so as to re-balance the density levels between lane groups 1 and 2 in view of ramp flows merging onto the downstream segment's lane group 1. The third term, $(\rho^{jam} - \rho_{i,j+1}(k))L_i$, is a straightforward approximation of the available space in lane group 2 to accommodate such lane-changing vehicles in segment 0 at time k.

Eq. (3-8) shows the number of lane-changing vehicles in the downstream segments (segments 1 to 3) of an on-ramp, based on the assumption that a freeway segment, after impacted by the on-ramp merging flows, will progressively redistribute its mainline and merged volumes between travel lanes over those downstream segments via drivers' discretionary lane changes until evolving back to the state that should have approximately the same density ratios between neighboring lane groups as those prior to the impacts by on-ramp flows.

$$N_{i,j,j+1}(k)$$

$$= \begin{cases} \min(\lambda_{i,j}\lambda_{i,j+1}L_i\dfrac{\rho_{i,j}(k) - \alpha_{j,j+1}\rho_{i,j+1}(k)}{\lambda_{i,j}\alpha_{j,j+1} + \lambda_{i,j+1}}, \; (\rho^{jam} - \rho_{i,j+1}(k))L_i), \; if \, \rho_{i,j}(k) > \alpha_{j,j+1}\rho_{i,j+1}(k) \\ \qquad\qquad 0, \; otherwise \end{cases} \quad (3\text{-}8)$$

Where,

$N_{i,j,j+1}(k)$ is the number of lane change vehicles from lane groups j to $j+1$ in segment i at time k; and

$\alpha_{j,j+1}$ is the target density ratio between lane groups j and $j+1$.

Same as in Eq. (3-7), the term, $\lambda_{i,j}\lambda_{i,j+1}L_i\frac{\rho_{i,j}(k)-\alpha_{j,j+1}\rho_{i,j+1}(k)}{\lambda_{i,j}\alpha_{j,j+1}+\lambda_{i,j+1}}$, reflects the number of

vehicles that needs to change lanes from lane groups j to $j+1$ at time k in order to reach the target density ratio between lane groups j and $j+1$ when $\rho_{i,j}(k)$ is larger than the value of $\alpha_{j,j+1}\rho_{i,j+1}(k)$.

Module for updating flow rate and density

Using the flow conservation relation as in METANET, one can formulate the dynamics of density evolution for each lane group as follows:

$$
\rho_{i,j}(k+1) = \begin{cases} \rho_{i,j}^*(k) + \dfrac{T}{L_i\lambda_{i,j}}\left[\dfrac{\lambda_{i,j}}{\lambda_{i-1,j}}q_{i-1,j}(k) - q_{i,j}(k)\right], & \text{if } \lambda_{i,j} \leq \lambda_{i-1,j} \\[4mm] \rho_{i,j}^*(k) + \dfrac{T}{L_i\lambda_{i,j}}\left[\left[\displaystyle\sum_{m\in S_{i,j}} \lambda_{i-1,m}\, q_{i-1,m}(k)\right] - q_{i,j}(k)\right], & \text{if } \lambda_{i,j} > \lambda_{i-1,j} \end{cases}
\tag{3-9}
$$

$$
q_{i,j}(k) = \lambda_{i,j}\rho_{i,j}^*(k)v_{i,j}(k)
\tag{3-10}
$$

Where,

$\rho_{i,j}(k+1)$ is density of lane group j in segment i at time $k+1$ prior to accommodating the lane-changing vehicles;

$\rho_{i,j}^*(k)$ is density of lane group j of segment i at time k after receiving those lane-changing vehicles;

$\lambda_{i-1,m}$ is the number of lanes in lane group m of the adjacent upstream segment connected to lane group j of segment i; and

$S_{i,j}$ is the set of lane groups in the adjacent upstream segment, which are connected with lane group j of segment i.

Note that, the term, $\frac{\lambda_{i,j}}{\lambda_{i-1,j}}q_{i-1,j}(k)$, is to reflect the in-flow rate if the number of lanes for

each lane group differs between successive segments. Also note that $\rho_{i,j}^*(k)$ in Eq. (3-9) and Eq. (3-10) denotes the density after receiving the lane-changing vehicles, as shown in Eq. (3-11).

$$\rho_{i,j}^*(k) = \rho_{i,j}(k) + \frac{N_{i,j-1,j}(k) - N_{i,j,j+1}(k)}{L_i \lambda_{i,j}} \tag{3-11}$$

$N_{i,j-1,j}(k) - N_{i,j,j+1}(k)$ is the net number of lane changes from two neighboring lane groups in lane group j of segment i at time k. For the rightmost lane group, $N_{i,j-1,j}(k)$ equals 0. In addition, for the leftmost lane group, $N_{i,j,j+1}(k)$ is equal to 0.

Speed update module

Again, by replacing the segment-based notion in METANET with lane-group specific relations, one can formulate the speed dynamics for each lane group as follows:

$$v_{i,j}(k+1) = \min\{v^m, v_{i,j}(k) + \frac{T}{\tau}\left[V_i\left(\rho_{i,j}^*(k)\right) - v_{i,j}(k)\right] + \frac{T}{L_i} v_{i,j}(k)\left[\frac{\Sigma_{m \in S_{i,j}}\left(v_{i-1,m}(k)\right)}{|S_{i,j}|} - \right.$$

$$v_{i,j}(k)\right] - \frac{\upsilon T}{\tau L_i} \frac{\left[\frac{\Sigma_{w \in D_{i,j}}\left(\rho_{i+1,w}^*(k)\right)}{|D_{i,j}|} - \rho_{i,j}^*(k)\right]}{\rho_{i,j}^*(k)+\kappa} - \frac{\phi \max(v_{i,j}(k)-v_{i,j-1}(k),0)N_{i,j-1,j}(k)}{L_i \lambda_{i,j} \rho_i^C}\} \tag{3-12}$$

Where,

$v_{i,j}(k)$ is speed of lane group j in segment i at time k;

$D_{i,j}$ is the set of lane groups in the adjacent downstream segment, which are connected with lane group j of segment i ($|D_{i,j}|$ is the number of lane groups in $D_{i,j}$);

$N_{i,j-1,j}(k)$ is the number of lane change vehicles from lane groups j-1 to j in segment i at time k;

ρ_i^C is the critical density of segment i; and

$\tau, \upsilon, \kappa,$ and ϕ are parameters.

Note that the last term, $-\phi \max(v_{i,j}(k) - v_{i,j-1}(k), 0)N_{i,j-1,j}(k)/L_i \lambda_{i,j}\rho_i^C$, in Eq. (3-12) is proposed to reflect the impacts of lane changes in each lane group on its resulting speed that increases with the speed difference between lane groups and the frequency of such changes. The functional form of the speed-density relationship of segment i is the same as Eq. (3-3).

To reflect the on-ramp merging impacts on the directly connected lane group's speed, one can add an extra term, $-v_{i,1}(k)\frac{\delta Tr_i(k)}{L_i(\rho_{i,1}^*(k)+\kappa)}$, to Eq. (3-12), indicating that such impacts increase with the ratio between the number of on-ramp vehicles, $Tr_i(k)$, and the number of vehicles in the lane group, $L_i \rho_{i,1}^*(k)$.

Note that such impacts due to on-ramp merging under the METANET model are assumed to evenly distributed over all lanes in the segment. In contrast, the proposed model captures such impacts first with the directly connected lane group, and then propagate such impacts through the estimation of lane-group density before and after receiving the lane-changing vehicles between lane groups in the same segment and the downstream segments.

3.3 Model evaluation with field data

Figure 3-5 shows the geometric features and detector locations of a freeway on-ramp area from Taiwan Freeway No-1 for calibration and evaluation of the proposed lane-group-based traffic model. The entire area for field study has been divided into four segments, about 1,640 feet each in length, based on the ramp location and exhibited lane-changing activities. Those three travel lanes in each segment are further grouped into two or three lane groups, as shown in Figure 3-5, using the information of detected speed and flow rate distribution across all lanes.

Figure 3-6 illustrates the temporal distribution of ramp and mainline flow rates on a typical date, and Figure 3-7 highlights the significant speed reduction on segment 0 and segment 2 due to the on-ramp waving flows and vehicles performing discretionary lane changes.

Some key data associated with the target freeway segment for evaluation are summarized below:

- Date of data for calibration: 2-6 p.m. on March 17, 2019
- Date of data for evaluation: 2-6 p.m. on March 24, 2019
- Collected traffic flow data: speed (mph) and flow rate (vph) per lane per minute
  from detectors at 108.15 mile point (MP) and 107.51 MP
- Average freeway mainline flow rate: 3,400 - 4,200 vph for all lanes
- Average ramp flow rate: 1,400 - 1,800 vph (see Figure 3-6)
- Speed limit: 65 mph
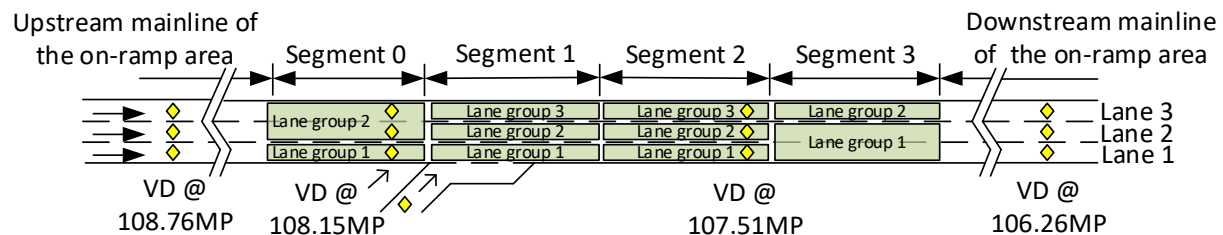
Figure 3-5: Locations of the detectors and segmentation
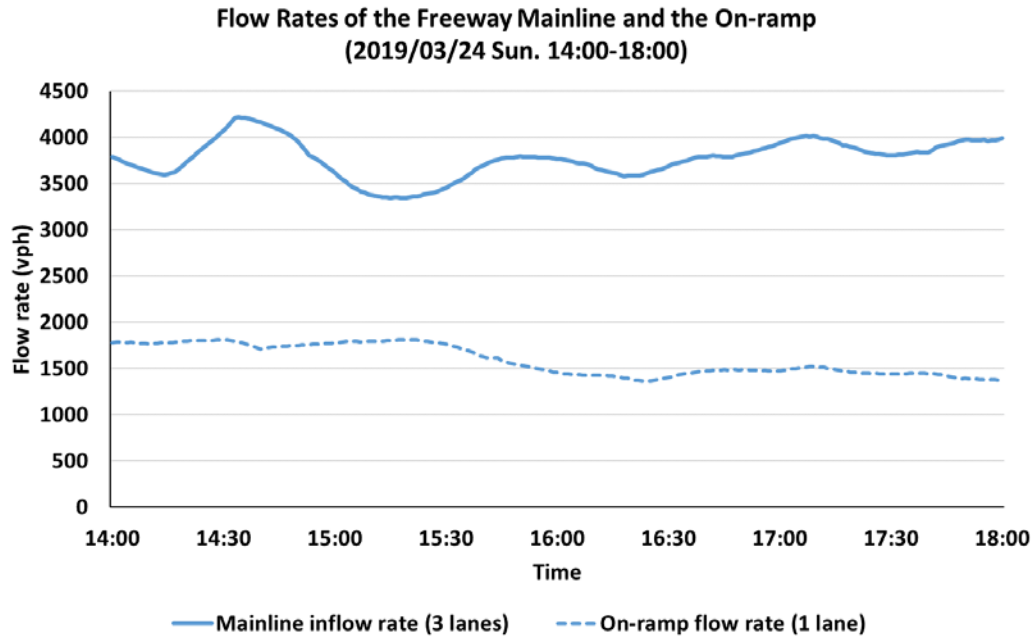
Figure 3-6: Flow rates of the freeway mainline and the on-ramp
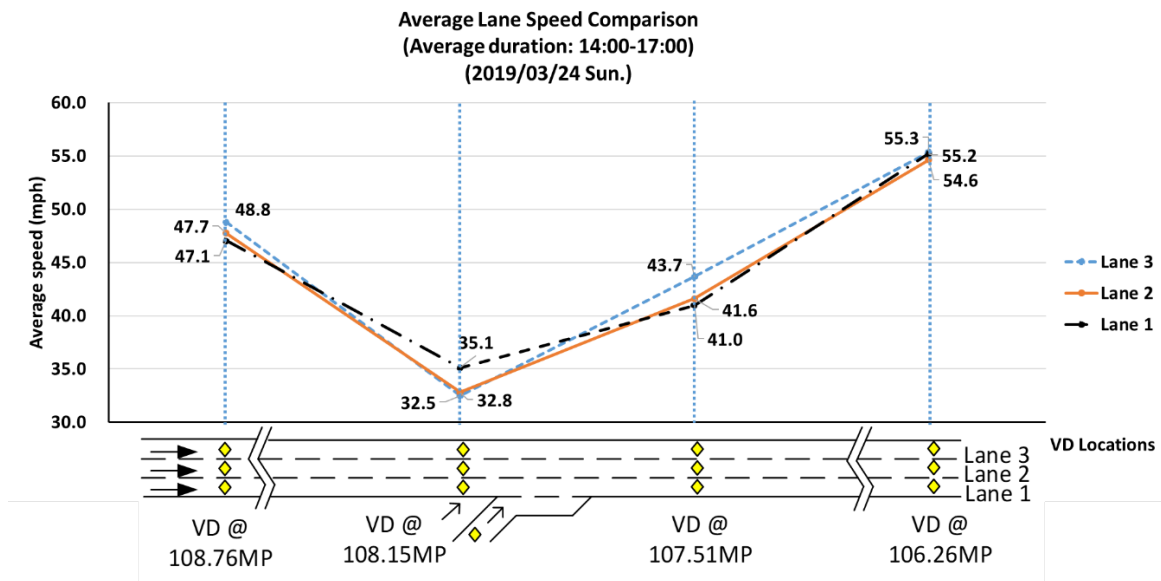
Figure 3-7: Average lane speed comparison

Evaluation results at the lane-group level

To evaluate the proposed model's unique feature, the performance evaluation first compares the predicted traffic conditions by lane group with those measured by the two sets of detectors, based on the following three statistics: mean absolute errors (MAE), mean absolute percentage error (MAPE), and Theil's inequality coefficient (Koutsoyiannis, 1973), as shown in Eq. (3-13) The benefits of deriving the segment-based average traffic conditions from the lane-group-based

results will also be demonstrated by the performance comparisons between the proposed model and METANET.

$$Theil's\ Inequality\ Coefficient: U = \sqrt{\frac{\sum(P_i - A_i)^2/n}{\sum A_i^2/n}} \quad 0 \le U \le \infty \qquad (3\text{-}13)$$

Where, P_i are predicted values; A_i are actual values; n is the number of data points; and the model is viewed to attain perfect forecasts if $U = 0$ (i.e., $P_i = A_i$).

As shown in Table 3-2, the comparison results with respect to speeds and flow rates at both detector locations over all lane-groups are all far less than 1 when evaluated with Theil's inequality coefficients, reflecting that the predicted traffic states, before and after impact by the on-ramp flows, are sufficiently closed to detected filed data. Such desirable properties for traffic state prediction can also be seen from the resulting MAEs which are less than 3 mph for the speeds and below 3 vehicles per minute for the predicted flow rates on all lane groups at the location of 108.15 MP and 107.51 MP. Most of such predicted deviations across all lane groups at both detector locations are less than 5 mph for the predicted speed deviation (see Figure 3-8), and 94% within the range of 4 vehicles per minute regarding the difference with the detected flow rate (see Figure 3-9).

Note that the approximate same level of very low MAEs for the freeway's traffic states, before and after the impacts of ramp flows, seems to confirm the proposed model's effectiveness in capturing the impacts of mainline vehicles' lane-changing maneuvers and ramp flows' merging frequency on the resulting speed and flow rate at the lane-group level.

As for the model performance with MAPE, the predicted errors for lane-group speed with the proposed model range from the lowest of 4.6 % for lane group 2 at the location of 107.51 MP to the highest of 6.7% for lane group 2 at the location of 108.15 MP. The MAPEs for flow rate prediction for all lane groups at both locations are all within the range of 5%, except for the 7.2% for lane group 1 at 108.15 MP where there are heavy discretionary lane-changing activities.

In brief, considering the data accuracy from most existing traffic detectors, one can expect that the model offers sufficient accuracy for traffic engineers to take full advantage of available sensor information and to best design the freeway control strategies at the lane-group level.

Table 3-2: Comparison results with respect to lane-group-based speeds and flow rates

Indicator	@108.15 MP		@107.51 MP		
	Lane group 1	Lane group 2	Lane group 1	Lane group 2	Lane group 3
Theil's Inequality Coefficient					
Speed	0.0721	0.0835	0.0569	0.0555	0.0600
Flow rate	0.1014	0.0620	0.0469	0.0531	0.0605
Mean Absolute Error (MAE)					
Speed (mph)	2.40	2.41	2.13	2.04	2.37
Flow rate (veh/min)	1.27	2.20	0.93	1.32	1.55
Mean Absolute Percentage Error (MAPE)					
Speed	6.3%	6.7%	4.8%	4.6%	5.1%
Flow rate	7.2%	4.8%	3.6%	4.1%	5.0%
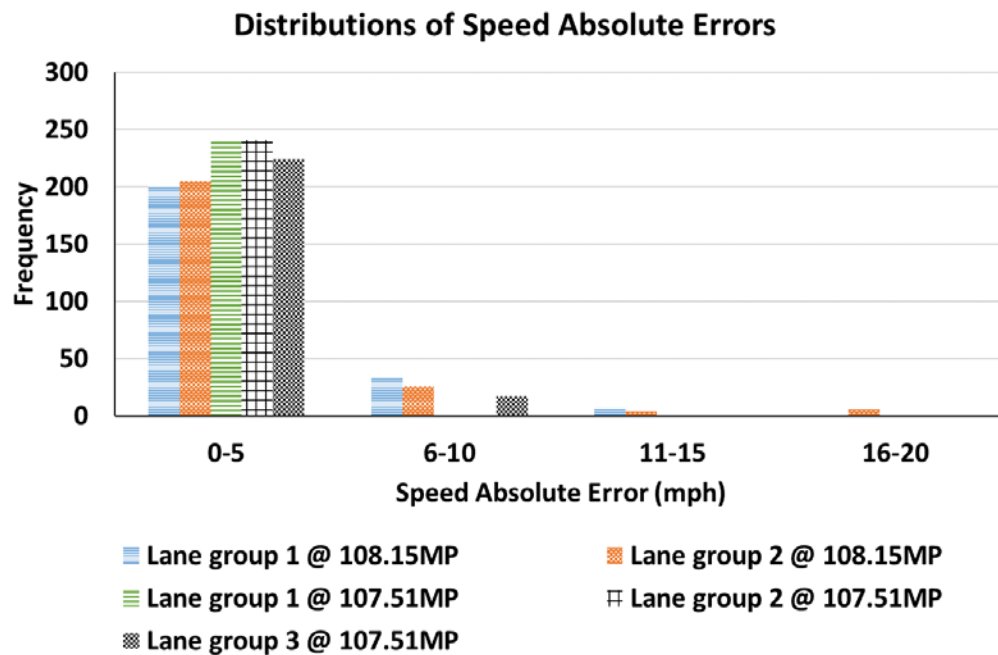
Figure 3-8: Distributions of the estimated absolute errors for speed by lane group
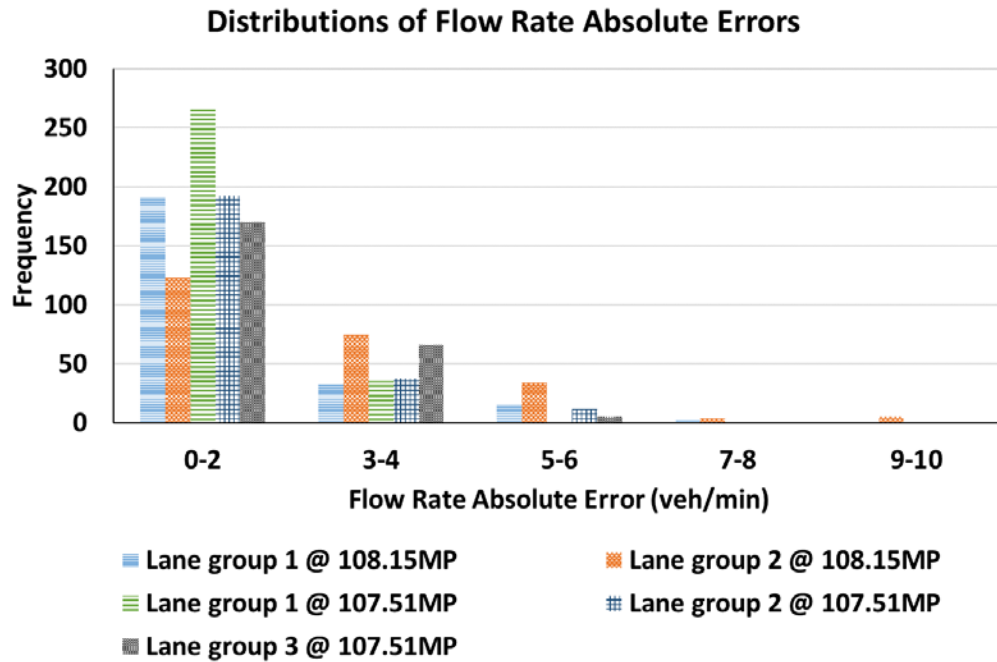
Figure 3-9: Distributions of estimated absolute errors for flow rate by lane group

Evaluation results at the segment level

To assess the benefits of applying the proposed lane-group-based model for predicting the average flow rate and speed across all lanes as in most existing models, the study has further compared its performance at the segment level with respect to speed and flow rates using the field data averaged from all lane detectors. The results from the well-established METANET model have also been computed to serve as the baseline for assessing the proposed model's performance improvement.

As shown in Table 3-3, the predicted average flow rates over all lanes by both the proposed model and MENTANT at two detector stations are at the same high level of accuracy, based on the statistics of Theil's inequality coefficient (i.e., less than 0.1). However, the prediction power of the proposed lane-group-based model with respect to the average speeds at the segment level clearly outperform MENTANT, and is comparable to its prediction accuracy for the average flow rate (also less than 0.1). Such interesting findings seem to confirm the observations that the lane-changing maneuvers in a freeway's interchange area due to the on-ramp merging flows indeed often incur substantial speed variance between travel lanes, thus justifying the need to employ the lane-group-based model for estimating the projected speeds for either individual lanes or across all lanes.

38

In contrast, as for use in projecting the average flow rate over all lanes, the segment-based model, such as MENTANT, appears to achieve the same quality of prediction as with the proposed lane-group-based model that produces the average from all individual lanes. Note that the performance discrepancy between these two models with respect to the speed and flow rate is consistent with the field observation that the impedance-created lane-changing vehicles will inevitably cause speed variation between travel lanes, and thus yield an average speed that may differ significantly from that with the segment-based method grounded on the uniformity assumption of traffic conditions across all lanes. However, since all such lane changes, triggered by on-ramp flows, occur mainly between lanes (less likely to subsequent segments), it is expected that the number of vehicles with the same freeway segment ought to remain at approximately the same level. Hence, the total flow rate for all lanes, insensitive to the lane-changing frequency within the same segment, can be predicted to the acceptable level of accuracy with either the segment-based model or the lane-group-based model.

Note that the above findings with respect to the performance of the proposed model and METANET are further supported by the evaluation results with MAE and MAPE as shown in Table 3-3. For instance, at the location of 108.15 MP, both models yield the same level of accuracy (i.e., about 2% in difference) for the flow rate prediction, but vary significantly in their forecasts of the average speed, i.e., MAE of 2.47 vs. 10.04 mph. The same conclusions can also be made from the comparison results with MAPE.

The performance discrepancy between these two models can be further verified with the detector data shown in Figure 3-10. Noticeably, the proposed model (but not the METANET model) can replicate the drop in average speed from 14:30 to 15:30 at the location of 108.15 MP, where many drivers may have exercised lane changes to avoid the speed impedance by on-ramp flows. Such a speed-drop pattern, triggered by lane-changing activities, often follows a slow recovery process, as shown in its temporal evolution during the time period between 15:30 to 17:30, likely due to propagation of the impacts by the on-ramp merging flows, measured at downstream location of 107.51 MP.

Figure 3-11 illustrates the temporal evolution patterns of the average flow speed at the freeway of 107.51 MP, produced from both models and the detectors, where most on-ramp flows may have merged onto the mainline segment. Again, it is evident that the proposed lane-group-based model can better capture the impacts incurred by the ramp flows and those mainline vehicles exercising discretionary lane changes, on both the freeway segment's average speed and the speed variance between lanes. Finally, it is worth noting that the overall traffic impacts by the on-ramp flows on the upstream segment (e.g., at 108.15 MP) seem more pronounced than on the

ramp's downstream segment (e.g., at 107.51 MP), reflecting the need to employ some information strategies to advise drivers to take early-lane changes so as to minimize the resulting impacts on the overall traffic conditions.

Table 3-3: Validation results of speed and flow rate between the proposed model and METANET

Indicator	The proposed model	The METANET model	Percentage Improvement
Theil's Inequality Coefficient			
Speed			
@108.15 MP	0.0946	0.3478	72.8%[1]
@107.51 MP	0.0484	0.1463	66.9%[1]
Flow rate			
@108.15 MP	0.0570	0.0572	0.3%[1]
@107.51 MP	0.0392	0.0452	13.3%[1]
Mean Absolute Error (MAE)			
Speed (mph)			
@108.15 MP	2.47	10.04	75.4%[1]
@107.51 MP	1.79	4.84	63.0%[1]
Flow rate (veh/min)			
@108.15 MP	3.10	3.04	-2.0%[1]
@107.51 MP	2.94	3.46	15.0%[1]
Mean Absolute Percentage Error (MAPE)			
Speed			
@108.15 MP	7.0%	33.9%	26.9%[2]
@107.51 MP	4.1%	11.5%	7.4%[2]
Flow rate			
@108.15 MP	4.9%	4.8%	-0.1%[2]
@107.51 MP	3.3%	3.9%	0.6%[2]

[1](the indicator value of METANET – the indicator value of the proposed model)/ (the indicator value of METANET)*100 (%)
[2](the MAPE of METANET – the MAPE of the proposed model)
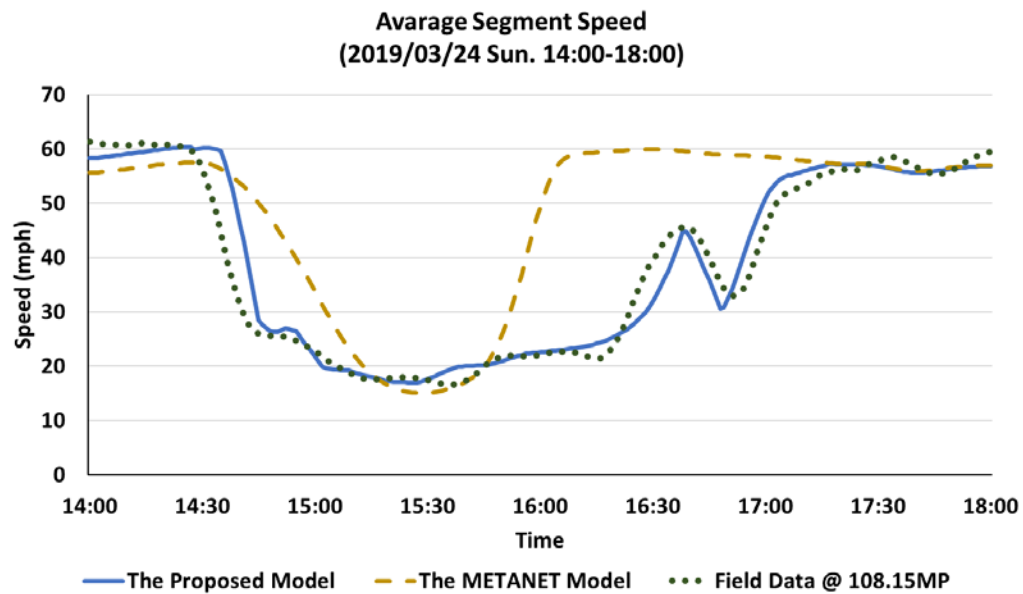
Figure 3-10: Speed comparison among the proposed model, the METANET model, and field data (@ 108.15 MP)
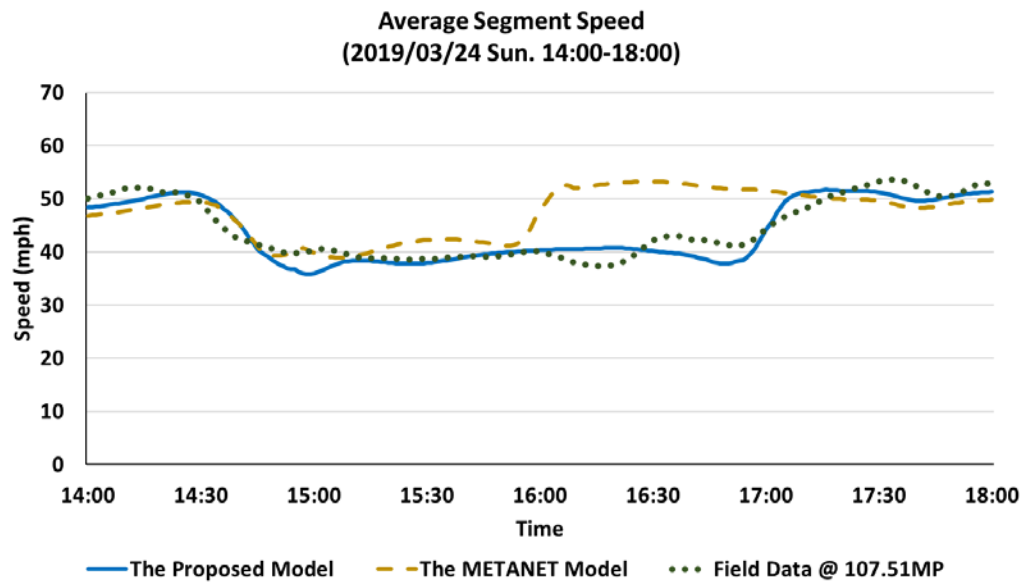

Figure 3-11: Speed comparison among the proposed model, the METANET model, and field data (@ 107.51 MP)

41

Chapter 4
Optimizing the Off-Ramp Signal Control to Prevent Queue Spillback to the Freeway Mainline

4.1 Research background

As is well recognized by the traffic community, weaving maneuvers by on-ramp vehicles and existing off-ramp flows are two primary contributors to the formation of local freeway bottlenecks, as both may result in substantial speed reduction and congestion increase in the vicinity of an interchange due to either mandatory or discretionary lane-changing activities. Over the past several decades, a large body of ramp metering studies, ranging from pre-timed to real-time adaptive controls, has been proposed in the freeway control literature to address the impacts of high on-ramp flows and the resulting merges on the target freeway segments' traffic conditions.

In contrast, the equally critical off-ramp control issue has not received the same level of attention by the traffic community, likely because off-ramp signals in most states are mostly operated by local traffic agencies rather than by their highway departments. As such, an off-ramp signal's vital role in balancing the congestion level between the freeway and arterials in the vicinity of an interchange has mostly been neglected, and its signal settings are based typically on the volume distributions over all intersection approaches, supplemented with the progression offsets to facilitate the arterial through-traffic flows.

Note that failing to account for the impacts of off-ramp queue spillback for an intersection receiving heavy off-ramp volume may yield the green duration insufficient to discharge the rapidly increasing queues from the off-ramp flows, and even spill such queues back to the freeway's rightmost lane during the peak hours. The mandatory lane-changing maneuvers by the exiting-to-off-ramp vehicles on a congested freeway segment will inevitably cause uneven speed reduction across all travel lanes, and consequently trigger extensive discretionary lane change. As such, a freeway segment's traffic condition is likely to evolve to a near chaotic state and propagate the congestion to its upstream segments, if concurrently plagued by both types of extensive lane-changing maneuvers and capacity reduction due to partial lane blockage by the off-ramp queue spillback. Hence, it is imperative that an off-ramp signal be designed with the control objective to benefit both the intersection and freeway segment within the impact range of off-ramp queues.

This chapter presents an off-ramp signal control model developed in response to such concerns, including the formulation of mandatory and discretionary lane-changing maneuvers

from the macroscopic perspective, and their collective impacts on the freeway segment's speed and concentration. An off-ramp signal model specially designed to incorporate the off-ramp queue impacts on the freeway will also be detailed in this chapter along with extensive experimental results to demonstrate its effectiveness with different measures of effectiveness (MOEs).

4.2 Modeling the impacts of ramp queue spillback on mainline traffic flows

Traffic flows on a freeway segment that are impeded by off-ramp queues generally exhibit a high frequency of lane-changing activities across all travel lanes, where the rightmost and its neighboring lanes often need to accommodate more lane changes and consequently experience more speed reduction. Such lane-changing activities, typically classified as either mandatory or discretionary in nature, are exercised by drivers intending to exit the freeway or those avoiding the perceived speed reduction due to the spillback of off-ramp queues. Conceivably, the frequency and the distribution of these two types of lane-changing activities, varying with the freeway and off-ramp volumes, will characterize the nature and determine the degree of off-ramp queue impacts on the mainline segment.

To model the impacts of such lane-changing activities, it is essential to address the following three critical issues under the available traffic information: (1) the number of vehicles performing either type of lane-changing maneuvers in each travel lane; (2) the available space in each lane for such vehicles to complete their intended lane changes during each time interval; and (3) the resulting impacts on the freeway's traffic conditions.

Figure 4-1 illustrates all key steps in constructing the proposed macroscopic model for estimating ramp queue impacts; Table 4-1 summarizes variable notations used hereafter in key formulations. Note that the control area on a freeway for studying the impacts of off-ramp queues typically ranges from the traffic sign that displays the off-ramp exit, to the off-ramp gore or the end of the spillback queues.

As seen in Figure 4-1, the Off-ramp Queue Impact (OQI) model based on the macroscopic traffic simulation notion, can approximate the freeway's traffic conditions in the presence of ramp queues during each time step via the following sequential stages of computation and estimation:

Stage-1: estimating the number of intended lane-changing vehicles in each lane
Stage-2: computing the available roadway space for successful lane changes
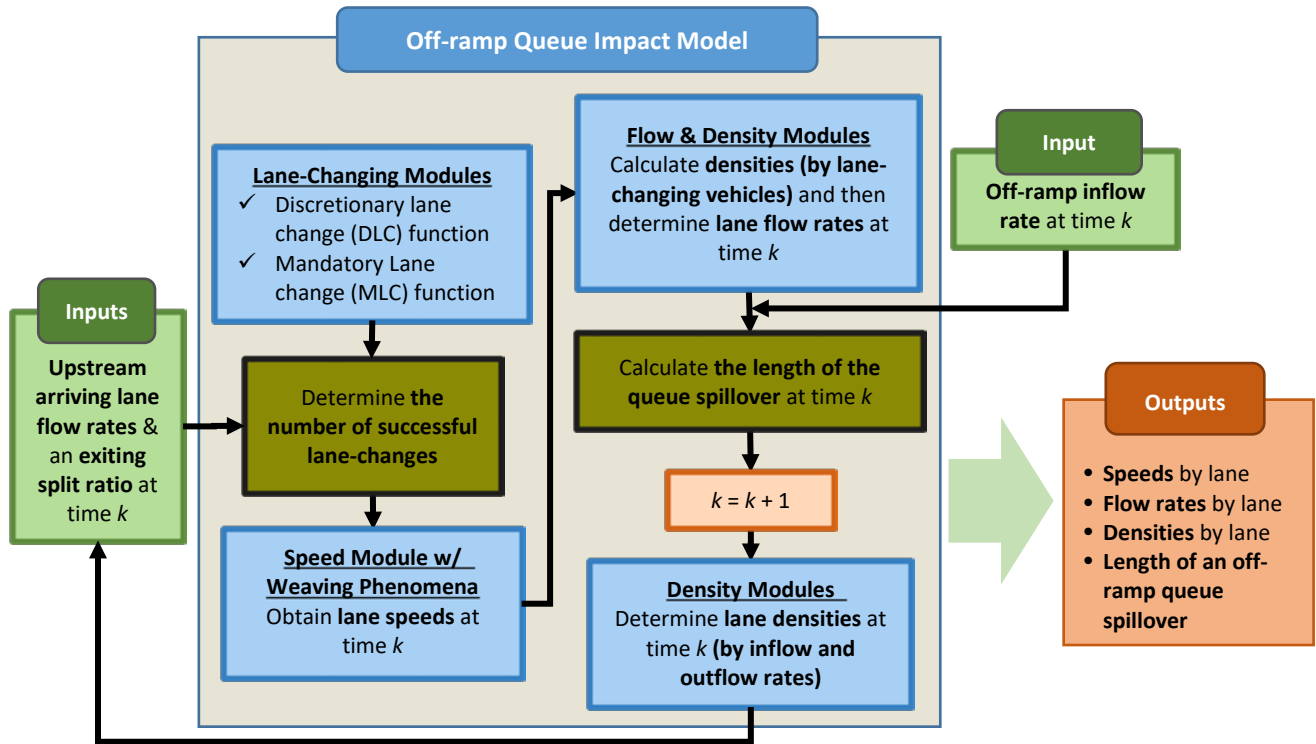*Stage-3: computing the impacts of the lane changes on the mainline' traffic speed*

Figure 4-1: The Off-ramp Queue Impact (OQI) model and its key components

Table 4-1: List of key variables used in the off-ramp queue impact model

$N_j(k)$	Number of moving vehicles in lane j at time k
$N_j^T(k)$	Number of **through** vehicles in lane j at time k
$N_j^E(k)$	Number of **exiting** vehicles in lane j at time k
$C_{j,l}^D(k)$	Number of vehicles **intending** to make **DLC** from lanes j to l at time k
$C_{j,l}^M(k)$	Number of vehicles **intending** to make **MLC** from lanes j to l at time k
$n_{j,l}(k)$	Number of lane-changing vehicles from lanes j to l at time k
$n_{j,l}^D(k)$	Number of **DLC** vehicles from lanes j to l at time k
$n_{j,l}^M(k)$	Number of **MLC** vehicles from lanes j to l at time k
$y_{j,l}(k)$	Percentage of vehicles intending to make a **DLC** from lanes j to l at time k
$p_{j,i}(k)$	**MLC** probability of vehicle i on lane j at time k
$S_l(k)$	Remaining space of lane l for lane-changing vehicles at time k (vehicles)
$\rho_j(k)$	The density of lane j at time k (prior to experience the lane changes by vehicles) (veh/mile)
$\rho_j^*(k)$	The density of lane j at time k (after accommodating lane-changing vehicles) (veh/mile)
$v_j(k)$	Speed on lane j at time k (ft/s)
$\hat{q}^\epsilon(k)$	Flow rate **joining** to a tail of **a queue spillover** at time k (vph)
$\hat{q}^o(k)$	Inflow rate of the off-ramp at time k (vph)
$q_j^\epsilon(k)$	Inflow rate of lane j at time k (vph)
$q_j(k)$	Flow rate of lane j at time k (vph)
L	Length of an off-ramp segment (ft)
$L^H(k)$	The horizontal queue spillover length on mainline at time k (ft)
λ	Longitudinal travel distance while making one lane change (ft)
g^m	A minimal acceptable gap for lane changes (ft)
v^b	Backward shockwave speed (ft/s)
h^m	Minimum space headway (ft)
$v_j^1(k)$	Speed of lane j at time k under **type-1** impact (ft/s)
$n_j^1(k)$	Number of vehicles impacted by **one** moving-out vehicle **to** a slower-speed lane
$v_j^2(k)$	Speed of lane j at time k under **type-2** impact (ft/s)
$n_j^2(k)$	Number of vehicles impacted by **one** moving-in vehicle **from** a slower-speed lane
$\bar{v}_j^*(k)$	Average speed of impacted vehicles in lane j during time k (ft/s)
$\bar{v}(k)$	Average speed across all freeway's travel lanes at time k (ft/s)
$t_j^f(k)$	The time duration that speeds of following vehicles of lane-changing vehicles are influenced (sec)
$g_j^s(k)$	Minimal safety gap between vehicles in lane j at time k (ft)
L^v	Average vehicle length (ft)
t	Time interval duration (sec)
$x_{j,i}(k)$	Distance of vehicle i on lane j at time k from an off-ramp gore if no queue spillover exists and from a tail of a queue spillover, otherwise (ft)
ρ^{jam}	Jam density (veh/mile)

A detailed description of mathematical formulations used in each stage is presented in sequence below:

Stage-1: estimating the number of intended lane-changing vehicles in each lane

Compute the number of discretionary lane changes

Except for designated exit-only lanes, one can approximate the number of vehicles, $C_{j,l}^D(k)$, likely to perform DLC in each lane at interval k as follows:

$$C_{j,l}^D(k) = N_j^T(k) * y_{j,l}(k) \tag{4-1}$$

Where, $N_j^T(k)$ is the total number of through vehicles within the subject lane segment at interval k, and $y_{j,l}(k)$ denotes the percentage of through vehicles intending to make DLC from lanes j to l at time k.

Note that the number of vehicles that may have the desire to increase their speeds by changing to a fast-moving lane in the presence of off-ramp queues often varies with the following factors:

- speed difference between the subject and the target lanes;
- perceived difference in concentration between the subject and the target lanes;
- the average speed across all freeway's travel lanes;
- the perceived speeds and concentrations across all lanes beyond the interchange off-ramps; and
- the posted speed limit.

Hence, one shall calibrate a location-specific function with all the above factors for field implementation. The following function, calibrated with the popular NGSIM dataset (FHWA, https://ops.fhwa.dot.gov/trafficanalysistools/ngsim.htm) from this study, can serve as an alternative if field data for model development and application are not available.

$$y_{j,l}(k) = \left(\frac{\exp(\bar{v}(k)-v_j(k)-\mu)}{1+\exp(\bar{v}(k)-v_j(k)-\mu)} \right)^{\varpi_1} \left(\frac{\exp(v_l(k)-v_j(k)-\hat{\mu})}{1+\exp(v_l(k)-v_j(k)-\hat{\mu})} \right)^{\varpi_2} \left(\frac{\left(\rho^{jam}-\rho_l(k)\right)}{|v_l(k)-v_j(k)|+\xi} \right)^{\varpi_3} e^{(1-\delta)\varpi_4} \tag{4-2}$$

$$\ln(y_{j,l}(k)) = \beta_1 X_1 + \beta_2 X_2 + \beta_3 X_3 + \beta_4 X_4 + \beta_5 X_5 + \beta_6(1-\delta) \tag{4-3}$$

Where,

$X_1 = \bar{v}(k) - v_j(\mathrm{k}) - \mu;\ \beta_1 = 0.040\ (t\text{-}value = 3.0);$

$X_2 = v_l(\mathrm{k}) - v_j(\mathrm{k}) - \hat{\mu};\ \beta_2 = 0.596\ (t\text{-}value = 11.4);$

$X_3 = \ln(\frac{\left(\rho^{jam}-\rho_l(k)\right)}{|v_l(k)-v_j(k)|+\xi});\ \beta_3 = 0.491\ (t\text{-}value = 14.9);$

$X_4 = \ln(1 + e^{\bar{v}(k)-v_j(\mathrm{k})-\mu});\ \beta_4 = -0.037\ (t\text{-}value = -2.1);$

$X_5 = \ln(1 + e^{v_l(\mathrm{k})-v_j(\mathrm{k})-\hat{\mu}});\ \beta_5 = -0.845\ (t\text{-}value = -15.6);$

$\beta_6 = -4.380\ (t\text{-}value = -77.3);$

$\delta = 1$, if changing to the left; $\delta = 0$, otherwise; and

ξ is a very small value to prevent the denominator of the term, $\frac{\left(\rho^{jam}-\rho_l(k)\right)}{|v_l(k)-v_j(k)|+\xi}$, from equaling 0.

Note that those three terms in Eq. (4-2) are specified to reflect the following three consecutive conditions that will collectively work to motivate a driver to change lanes until actual completion of such a maneuver:

Condition-1: the current lane's speed less than the average speed of all travel lanes, and the difference exceeds a threshold;

Condition 2: the target lane's speed is higher than the speed of the current lane, and the difference exceeds a threshold;

Condition 3: the feasibility to complete a safe lane change that depends on the differences in both the speed and density between the subject and the target lanes.

Conceivably, the joint probability from those three conditions shall be the probability for a vehicle to successfully complete a discretionary lane change. All model parameters shall be calibrated from the field data to reflect the location-specific driving behaviors.

Compute the number of mandatory lane changes

With respect to the number of vehicles in each lane at time interval k intending to perform MLC, $(C_{j,l}^M(k))$, it is expected to be a function of the following factors:

- the distribution of off-ramp vehicles on the target highway segment, but not in the rightmost lane; and
- the distance to the off-ramp gore or the end of the spillback queue.

A mathematic expression for such vehicles over all travel lanes within the target area is shown below:

$$C_{j,l}^M(k) = \sum_{i=1}^{N_j^E(k)} p_{j,i}(k) \tag{4-4}$$

Where, $p_{j,i}(k)$ denotes each vehicle's probability of exercising MLC.

With the assumption that all vehicles intending to exit the ramp before perceiving the target exit sign are distributed randomly between lanes and within each lane segment, one can approximate each vehicle's probability, $p_{j,i}(k)$, of exercising MLC with the following procedures derived from the field data and results by Pahl (1972).

47

Step-1: estimating the frequency of MLC between neighboring lanes from the following empirical function, calibrated by Pahl (1972):

$$F_{r,j,l} = w_{r,j,l}/[\widehat{N}_r * 0.1135 \ mile]$$

Where,

$F_{r,j,l}$ is the frequency per mile of exiting-vehicles changing from lane j to lane l in zone r;

$w_{r,j,l}$ is the number of exiting-vehicle changes from lane j to lane l in zone r; and

$\widehat{N}_r$ is the total number of exiting vehicles in zone r.

Step-2: converting the estimated lane-changing frequency between neighboring lanes to the following three figures showing the probability of changing lanes at different distances from the off-ramp gore.
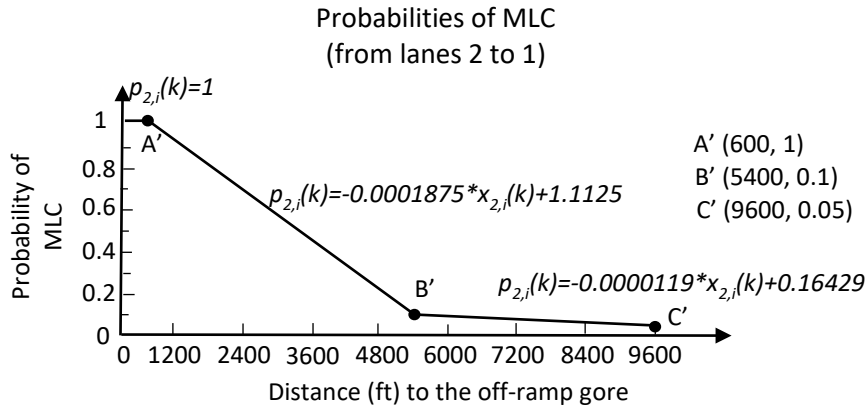
(a)   Probability functions for MLC from lanes 2 to 1

(b)   Probability functions for MLC from lanes 3 to 2

48
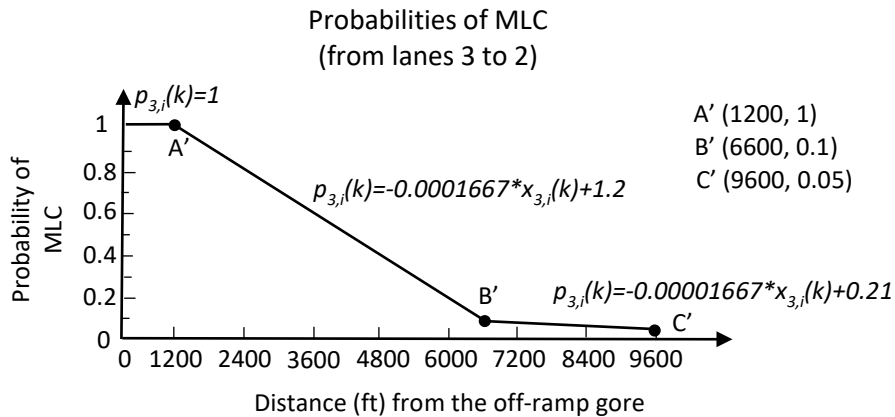
Probabilities of MLC
(from lanes 4 to 3)
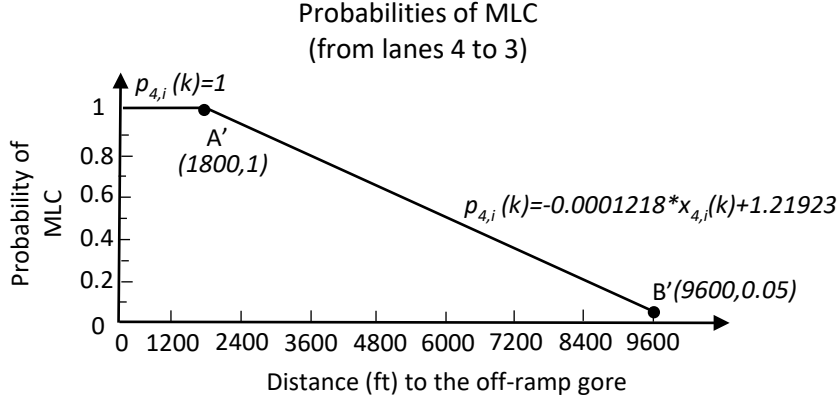
(c)   Probability functions of MLC from lanes 4 to 3

Figure 4-2: Probability functions for mandatory lane changes between neighboring lanes

Step-3: compute the MLC probability for vehicles at a given distance from the off-ramp gore at each interval k with the above figures or from their mathematical expressions shown below:

$$\begin{cases} p_{j,i}(k) = 1, & \text{if } 0 \leq x_{j,i}(k) < \dfrac{\alpha_j^2 - 1}{\alpha_j^1} \\[2mm] p_{j,i}(k) = -\alpha_j^1 * x_{j,i}(k) + \alpha_j^2, & \text{if } \dfrac{\alpha_j^2 - 1}{\alpha_j^1} \leq x_{j,i}(k) < \dfrac{\alpha_j^2 - \alpha_j^4}{\alpha_j^1 - \alpha_j^3} \\[2mm] p_{j,i}(k) = -\alpha_j^3 * x_{j,i}(k) + \alpha_j^4, & \text{if } \dfrac{\alpha_j^2 - \alpha_j^4}{\alpha_j^1 - \alpha_j^3} \leq x_{j,i}(k) \leq 9,600 \ (ft) \end{cases}$$

Where,

$p_{j,i}(k)$ is lane-changing probability of vehicle i on lane j at time k;

$x_{j,i}(k)$ is distance of vehicle i on lane j at time k from an off-ramp gore if no queue spillover
exists and from the tail of a queue spillover (ft), otherwise; and

$\alpha_j^1, \alpha_j^2, \alpha_j^3$, and α_j^4 are parameters for lane j.

Note that with the above procedures for MLC probability and the assumption that all such vehicles are distributed uniformly in each lane, one can approximate the total number of MLC vehicles in each lane over time from the macroscopic perspective.

Stage-2: computing the available roadway space for successful lane changes

Note that a driver's lane-changing exercise can be accomplished only if the target lane at time interval k has sufficient space for doing so. Hence, by assuming that the space headways on each lane follow a normal distribution, one can approximate the number of space headways, $S_l(k)$, sufficient for lane changes with the following expression:

49

$$S_l(k) = \begin{cases} N_l(k) * p(g \geq \dfrac{v_l(k)^2 - v_j(k)^2}{2a} + L^v\}), & if \ v_l(k) > v_j(k) \\ N_l(k) * p(g \geq g^m) & , otherwise \end{cases} \tag{4-5}$$

Where, $N_l(k)$ is the number of moving vehicles in the target lane l within the study area, which can be estimated with the lane density and its length not occupied by the spillback queues. The probability, $p(g \geq g^m)$, to reflect the available gaps that are longer than the minimum threshold, denoted as g^m, for vehicles to change from a higher-speed lane to a lower one. In contrast, only those gaps on the target lane, exceeding the safety distance, $(v_l(k)^2 - v_j(k)^2)/2a + L^v$, can be taken by vehicles to move from a slower lane to the faster-moving one.

Note that the time-varying length, $L^H(k)$, of spillover queues on the freeway mainline, used for estimating the available gaps for vehicles from its left lanes to conduct MLC, can be expressed as follows:

$$L^H(k) = L^H(k-1) + (\hat{q}^\epsilon(k-1) - \hat{q}^o(k - t^b - 1)) * \frac{t}{3600} * h^m \tag{4-6}$$

$$t^b = L^H(k-1)/v^b \tag{4-7}$$

Where, the second term in Eq. (4-6) shows the queue length variation based on the number of vehicles joining the queues and those flowing to the off-ramp. Note that Eq. (4-7) is for computing the time lag, t^b, for the off-ramp queue discharging shockwave at the speed of v^b to reach the end of the spillback queues.

Conceivably, the distributions of DLC and MLC from the microscopic perspective may vary across freeway lanes. However, for assessing their collective impacts of such lane changes on the freeway segment's overall traffic conditions, it is reasonable to assume that each of such changing vehicles has the same opportunity to do so under the given available space headways. Hence, one can approximate the number of vehicles completed MLC ($n_{j,l}^M(k)$) and DLC ($n_{j,l}^D(k)$) based on their ratios and with the following expressions:

$$n_{j,l}^M(k) = \min\{S_l(k) * \frac{C_{j,l}^M(k)}{\sum_{\hat{j} \in \Omega_l}\left(C_{j,l}^D(k) + C_{j,l}^M(k)\right)}, \ C_{j,l}^M(k)\} \tag{4-8}$$

50

$$n_{j,l}^D(k) = \min\left\{S_l(k) * \frac{C_{j,l}^D(k)}{\sum_{j\in\Omega_l}\left(C_{j,l}^D(k) + C_{j,l}^M(k)\right)}, C_{j,l}^D(k)\right\}$$ (4-9)

Where, Ω_l is the set of neighboring lanes of lane l.

Naturally, the total number of lane-changing vehicles, $n_{j,l}(k)$, can be shown with Eq. (4-10).

$$n_{j,l}(k) = n_{j,l}^M(k) + n_{j,l}^D(k)$$ (4-10)

Stage-3: computing the impacts of the lane changes on the mainline' traffic speed

For each lane segment near the off-ramp, its average speed is likely to be impacted by the following two types of lane-changing activities: moving into the slower-moving neighboring lane to get off the ramp (denoted as Type-1), and discretionary lane changes by vehicles from a neighboring lane to increase speed (named Type-2). In either case, vehicles in the subject lane will generally be forced to first decelerate to accommodate the speed of the lane-changing vehicle, and then accelerate to get back to their original speed.

For Type-1 impact, each vehicle, prior to changing to the slower-speed lane, is expected to decelerate to the same speed as the target lane (denoted as lane l). Hence, let $t_j^f(k)$ and $\Delta\eta_{j,l}(k)$ be defined as the required time duration and resulting travel distance for the subject lane vehicles to decelerate from its current speed, $v_j(k)$, to the target lane speed, $v_l(k)$, and then recover to the same speed after the lane-changing vehicle completed its maneuver. And $\Delta\theta_j(k)$ denotes the average space headway between vehicles on the subject lane at time interval k. Then, one can approximate the number of vehicles ($n_j^1(k)$) on the subject lane constrained to the impact of one such lane-changing vehicle as $\Delta\eta_{j,l}(k)/\Delta\theta_j(k)$, where,

$$\Delta\eta_{j,l}(k) = t_j^f(k) * \frac{v_j(k)-v_l(k)}{2}, \text{ for } v_j(k) > v_l(k);$$

$$\Delta\theta_j(k) = \frac{5280}{\rho_j(k)} - L^v - g_j^s(k);$$

$g_j^s(k)$ is the minimum safety gap between vehicles in lane j at time interval k (ft); L^v is the average vehicle length (ft); and $\rho_j(k)$ is the density of the subject lane (veh/mile).

As for the resulting impacts on the subject lane's average speed, it depends on both the total estimated lane changes ($n_{j,l}(k)$) for the subject lane during interval k, and the number of vehicles

impacted by each of such lane changes $(n_j^1(k))$. From the macroscopic perspective, one can naturally approximate the resulting average speed under such Type-1 lane-changing vehicles as follows:

$$v_j^1(k) = \begin{cases} \bar{v}_j^*(k) & \text{, if } n_{j,l}(k) * n_j^1(k) \geq N_j(k) \\ \frac{\bar{v}_j^*(k)*n_{j,l}(k)*n_j^1(k)+v_j(k)*(N_j(k)-n_{j,l}(k)*n_j^1(k))}{N_j(k)} & \text{, otherwise} \end{cases} \tag{4-11}$$

Where the condition, if $n_{j,l}(k) * n_j^1(k) \geq N_j(k)$, indicates that all subject lane vehicles, $(N_j(k))$, are subject to the speed impacts due to those Type-1 lane changes $(n_{j,l}(k) * n_j^1(k))$; and the resulting average lane speed, $v_j^1(k)$ shall equal $\bar{v}_j^*(k)$ shown in Eq. (4-12):

$$\bar{v}_j^*(k) = \frac{1}{t}\left\{t_j^f(k) * \frac{v_l(k)+v_j(k)}{2} + \left(t - t_j^f(k)\right) * v_j(k)\right\}, \ v_j(k) > v_l(k) \tag{4-12}$$

Otherwise, $v_j^1(k)$ can be approximated with the weighted speed average of both vehicles free from and subject to the Type-1 lane-changing vehicles.

Note that by following the same logic, one can also derive the average speed of lane j, subjected to the Type-2 impacts of moving-in vehicles from a slower-speed lane, as shown in Eq. (4-13):

$$v_j^2(k) = \begin{cases} \bar{v}_j^*(k) & \text{, if } n_{l,j}(k) * n_j^2(k) \geq N_j(k) \\ \frac{\bar{v}_j^*(k)*n_{l,j}(k)*n_j^2(k)+v_j(k)*(N_j(k)-n_{l,j}(k)*n_j^2(k))}{N_j(k)} & \text{, otherwise} \end{cases} \tag{4-13}$$

Where, $n_j^2(k)$ denotes the number of vehicles in lane j impacted by one moving-in vehicle from a slower-speed lane.

Flow and density modules

With the estimated number of lane-changing vehicles, one can update the resulting lane density and densities at the current time interval with the following expressions:

$$\rho_j^*(k) = \rho_j(k) + \frac{5280}{(L-L^H(k)-(j-1)*\lambda)}(n_{l,j}(k) - n_{j,l}(k)) \tag{4-14}$$

$$q_j(k) = \rho_j^*(k) * \min[v_j^1(k), v_j^2(k)] * 0.68 \qquad (4\text{-}15)$$

$$\rho_j(k+1) = \rho_j^*(k) + \frac{t}{0.68*(L-L^H(k)-(j-1)*\lambda)}(q_j^\epsilon(k) - q_j(k)) \qquad (4\text{-}16)$$

4.3 Model evaluation and application

This section presents the results of two numerical investigations: one for model validation with field data and the other for its application in design of an off-ramp signal. The necessity of accounting for the potential off-ramp queue spillback under different volume levels in analyzing interchange traffic conditions will also be discussed.

Experimental site for model evaluation

Figure 4-3 illustrates the freeway segment for model evaluation and the locations of its six vehicle detectors (VD), as well as one ETC (electric toll collection) sensor for data collection. Both the speeds and flow rates collected from 15:00 to 21:00 on March 7, 2019 are used as the dataset for model calibration. The same data set available on March 14, 2019 serves as the basis for evaluating the calibrated model's performance.
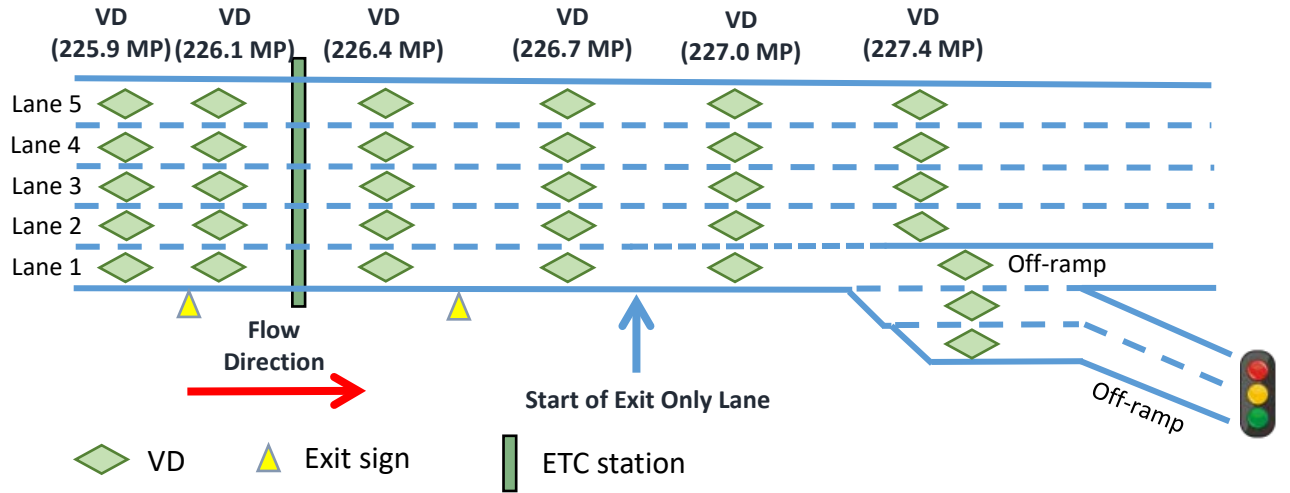
Figure 4-3: Locations of the detectors and the ETC station

Figure 4-4 shows the observed time-varying flow rates on the freeway segment and to the off-ramp in the dataset for model validation. Noticeably, the maximum freeway flow rate was up to 10,100 vph, and the inflow rates to the off-ramp varied between 1,350 vph to 2,400 vph during the same period.
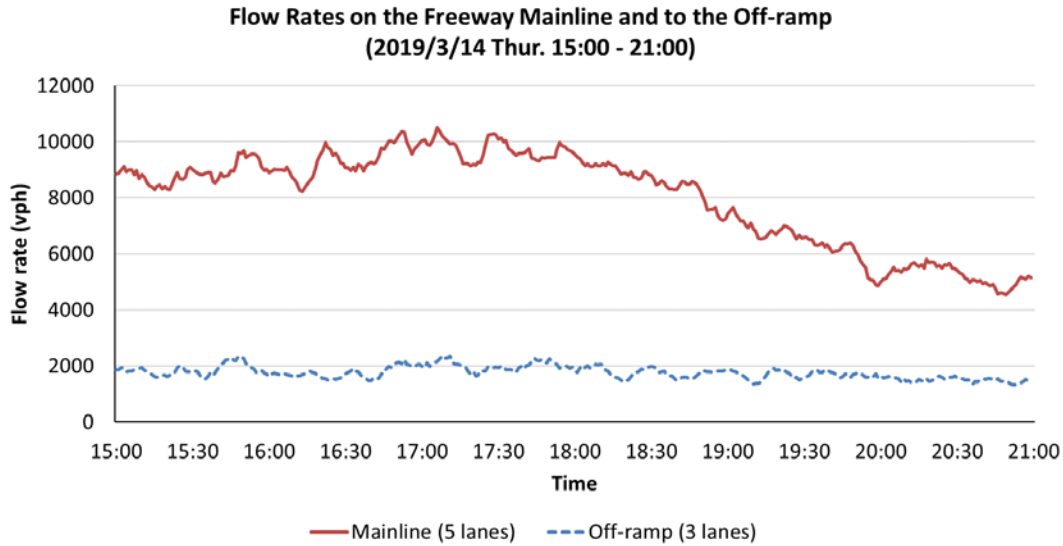
Figure 4-4: Time-varying flow rates on the freeway mainline and to the off-ramp

Model evaluation results

To assess the calibrated model's performance under different traffic conditions, Table 4-2 presents the statistical test results with respect to the predicted speeds for both the peak (16:30-19:30) and off-peak (15:00-16:30 & 19:30-21:00) hours, based on the Theil's Inequality Coefficient, a well-recognized test in econometrics to test a model's prediction power (Koutsoyiannis, 1973), MAE (*mean absolute error*), and MAPE (*mean absolute percentage error*). Noticeably, the model, after careful calibration, can reasonably capture the complex off-ramp queue impacts on the freeway's speed and flow rate as well as their distributions across lanes.

All MAPEs for all travel lanes' speeds during both peak and off-peak hours are less than 5%, except the 5.5% for lane-1 during the peak hours. This is further supported by the resulting MAEs, where the differences between the detected and predicted speeds across all five lanes during both peak and off-peak hours are less than 3 mph.

Figure 4-5 further illustrates the distributions of predicted errors with respect to the speed by the freeway travel lane during both peak (Figure 4-5(a)) and off-peak hours (Figure 4-5(b)), mostly less than 4 mph. The results with Theil's Inequality Coefficient also reveal that the model's prediction errors are mostly less than 0.05, as shown in Table 4-2.

Table 4-3 highlights the evaluation results with respect to the freeway mainline outflow rate under the same performance test statistics during the same peak and off-peak periods. Noticeably, the MAPEs for the flow rate on all travel lanes are less than 10%, varying between

the lowest of 4.9% on lane-5 in peak hours and the highest of 8.7% on lane-2 during the off-peak hours. In addition, the predicted discrepancies with respect to the flow rates (vehicles per minute on each lane) lie within the range of less than three vehicles per minute for all travel lanes during the entire period. The proposed model's potential for predicting the flow rate variation and evolution on the freeway segment due to off-ramp flows is also confirmed from the test results with the Theil's Inequality Coefficient, as mostly within the range of 0.1. This is consistent with the distribution of predicted discrepancies with respect to the freeway mainline outflow rate by lane shown in Figure 4-6 over both the peak and off-peak hours.

Table 4-2: Comparison between the detected and predicted freeway speeds

Test statistics	Lane No.				
	1	2	3	4	5
Theil's Inequality Coefficient					
Peak hours	0.062	0.033	0.036	0.038	0.044
Off-peak hours	0.028	0.028	0.032	0.023	0.024
Mean Absolute Error (MAE) (mph)					
Peak hours	2.08	1.27	1.30	1.55	1.80
Off-peak hours	1.19	1.25	1.38	1.09	1.28
Mean Absolute Percentage Error (MAPE)					
Peak hours	5.5%	2.9%	2.8%	3.2%	3.4%
Off-peak hours	2.4%	2.3%	2.8%	2.3%	2.0%

Table 4-3: Validation results of freeway mainline outflow rates

Test statistics	Lane No.				Cross Section[a]
	2	3	4	5	
Theil's Inequality Coefficient					
Peak hours	0.092	0.084	0.082	0.058	0.115
Off-peak hours	0.097	0.071	0.068	0.076	0.172
Mean Absolute Error (MAE) (veh/min)					
Peak hours	1.41	1.79	2.13	1.51	3.73
Off-peak hours	1.37	1.32	1.58	1.34	3.84
Mean Absolute Percentage Error (MAPE)					
Peak hours	7.5%	6.9%	6.5%	4.9%	3.0%
Off-peak hours	8.7%	5.7%	5.2%	6.4%	4.4%

[a]*Outflow rate for the entire freeway mainline segment.*
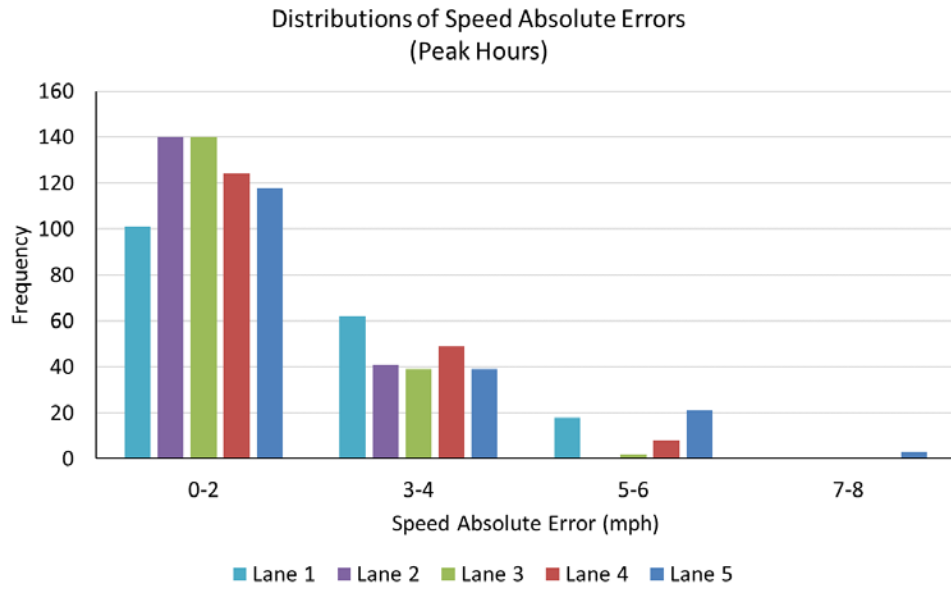
(a) Peak hours
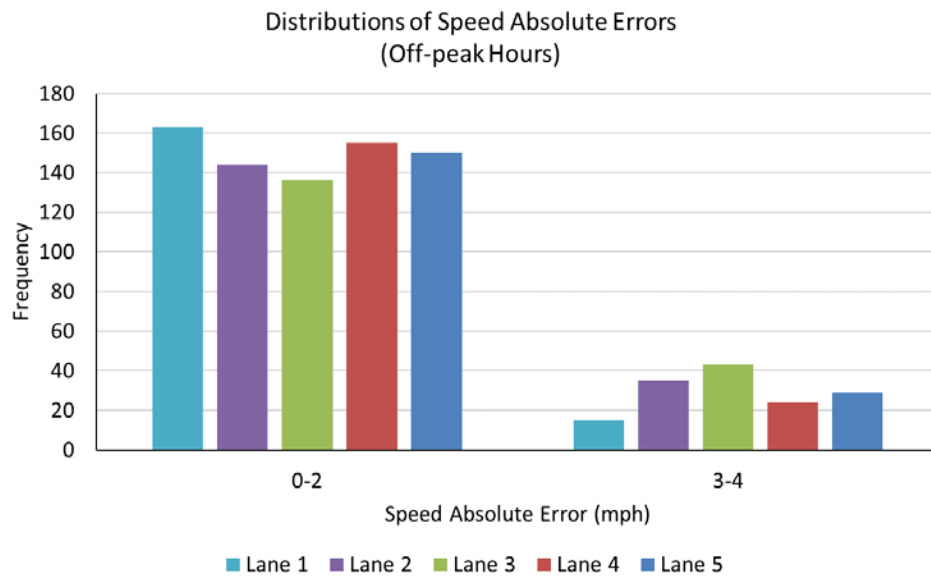
(b) Off-peak hours

Figure 4-5: Distributions of speed absolute errors

Distributions of Mainline Outflow Rate Absolute Errors (Peak Hours)

(a) Peak hours

Distributions of Mainline Outflow Rate Absolute Errors (Off-peak Hours)

(b) Off-peak hours
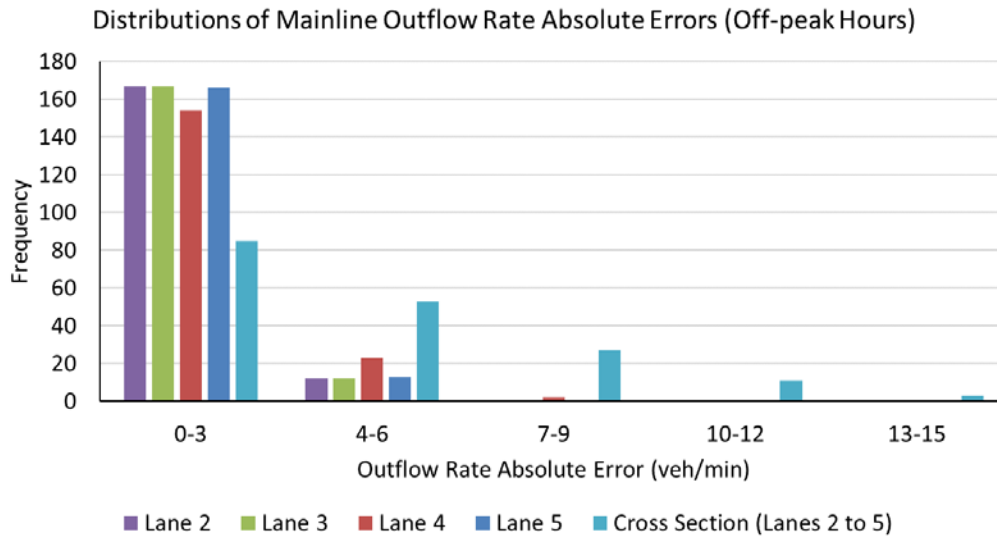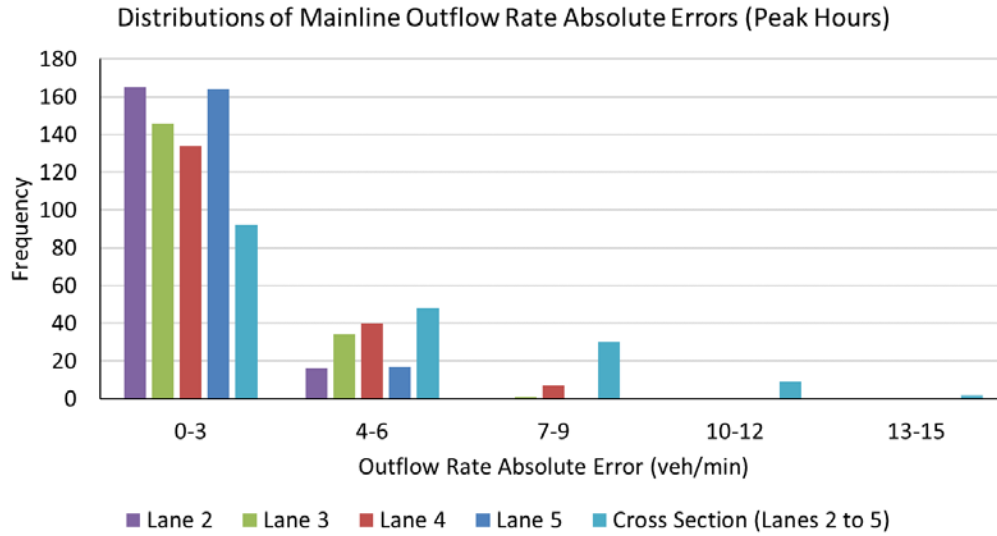
Figure 4-6: Distributions of mainline outflow rate absolute errors

Queue Length prediction

Since the core of this study is to reflect the impacts of off-ramp queues on the freeway's traffic condition, evaluating the predicted accuracy of the proposed model with respect to the time-varying queue length is an essential task. Figure 4-7 shows the time-varying off-ramp queues predicted by the model and the discrete queues observed from the field data. Note that the field-developed off-ramp queue length is observable only when it occupies or exceeds the deployed VD. As such, the evolution of the field-detected queue length can only be recorded with its times to reach the set of deployed queue detectors.

57

Due to the discrepancy in data nature between the field-observed and model-produced queues, this study has adopted two non-parameter tests, Mann-Whitney and Siegel-Tukey tests, to evaluate if the differences between these two sets of queues are statistically insignificant. The results from both tests indicate that these two graphical patterns shown in Figure 4-7 are statistically indifferent at the 5% significant level.
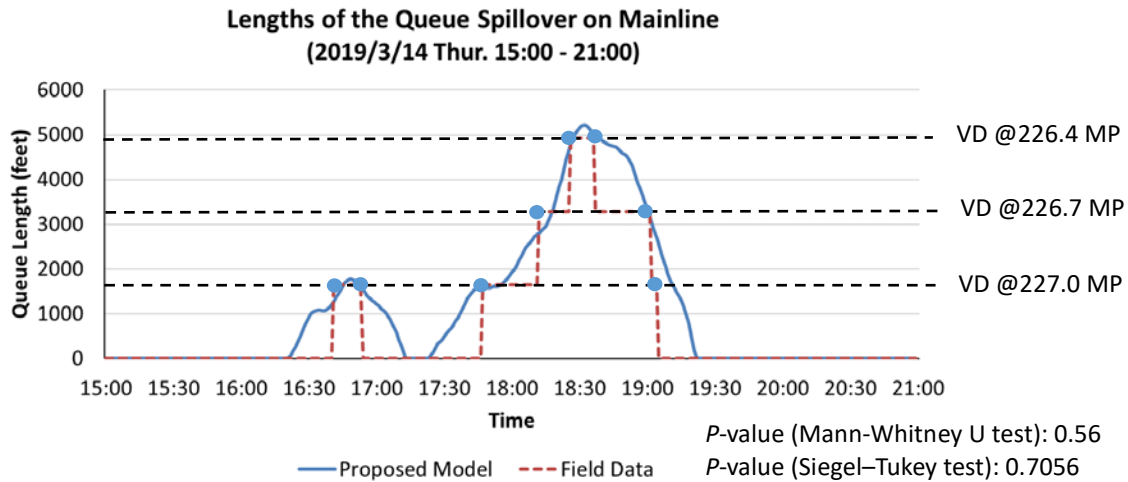
Figure 4-7: Comparison between the field-observed and model-produced time-varying queues

Application for design of off-ramp signal

Figure 4-8 shows the control area for the case study site, designed to demonstrate the necessity of accounting for the impacts of ramp queues on the freeway segment in design of the local off-ramp signal. Both the key geometric features and existing intersection turning ratios, along with phase sequence, are further illustrated in Figure 4-9. Different from the state of the practice, the target area for the off-ramp signal design comprises not only all intersection legs, but also the freeway segment likely affected by queue length developed on its off-ramp leg. Hence, the control objective for the signal is thus to minimize the total delay or to maximize throughput for the entire control area, including both the freeway and all intersection approaches, based on the off-ramp impact models developed in this study.
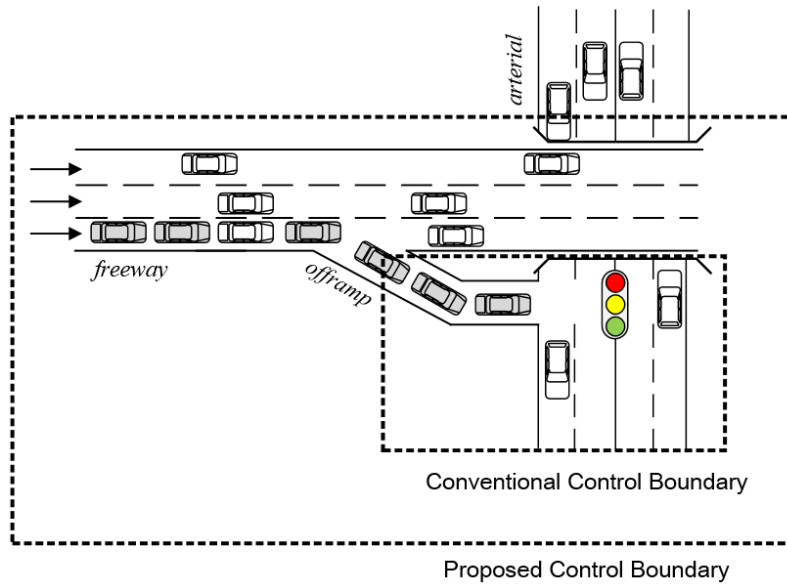
Figure 4-8: Conventional and proposed control boundaries
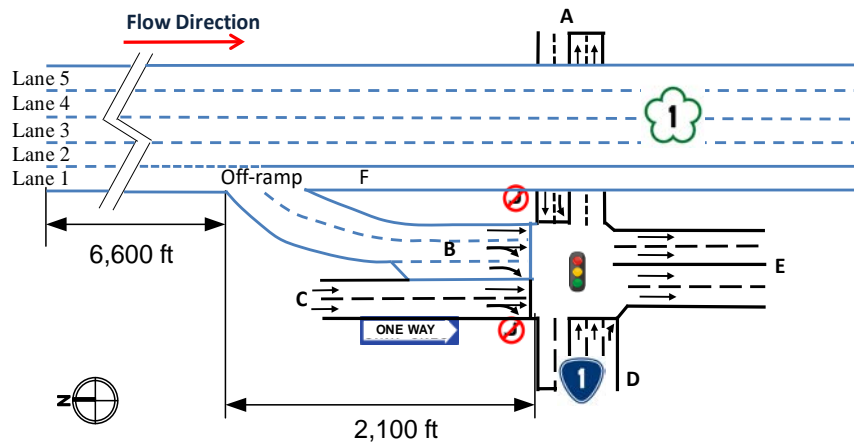
(a) Geometric features
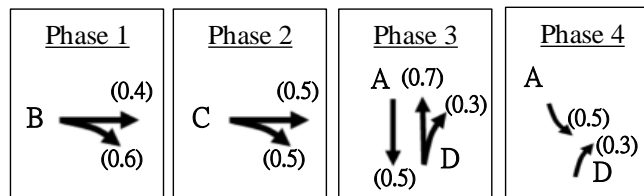
(b) Phase sequence and turning ratios

Figure 4-9: Key features of study site

Conceivably, the necessity of accounting for the off-ramp queue impacts in the signal design varies with not only the distribution of intersection volumes among all approaches, but also the flow rates on the off-ramp and the freeway mainline segment. Hence, the case study is

designed to show their interrelations with the following three scenarios summarized in Table 4-4:

- **Scenario 1**: high volumes on the freeway mainline, the off-ramp, and the local arterial traffic.
- **Scenario 2**: same freeway and the off-ramp volumes as in Scenario 1 but low flow rates for all other intersection approaches.
- **Scenario 3**: low freeway and the off-ramp volumes but the same high flow rates as in Scenario 1 at all other intersection approaches.

Table 4-4: Scenarios

Scenarios	Demand entries (in vph)				
	Freeway	A	B (off-ramp)	C	D
1	10,000	1,000	1,200	600	1,000
2	10,000	600	1,200	300	600
3	6,000	1,000	720	600	1,000

Comparison results with respect to the cycle length and green splits produced with the proposed model and the exiting practice using TRANSYT-7F (but with a queuing penalty added to its performance index for a fair comparison) are summarized in Table 4-5. Noticeably, under Scenario-1 of congested traffic conditions and high off-ramp volume, incorporating the queue spillback impacts in the design for the proposed model yields the cycle length of 115 seconds and the green split of 0.4 for the off-ramp approach, much higher than the split of 0.22 for the same intersection approach under the comparable cycle length of 120 seconds by TRANSYT-7F.

By reallocating a longer green duration to accommodate the high off-ramp volume, the signal plan with the proposed model can achieve about a 9% (see Table 4-6) increase in the total system throughput, mostly on the freeway segment (from 6,681 vph to 8,087 vph) due to the prevention of queue spillback from the off-ramp flows (see Figure 4-10(a)). The benefits of minimizing the off-ramp queue impacts are also reflected on the 56% reduction in the total system delay (see Table 4-6), attributing mainly to the decrease in total vehicle delay, from 15,160 to 720 vehicle-minutes (Figure 4-11(a)) on the freeway segment.

Note that such substantial improvements on the freeway in Scenario-1 are due to the allocation of a longer green time to the off-ramp flows, which will inevitably reduce the available green times for all other intersection approaches and thus increase their total delays. For instance, the conventional design practice with TRANSYT, neglecting the off-ramp queue impacts, tends to allocate more green times to phases 2 (0.21 vs. 0.13) and 3 (0.31 vs. 0.18) to discharge more non-off-ramp flows, and thus result in more throughput and less delays for those

intersection approaches (see Figure 4-10(a) and Figure 4-11(a)).

However, since the off-ramp queue spillback, if taking place, may cause an exponential delay increase and throughput reduction on the freeway segment due to the non-linear nature of traffic flow dynamics, such a trade-off, reflecting the minimal impacts on the surface traffic delays, certainly deserves the implementation by the traffic agency responsible for contending with corridor traffic congestion.

Scenario-2 highlights the traffic conditions where the intersection receiving the off-ramp flows must accommodate only relatively low surface traffic volumes from all other approaches. Hence, both the proposed model and the TRANSYT-7F are expected to be capable of allocating sufficient green duration to the off-ramp flows so that the traffic queues are less likely to spill back onto the freeway mainline. The results of green splits and MOEs shown in Table 4-5 and Table 4-6, respectively, clearly confirm such pre-assessment, where both models yield a quite similar set of green splits, and the shorter cycle length produced by the proposed model seems to contribute to the 16% delay reduction (see Table 4-6) for the entire control area. Further comparisons with respect to the delay by intersection approach are also evidence that off-ramp vehicles (Figure 4-11(b)) experience the most delay reduction under the proposed model's signal plan. Note that all intersection approaches and the freeway segment have nearly the same throughputs under both models, due mainly to the distribution of low arterial volumes that produce no-residual queues per cycle and no off-ramp queues during the control period.

Scenario-3 is designed to evaluate the proposed model's sensitivity, as it should view the off-ramp intersection as a typical local intersection if the freeway volume is relatively light and the off-ramp queue is of no concern to the traffic control operations. As such, both models are expected to yield approximately the same level of MOEs at either the entire system level or by intersection approach. The simulation results, shown in Table 4-6, Figure 4-10(c) and Figure 4-11(c), indeed are consistent with the expectation that both models perform indifferently under a standard statistical test in this traffic scenario, regardless of the selected MOE.

Note that genetic algorithm (GA) has been applied in the case study to generate the optimized cycle length and splits of the traffic signals with the control objective of maximizing the total system throughput (Chen and Chang, 2013). The resulting MOEs under the optimized signal plan for performance comparison are from the simulation output of TSIS 6.3, a stochastic microsimulation software by FHWA (https://ops.fhwa.dot.gov/trafficanalysistools/corsim. htm).

Table 4-5: Optimal signal plans

Scenario	Model	Cycle Length (sec)	Green split			
			Phase 1	Phase 2	Phase 3	Phase 4
1	The proposed model	115	0.40	0.13	0.18	0.18
	TRANSYT-7F	120	0.22	0.21	0.31	0.17
2	The proposed model	103	0.36	0.15	0.19	0.18
	TRANSYT-7F	126	0.34	0.14	0.22	0.20
3	The proposed model	95	0.16	0.20	0.32	0.20
	TRANSYT-7F	84	0.19	0.21	0.24	0.21

Table 4-6: MOEs

Scenario	Delay (veh-min)			Throughput (vph)		
	TRANSYT	Proposed	Percent Change[1]	TRANSYT	Proposed	Percent Change[1]
1	25,583	11,200	-56.2%	10,715	11,680	9.0%
2	2,823	2,369	-16.1%	10,809	10,755	-0.5%
3	5,575	5,530	-0.8%	8,153	8,325	2.1%

[1] Percent Change = $(MOE_{\text{proposed model}} - MOE_{\text{TRANSYT-7F}})/MOE_{\text{TRANSYT-7F}} *100\%$
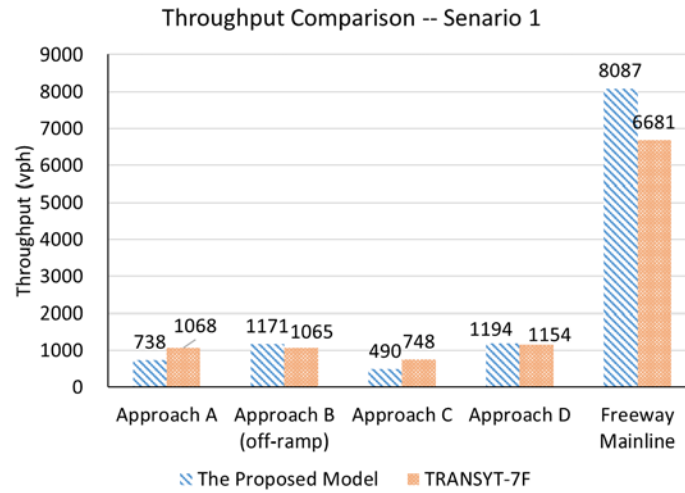
(a) Scenario 1
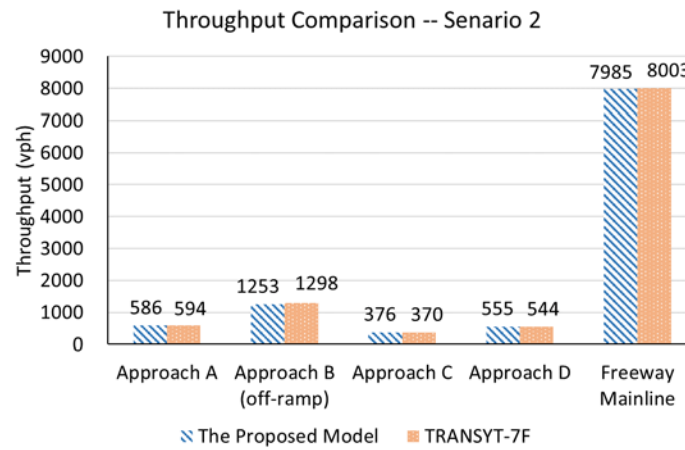
(b) Scenario 2
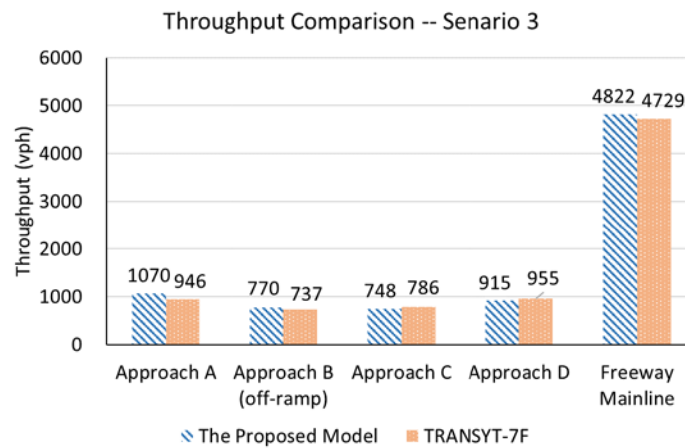
(c) Scenario 3

Figure 4-10: Throughputs of scenarios
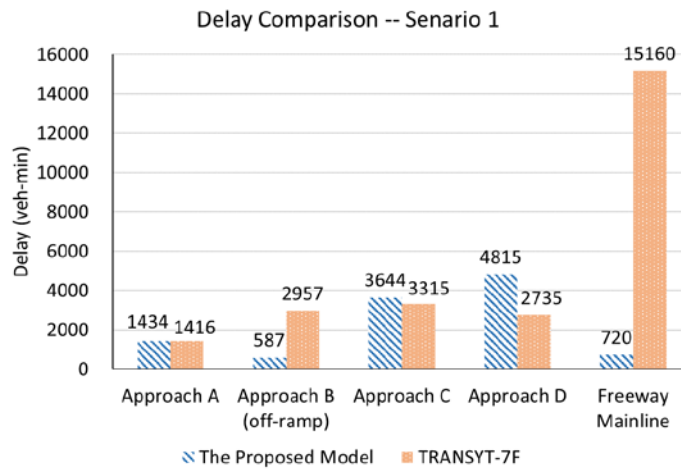
(a) Scenario 1
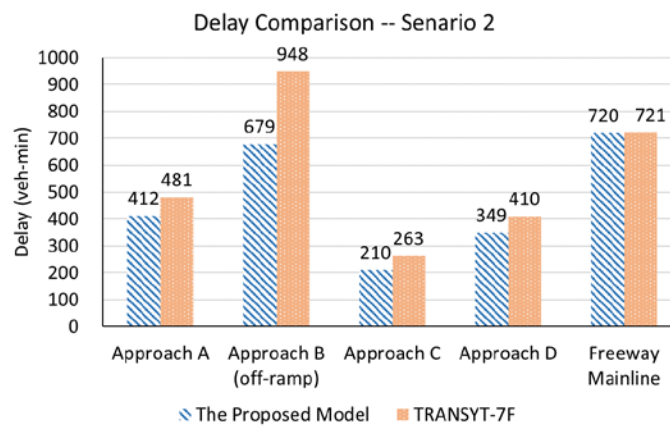
(b) Scenario 2
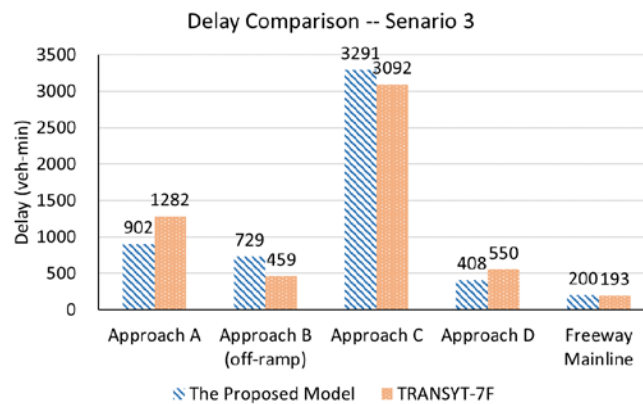
(c) Scenario 3

Figure 4-11: Delays of scenarios

Chapter 5
An Arterial Multi-Path Model for Progressing Heavy Off-Ramp Flows

5.1 Introduction

As noted in the last chapter, an intersection receiving the off-ramp flows from a freeway corridor must be designed with a specially developed signal model that accounts for the potential impacts of ramp queue spillback on the freeway traffic conditions. Conceivably, the large volume of off-ramp flows from such an intersection, compounded with the typically high commuting volume, will inevitably pose a serious challenge to the design of signal control for the subject arterial. Since both the off-ramp and arterial flows may be bound to different destinations via turning movements at different intersections, it is essential for the arterial signals to offer progression bands for not only the through movement, but also all major path-flows along the arterial. The multi-path arterial progression model presented in the chapter is developed primarily for such a need.

Figure 5-1 shows the overall structure of the proposed multi-path arterial progression model (denoted as MAP model), and the relations between its principal components. Grounded in the core notion of providing a progression band for any pair of flow movements between each arterial link's upstream and downstream intersections, the MAP model has the following unique features:

- accounts for the off-ramp queues and their spillback impacts on the freeway delays in design of signal plan for the intersection receiving the off-ramp flows;
- offers a progression band (named local band) for each pair of flow movements between an arterial link's upstream and downstream intersections;
- concurrently optimizesthe signal timings and phase sequence for each intersection, based on the volume distribution for different movements and the available turning-bay length; and
- innovatively connects all local bands to construct the set of though progression bands for traffic flows moving over different number of arterial links.
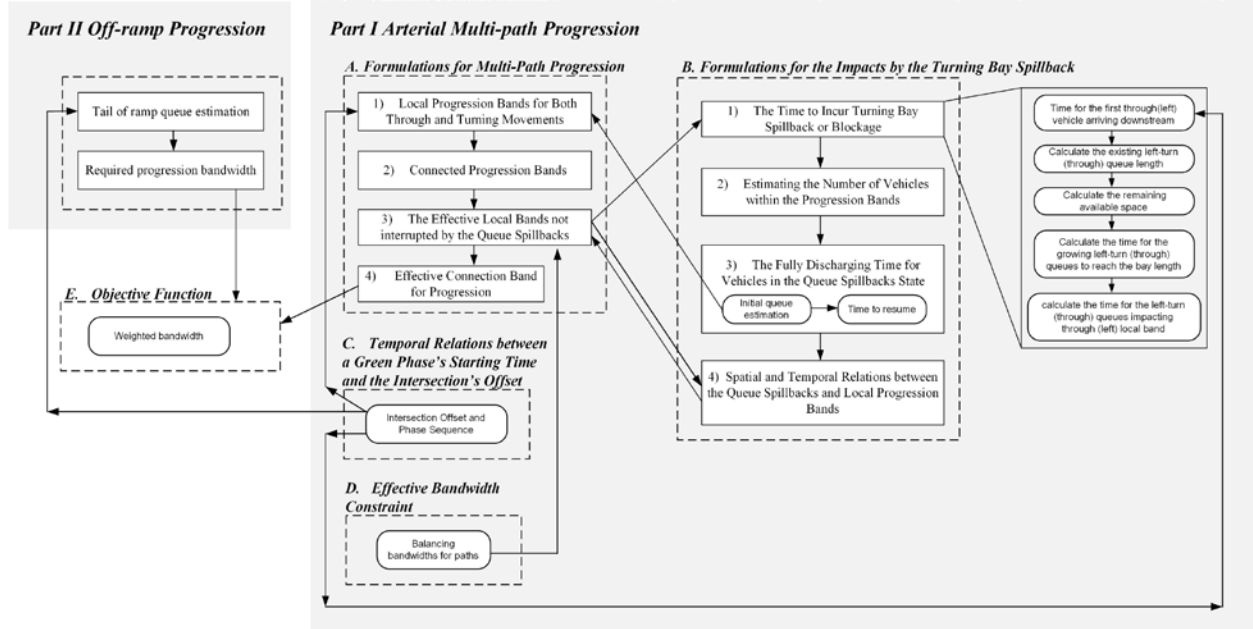
Figure 5-1: Structure of the MAP model and the interrelations between its key components

The key logic, along with the mathematical formulations to reflect the MAP model's features, will be presented in sequence in the ensuing sections.

5.2 Formulations of local progression bands for through and turning flows

Considering an arterial link, denoted as link *I* and shown in Figure 5-3(a), it generally may accommodate multiple inflow streams from its upstream intersection and discharge up to three outflow streams. Hence, for the convenience of presenting the formulations, one can then classify all its upstream traffic movements m as follows:

- m_1: moving into the link from its upstream through-movement flows;
- m_2: from a crossing street left-turning into the link; or
- m_3: from a crossing street right-turning into the link.

Similarly, all discharging traffic streams, denoted as n, from the link can be defined as follows:

- n_1: moving out of the link via the through movement;
- n_2: moving out of the link via left turn; or
- n_3: moving out of the link via right turn.

Note that a local path, $<m,n> \in \mathcal{L}_i$, is defined as the traffic stream between two

movements: one is for moving-in flows taking a turn/through movement out of $\boldsymbol{m}$ at the link's upstream intersection, and the other is for those via a turn/through movement from $\boldsymbol{n}$ to move out the link from its downstream intersection, where $\mathcal{L}_i$ is the set of all possible local paths passing link i.

As such, there are up to nine possible local paths, $<\boldsymbol{m},\boldsymbol{n}>$, on a single link (if both are four-leg intersections), based on the combination of all its inflow and outflow movements. Note that the actual number of local paths in the set of $\mathcal{L}_i$ varies with an intersection's geometric features and signal phasing plan. For example, if no left-turn movement is allowed at the downstream intersection, then the possible outflows shall be set as follows: $\boldsymbol{n} \in \{n_1, n_3\}$.

Interference constraints

The set of constraints to ensure the progression for each local path on a link between two adjacent intersections, as shown in Figure 5-2(a), can be formulated as follows for MAXBAND:

$$v_{i,m,n} + b_{i,m,n} \leq \phi_{i,m} \quad \forall <\boldsymbol{m},\boldsymbol{n}> \in \mathcal{L}_i \quad \forall i \tag{5-1}$$

$$w_{i,m,n} + b_{i,m,n} \leq \phi_{i,n} \quad \forall <\boldsymbol{m},\boldsymbol{n}> \in \mathcal{L}_i \quad \forall i \tag{5-2}$$

$$w_{i,m,n} \geq \tau_{i,n} \quad \forall <\boldsymbol{m},\boldsymbol{n}> \in \mathcal{L}_i \quad \forall i \tag{5-3}$$

Where, $v_{i,m,n}(w_{i,m,n})$ refers to the time difference between the start of a progression band for each local path and the corresponding green phase at the upstream (downstream) intersection of link i; $b_{i,m,n}$ is the local progression bandwidth; $\phi_{i,m}$ is the green duration of movement m; $\tau_{i,n}$, is a variable, indicating the initial queues discharging time for movement $\boldsymbol{n}$ on link i, as shown in Figure 5-3. Eqs. (5-1)-(5-3) serve as the interference constraints for the local progression at each intersection. Table 5-1 lists all key variables used in the hereafter model presentation.
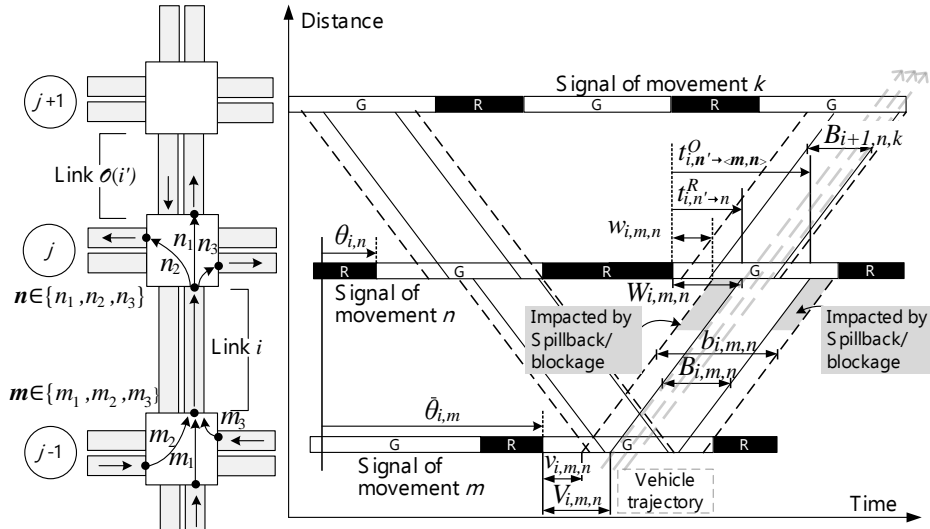
(a) Local progression bands
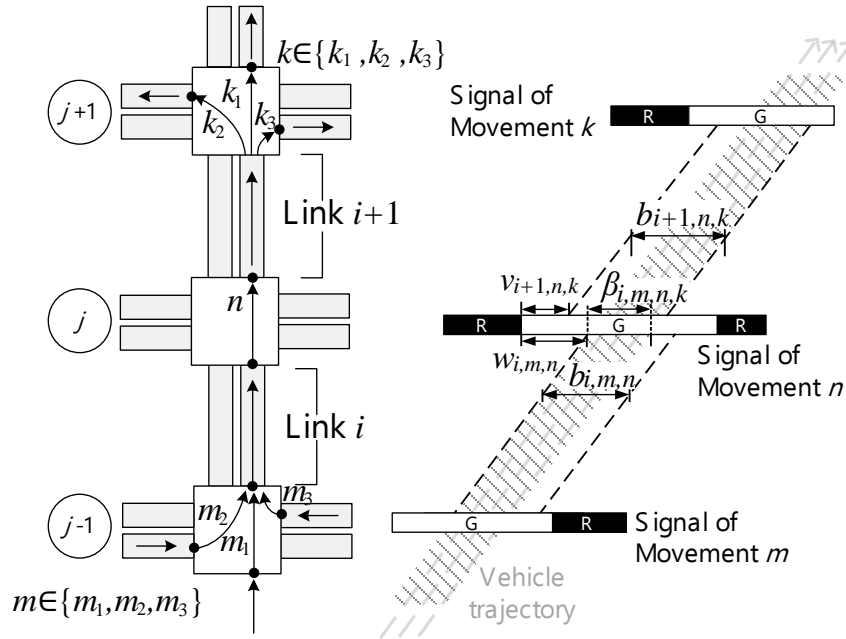
(b) Connection bands

Figure 5-2: Key variables for formulating

Table 5-1: List of key variables used in the MAP model

Part I

i	Link
$<m,n> \in \mathcal{L}_i$	Local paths of link i turning in from movement m and turning out via movement n
$v_{i,m,n}$	Time difference between the start of a progression band for each local path and the corresponding green phase at the upstream intersection of link i
$w_{i,m,n}$	Time difference between the start of a progression band for each local path and the corresponding green phase at the downstream intersection of link i
$b_{i,m,n}$	Local progression bandwidth
$\phi_{i,m}$	Green duration of movement m
$\tau_{i,n}$	The initial queue discharging time for movement n on link i
$\bar{\theta}_{i,m}$	Starting time of the green phase for the upstream movement of path $<m,n>$ at link i
$\theta_{i,n}$	Starting time of the green phase for the downstream movement of path $<m,n>$ at link i
$T_{i,m,n}$	Travel time to complete the local path over link i
C	Signal cycle length
$\beta_{i,m,n,k}$	Connection bandwidth from upstream movement m on link i, to downstream movement k on link i+1, via the through movement at the common intersection of those links
$B_{i,m,n}$	Effective local bandwidth for a local path $<m,n>$ on link i
$V_{i,m,n}$	Starting time of the effective local band at the upstream intersection of link i (reference to the start time of a green phase)
$W_{i,m,n}$	Starting time of the effective local band at the downstream intersection of link i (reference to the start time of a green phase)
$\beta'_{i\,m\,n\,k}$	Denotes the effective bandwidth for the connection bands
$\tilde{m} \in \tilde{\mathcal{M}}$	Upstream movements contributing to the left-turn queue before the first vehicle in the through path arrives at the downstream intersection
ρ^J	Jam density
$\mathcal{A}(n)$	The set of downstream movements that can have some impact to movement n
$\hat{S}_{i,m,n}$	Dispersed flowrate for local path $<m,n>$ on link i
$\tau_{i,n'}$	Discharging time of the initial queue defined in (3), and can be computed from the maximum queue
$Y_{i,n'}$	Maximum queue (in number of vehicles)
$q_{i,n'}$	Per-cycle outflow rate of movement n' from link i
$p_{i,n'}$	Per-cycle outflow rate receiving progression of movement n' from link i
$\alpha_{i,m,n}$	Binary variable indicating the existence of an effective local band
Θ_i	Offset at the downstream intersection j of link i, or $\mathcal{D}(i)$
$\phi_{i,n}$	Duration of the green of signal of movement n
χ_j	Binary variable indicating the phase sequence, which equals 1 if the green phase of the outbound through is before that of the inbound left-turn
$\bar{\chi}_j$	Binary variable indicating the phase sequence, which equals 1 if the green phase of the outbound left-turn is before that of the inbound through

Part II

$\mathcal{O}$	Set of off-ramp (link o is offramp if $o \in \mathcal{O}$)
b_o	Bandwidth of off-ramp
b_O^m	Minimum bandwidth
Y_O	Queue length of off-ramp
Y_O^M	Storage space of off-ramp
s^-	Discharge flowrate if not receiving progression
b_O^-	Green time not having progression while the queue is still dissipating
ϕ_o	Off-ramp green duration
q_o	Off-ramp volume
z_o	Queue length that spills back onto the freeway mainline
Z'	Objective function with penalty on queue spillback

Loop integer constraint for all paths over each arterial link

To synchronize signals between two intersections and allow vehicles to progress over the arterial within their designated local bands, one shall specify the following progression constraints for each local path, $<\boldsymbol{m},\boldsymbol{n}>$:

$$\bar{\theta}_{i,m} + v_{i,m,n} + T_{i,m,n} = \theta_{i,n} + w_{i,m,n} + K_{i,m,n} \times c \quad \forall <\boldsymbol{m},\boldsymbol{n}> \in \mathcal{L}_i \quad \forall i \tag{5-4}$$

Where, $\bar{\theta}_{i,m}(\theta_{i,n})$ is the starting time of the green phase for the upstream (downstream) movement of path $<\boldsymbol{m},\boldsymbol{n}>$ at link i; $T_{i,m,n}$ denotes the travel time for the local path over link i; $K_{i,m,n}$ is an integer variable, and c refers to the signal cycle length.

Path selection

To maximize the total benefits of the entire arterial flows, it may not be necessary for all path flows to receive local progression bands. Hence, only those path flows, selected for having progression bands, should follow Eq. (5-4), and the binary variable, $y_{i,m,n}$, specified below is used for the model to execute such a selection:

$$\bar{\theta}_{i,m} + v_{i,m,n} + T_{i,m,n} \geq \theta_{i,n} + w_{i,m,n} + K_{i,m,n} \times c - M(1 - y_{i,m,n}) \quad \forall <\boldsymbol{m},\boldsymbol{n}> \in \mathcal{L}_i \quad \forall i \tag{5-5}$$

$$\bar{\theta}_{i,m} + v_{i,m,n} + T_{i,m,n} \leq \theta_{i,n} + w_{i,m,n} + K_{i,m,n} \times c + M(1 - y_{i,m,n}) \quad \forall <\boldsymbol{m},\boldsymbol{n}> \in \mathcal{L}_i \quad \forall i \tag{5-6}$$

Where, M is a large number. When $y_{i,m,n} = 0$, Eqs. (5-5)-(5-6) are relaxed, indicating that the no local band exists for a local path (m, n) on the link i. Otherwise, the existence of the local band can be ensured with $y_{i,m,n} = 1$, for enforcing the integer loop constraints in Eq. (5-4). With such a binary variable, one can formulate the selection of local paths for having progression bands as follows:

$$b_{i,m,n} \leq M y_{i,m,n} \quad \forall <\boldsymbol{m},\boldsymbol{n}> \in \mathcal{L}_i \quad \forall i \tag{5-7}$$

$$b_{i,m,n} \geq b_0 - M(1 - y_{i,m,n}) \quad \forall <\boldsymbol{m},\boldsymbol{n}> \in \mathcal{L}_i \quad \forall i \tag{5-8}$$

The above equations function to ensure a minimum bandwidth of b_0 (e.g., 5 seconds in this study).

Connected progression bands

Note that an intersection's outgoing flows via a local through band will be the entry flows to its downstream link, as shown in Figure 5-2(b). Hence, the design of local progression bands needs to include the optimal connection between two consecutive local bands to facilitate the progression of through movements. To compute the connection bandwidth, defined as the overlapped duration between two adjacent local bands, one can adopt the following equations:

$$\beta_{i,\boldsymbol{m},\boldsymbol{n},\boldsymbol{k}} = \min\{w_{i,\boldsymbol{m},\boldsymbol{n}} + b_{i,\boldsymbol{m},\boldsymbol{n}}, v_{i+1,\boldsymbol{n},\boldsymbol{k}} + b_{i+1,\boldsymbol{n},\boldsymbol{k}}\} - \max\{w_{i,\boldsymbol{m},\boldsymbol{n}}, v_{i+1,\boldsymbol{n},\boldsymbol{k}}\}$$

$$(5\text{-}9)$$

$$\forall \langle \boldsymbol{m},\boldsymbol{n}\rangle \in \mathcal{L}_i, \langle \boldsymbol{n},\boldsymbol{k}\rangle \in \mathcal{L}_{i+1} \ \forall i$$

Where, $\beta_{i,\boldsymbol{m},\boldsymbol{n},\boldsymbol{k}}$ denotes the connection bandwidth from all upstream movements, $\boldsymbol{m}$, on link i, to downstream movements $\boldsymbol{k}$ on link $i+1$, via the through movement at the common intersection for those links. Note that $\boldsymbol{n}$ in Eq. (5-9) can only be a through movement n_1, but $\boldsymbol{m}$ and $\boldsymbol{k}$ can still be through or any turning movement. The overlapped duration, shown in Figure 5-2(b), can be calculated with its starting and terminating times. The former can be selected from either its upstream or downstream band that has a later starting time. The same selection logic can be extended for the latter by referencing to the earlier ending time between such two progression bands.
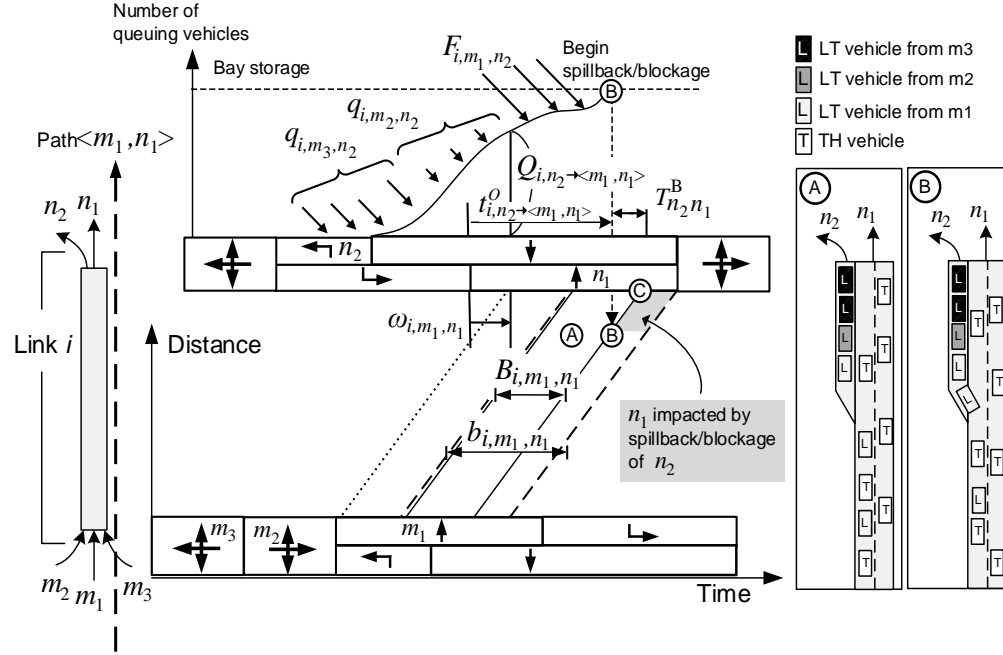
(a) Queue formation of left-turn movement (n_2) and its impacts on the through local path (m_1, n_1) movement
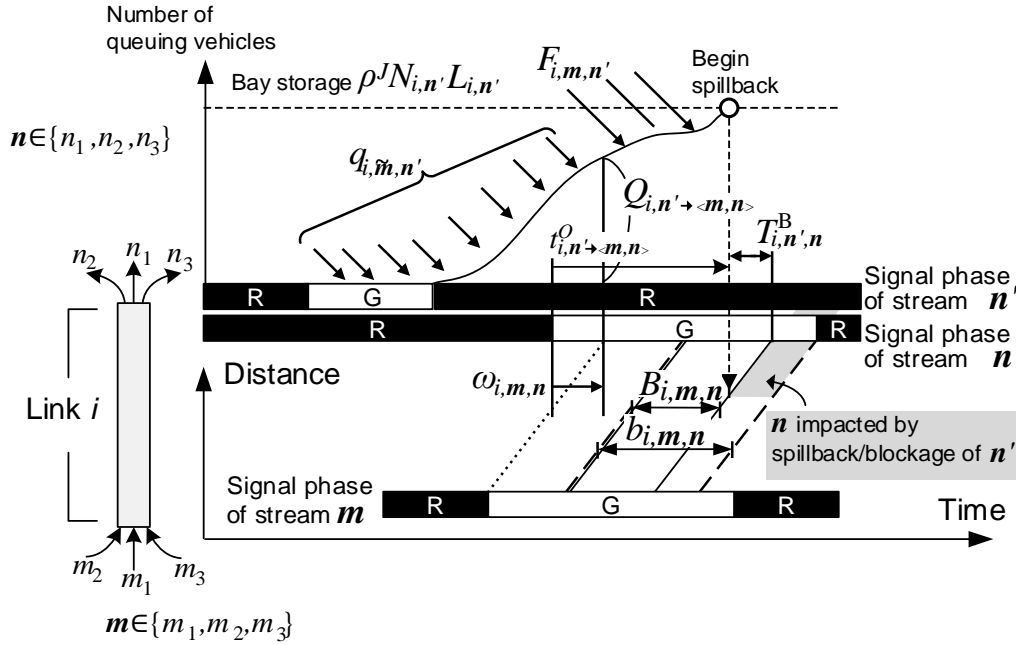
(b) Queue formation of movement n' and its impact on the local paths (m, n)

Figure 5-3: Graphical illustration of queue formations

The effective local bands not interrupted by the queue spillbacks

For a left-turn movement from the arterial, the local band for such a movement is likely to be impeded by the through queues at a link's downstream intersection. The spillback from turning queue can in turn interrupt the through bands. As shown in Figure 5-3(a), the effective local band, $B_{i,m,n}$, (shown with solid lines) is a portion of local band, $b_{i,m,n}$, (shown with dashed lines) that is not blocked by the excessive queues, which can be expressed with the following constraints:

$$V_{i,m,n} \geq v_{i,m,n} \quad \forall <\boldsymbol{m,n}> \in \mathcal{L}_i \quad \forall i \tag{5-10}$$

$$W_{i,m,n} \geq w_{i,m,n} \quad \forall <\boldsymbol{m,n}> \in \mathcal{L}_i \quad \forall i \tag{5-11}$$

$$V_{i,m,n} + B_{i,m,n} \leq v_{i,m,n} + b_{i,m,n} \quad \forall <\boldsymbol{m,n}> \in \mathcal{L}_i \quad \forall i \tag{5-12}$$

$$W_{i,m,n} + B_{i,m,n} \leq w_{i,m,n} + b_{i,m,n} \quad \forall <\boldsymbol{m,n}> \in \mathcal{L}_i \quad \forall i \tag{5-13}$$

Where, $B_{i,m,n}$ refers to the effective local bandwidth for a local path $<\boldsymbol{m,n}>$ on link i; and $V_{i,m,n}(W_{i,m,n})$ is the starting time of the effective local band at the upstream (downstream) intersection of link i . Eqs. (5-10)-(5-13) ensure that an effective local band is less than its own local progression band.

Effective connection band for through progression

Following the same notion as with Eqs. (5-9) and (5-14) shows the effective bandwidth for the connection bands, referring to the overlapped portion that allows vehicles to progress over consecutive links.

$$\beta'_{i,m,n,k} = \min\{W_{i,m,n} + B_{i,m,n}, V_{i+1,n,k} + B_{i+1,n,k}\} - \max\{W_{i,m,n}, V_{i+1,n,k}\}$$

$$\forall <\boldsymbol{m,n}> \in \mathcal{L}_i, <\boldsymbol{n,k}> \in \mathcal{L}_{i+1} \quad \forall i \tag{5-14}$$

Where, $\beta'_{i,m,n,k}$ denotes the effective bandwidth for the connection bands, defined as the overlapped duration between two adjacent effective local bands.

5.3 Formulations for the impacts due to the turning-bay spillback

It should be noted the starting time and duration of the effective bands introduced in Eqs. (5-10)-(5-13) vary with the formation and dissipation of vehicle queues. For example, the impact of a left-turn (n_2) queue spillback on a local through band along the arterial (m_1, n_1) on the same link should be estimated from the following two time points:

- $t^O_{i,n_2 \to (m_1,n_1)}$: the time when queues from the left-turn movement, n_2, exceed the bay length and start to impact the progression band for a local path (m_1, n_1) on link i; and

- $t^R_{i,n_2 \to n_1}$: the time for queues from the left-turn movement, (n_2), to end its impact on the local band for arterial through movement (n_1) on link i.

The formulations presented in the next section are derived, as an example, for links shown in Figure 5-3(a)). The impacts of left-turn or through queues on other local bands can be formulated with the same logic and similar constraints.

The onset of turning-bay spillback or blockage

Note that the queue spillback from a left-turn bay will impact the band for the local through path along the arterial, as shown in Figure 5-3(a). Such impacts can be estimated with the following steps:

Step-1: compute the time point when the first vehicle from the through path arrives at the downstream intersection, denoted by ω_{i,m_1,n_1}.

The trajectory of the first vehicle following the through path is shown by dotted lines in Figure 5-2(a), and its arrival time at the downstream intersection, ω_{i,m_1,n_1}, should be calculated with the offsets between two intersections and the link's travel time, as expressed below (see Figure 5-3(a)),

$$\omega_{i,m_1,n_1} = \bar{\theta}_{i,m_1} + T_{i,m_1,n_1} - \theta_{i,n_1} - K_{i,m_1,n_1} \times c \qquad (5\text{-}15)$$

Step-2: calculate the left-turn queue length when the first vehicle from the through path arrives at the downstream intersection.

Such left-turn queues are formed by vehicles from other local paths, but not within their local progression bands. As shown in Figure 5-3(a), vehicles from both directions of the crossing street not moving within their local bands contribute to such queues. Hence, the left-turn queues that may impact the through local paths along the arterial can be expressed as follows:

$$Q_{i,n_2\to<m_1,n_1>}=(q_{i,m_2,n_2}-p_{i,m_2,n_2})+(\ q_{i,m_3,n_2}-p_{i,m_3,n_2}) \tag{5-16}$$

Where, $Q_{i,n_2\to<m_1,n_1>}$ denotes the left-turn queue length when the through path's first vehicle arrives at the downstream intersection; $q_{i,m,n}$ is the volume per cycle of local path $(\boldsymbol{m,n})$ on link i; and $p_{i,m,n}$ is the path volume per cycle that can experience a local progression band.

Note that Eq. (5-17) is a generalized expression for Eq. (5-16) that summarizes all upstream flows contributing to the left-turn queues, prior to the arrival of any vehicle from the through path to the target intersection, but excluding those experiencing local progression.

$$Q_{i,n_2\to<m_1,n_1>} = \sum_{\widetilde{m}\in\widetilde{\mathcal{M}}} q_{i,\widetilde{m},n_2} - \sum_{\widetilde{m}\in\widetilde{\mathcal{M}}} p_{i,\widetilde{m},n_2} \tag{5-17}$$

Where, $\widetilde{\boldsymbol{m}} \in \widetilde{\mathcal{M}}$ denotes those upstream movements contributing to the left-turn queue before the first vehicle in the through path arrives at the downstream intersection, i.e., $\widetilde{\boldsymbol{m}} \in \{m_2, m_3\}$ in this case.

Step-3: Compute the remaining storage space within the left-turn bay, based on the existing left-turn queues, as follows:

$$\rho^J N_{i,n_2} L_{i,n_2} - Q_{i,n_2\to<m_1,n_1>} \tag{5-18}$$

Where, ρ^J represents the jam density; N_{i,n_2} is the number of left-turn (n_2) lanes on link i; and L_{i,n_2} is the bay length for the left-turn, (n_2), on link i.

Step-4: calculate the duration for the left-turn queues to exceed the bay length.

During the phase for through vehicles to traverse the link, those using the same green phase but intending to turn left at the downstream intersection will form the left-turn queues, as shown in time period A in Figure 5-3(a). The accumulative rate of left-turn queues equals the flow rate of those moving in from the link's upstream intersection via a through movement and then taking a left turn at the downstream intersection. Therefore, one can show the starting time for the left-turn queues to reach the end of the bay and to consequently impede the local through path as follows:

$$\frac{\rho^J N_{i,n_2} L_{i,n_2} - Q_{i,n_2\to<m_1,n_1>}}{F_{i,m_1,n_2}} \quad \forall i \tag{5-19}$$

Where, F_{i,m_1,n_2}, is the flow rate of left-turn vehicles arriving from the upstream through green

phase.

Step-5: calculate the time for the left-turn queues to show their impacts on the through local band.

The time point, when the left-turn queues for movement n_2 exceed the bay length and start to partially block the progression of the local through path $<m_1, n_1>$ on link i, can be formulated with the following constraint:

$$t^O_{i,n_2 \to <m_1,n_1>} = \frac{\rho^J N_{i,n_2} L_{i,n_2} - Q_{i,n_2 \to <m_1,n_1>}}{F_{i,m_1,n_2}} + \omega_{i,m_1,n_1} + T^B_{i,n_2,n_1} \quad \forall i \qquad (5\text{-}20)$$

Where, T^B_{i,n_2,n_1} is the time duration from the onset of queue spillback to the time it starts to impact a local band, which equals the travel time for through vehicles to traverse the entire bay length. The last term in Eq. (5-20), T^B_{i,n_2,n_1}, accounts for the fact that after the left-turn queue spillback takes place, the progression can be sustained until the last unimpeded vehicle arriving at the stop bar, as shown in the duration between time points B and C in Figure 5-3(a).

Note that a negative value for the starting time, $t^O_{i,n_2 \to <m_1,n_1>}$, indicates the worst case that spillback has already existed prior to the arrivals of those vehicles coming during their progression bands. On the contrary, if such a starting time is larger than the cycle length, it implies that such spillback is unlikely to occur.

By the same notion, one can also derive the above formulations for all local paths likely impacted by the queues from other paths. To do so, this study adopts the compressed notations with $\boldsymbol{n}$ denoting the set of movements suffering from the queue blockage, and $\boldsymbol{n'}$ denoting the set of movements generating queues. More specifically, all potential conflicts between the queues and a local band include:

- when $\boldsymbol{n} = n_1$, $\boldsymbol{n'} \in \{n_2, n_3\}$, indicating that the through stream may be impacted by the spillbacks from either left- or right-turn queues; and
- when $\boldsymbol{n} \in \{n_2, n_3\}$, $\boldsymbol{n'} \in \{n_1\}$, indicating that right- and left- turn streams may be impacted by the through queue spillback.

With the above notations, one can formulate the time points when the spillback of queue $\boldsymbol{n'}$ starts its impacts on the band, $<\boldsymbol{m}, \boldsymbol{n}>$, with the following general expressions:

$$\omega_{i,m,n} = \theta_{i,m} + T_{i,m,n} - \theta_{i,n} - K_{i,m,n} \times c \quad \forall <\boldsymbol{m,n}> \in \mathcal{L}_i \quad \forall i \qquad (5\text{-}21)$$

$$Q_{i,n' \to <m,n>} = \sum_{\widetilde{m}} q_{i,\widetilde{m},n'} - \sum_{\widetilde{m}} p_{i,\widetilde{m},n'} \quad \forall <\boldsymbol{m,n}> \in \mathcal{L}_i \quad \boldsymbol{n'} \in \mathcal{A}(\boldsymbol{n}) \quad \forall i \qquad (5\text{-}22)$$

$$t^O_{i,n' \to <m,n>} = \frac{\rho^J N_{i,n'} L_{i,n'} - Q_{i,n' \to <m,n>}}{F_{i,m,n'}} + \omega_{i,m,n} + T^B_{i,n',n} \quad \forall <m,n> \in \mathcal{L}_i \quad n' \in \mathcal{A}(n) \quad \forall i \quad (5\text{-}23)$$

Where, $\mathcal{A}(n)$ refers to the set of downstream movements that can have some impacts on movement n.

Estimating the number of vehicles within the progression bands

One key challenge in Eq. (5-22) is to compute those vehicles in the progression band so as to better estimate the resulting queues. Note that vehicles can progress on all lanes if traveling within their effective local band. Otherwise, they can only use those lanes not blocked by the excessive queues, if within the remaining portion of the band. Hence, the number of vehicles in and out of the effective local bands should be computed. The former of Eq. (5-22) is the product of bandwidth and the discharge rate, and the latter is modified by a term to reflect the impacts of excessive queues on one lane in a local path. Therefore, such vehicles can be calculated with Eq. (5-24):

$$p_{i,m,n} = B_{i,m,n} \hat{S}_{i,m,n} + \left(b_{i,m,n} - B_{i,m,n} \right) \times \frac{N_{i,n} - 1}{N_{i,n}} \times \hat{S}_{i,m,n} \quad \forall <m,n> \in \mathcal{L}_i \quad \forall i \quad (5\text{-}24)$$

Where, $\hat{S}_{i,m,n}$ is the flowrate for local path $<m, n>$ on link i. When estimating the potential discharge rate, one should notice that a platoon of vehicles discharged at the saturation flow rate from an upstream stop line may not necessarily sustain such a high flow rate at the downstream intersection. Therefore, this study takes Robertson's platoon dispersion effect into consideration, and adopts the dispersed flow rate, $\hat{S}_{i,m,n}$, as the potential discharge rate at the downstream intersection.

The duration to fully discharge all vehicles in the spillback state

The local progression band can be recovered once the queues causing spillback are fully discharged. With the same definition for set n' as in the last section, the time for a local band for movement n to be free from the impacts of entire queues from n', as shown in Figure 5-2(a), can be expressed as follows:

$$t^R_{i,n' \to n} = \theta_{i,n'} - \theta_{i,n} + \tau_{i,n'} \quad n' \in \mathcal{A}(n) \quad \forall i \quad (5\text{-}25)$$

Where, $\tau_{i,n'}$ is the discharging time of the initial queues defined in Eq. (5-3), and can be computed from the maximum queue as follows:

$$\tau_{i,n'} = \frac{Y_{i,n'}}{s_{i,n'} \times N_{i,n'}} \quad \forall i \tag{5-26}$$

where, $s_{i,n'}$ is the saturation flow rate of movement $\boldsymbol{n'}$; and $Y_{i,n'}$ denotes the maximum queue (in number of vehicles) of movement $\boldsymbol{n'}$ that can be estimated from those volumes not within their designated progression bands, as shown in Eq. (5-27).

$$Y_{i,n'} = q_{i,n'} - p_{i,n'} \quad \forall i \tag{5-27}$$

Where, $q_{i,n'}$ is the per-cycle outflow rate of movement $\boldsymbol{n'}$ from link i, and $p_{i,n'}$ is the in-progression outflow rate per-cycle for movement $\boldsymbol{n'}$ from link i. Following the logic in Eq. (5-22), vehicles that can experience progression are also excluded from the calculation of the queue length, as shown with the last two terms.

Interrelations between the queue spillbacks and local progression bands

Given the starting and ending time points for the queue spillback to impact the local bands, one can formulate their spatial-temporal relations with a set of constraints. The effective bands, excluding the duration of the progression band blocked by spillback queues, can be expressed with the following equations:

$$W_{i,m,n} + M(1-\alpha_{i,m,n}) \geq t^R_{i,n'\to n} \quad \forall <\boldsymbol{m,n}> \in \mathcal{L}_i, \ \boldsymbol{n'} \in \mathcal{A}(\boldsymbol{n}) \quad \forall i \tag{5-28}$$

Where, $\alpha_{i,m,n}$ is a binary variable, indicating the existence of an effective local band.

By the same token, the effective band that can sustain until next queue spillback can be expressed with Eq. (5-29).

$$W_{i,m,n} + B_{i,m,n} \leq t^O_{i,n'\to(m,n)} + M(1 - \alpha_{i,m,n}) \quad \forall <\boldsymbol{m,n}> \in \mathcal{L}_i, \boldsymbol{n'} \in \mathcal{A}(\boldsymbol{n}) \quad \forall i \tag{5-29}$$

Eqs. (5-28)-(5-29) would be relaxed when $\alpha_{i,m,n} = 0$, indicating that the effective local band does not exist. Such conditions can be identified with the following relation:

$$M\alpha_{i,m,n} \geq B_{i,m,n} \quad \forall <\boldsymbol{m,n}> \in \mathcal{L}_i, \quad \forall i \tag{5-30}$$

Relations between a green phase's starting time and the intersection's offset

Note that the starting time of the green phase for each movement should be computed concurrently with the optimized intersection offsets and phase sequences. The constraints for doing so for each movement as used in MAXBAND (Little *et al.*, 1981) can be specified as follows:

$$\theta_{i,n_1} = \Theta_j + (1-\chi_j)\cdot(\phi_{\mathcal{O}(i),n_2}+I) \quad \forall i, \ j = \mathcal{D}(i) \tag{5-31}$$

$$\theta_{i,n_2} = \Theta_j + (1-\bar{\chi}_j)\cdot(\phi_{\mathcal{O}(i),n_1}+I) \quad \forall i, \ j = \mathcal{D}(i) \tag{5-32}$$

$$\theta_{i,n_1} = \bar{\theta}_{i+1,m_1} \quad \forall i \tag{5-33}$$

Where, Θ_j is the offset at the downstream intersection j of link i, as shown in Figure 5-2(a); $\phi_{i,n}$ is a variable denoting the duration of the green phase for movement n at intersection i, and the $\mathcal{O}(i)$ refers to the inbound link at the upstream of intersection j, as shown in Figure 5-2(a); $\chi_j(\bar{\chi}_j)$ is a binary variable indicating the phase sequence, which equals 1 if the green phase of the outbound through (left-turn) is ahead of the inbound left-turn (through). Eq. (5-33) shows that the outflows for the through movement are the inflows of the through movement to its downstream link. The side-street signal phases can also be formulated in the same manner.

Effective bandwidth constraints

Considering that the bandwidth is wider than needed and should be distributed to other movements if possible, one should set the following upper bound for each effective local band:

$$B_{i,m,n}\hat{S}_{i,m,n} \leq q_{i,m,n} \quad \forall <\boldsymbol{m,n}> \in \mathcal{L}_i \quad \forall i \tag{5-34}$$

Eq. (5-34) is specified to ensure the effective local bandwidth will be shorter than the discharge time for all vehicles traveling from movements $\boldsymbol{m}$ to $\boldsymbol{n}$ on link i.

5.4 Objective functions for the multi-path progression

The objective function of the proposed model will maximize the sum of all bandwidths for the selected local paths weighted by their corresponding volumes. These weights are used to reflect the number of vehicles that can benefit from their designated bands. For example, the portion of the local band interrupted by turning-bay blockage can only benefit these vehicles in the non-impeded lanes. Therefore, the objective function can further be expressed as follows:

$$Max \quad Z \tag{5-35a}$$

$$Z = \sum \mu_{1,i,m,n} \times B_{i,m,n} + \sum \mu_{2,i,m,n,k} \times \beta'_{i,m,n,k} + \sum \mu_{3,i,m,n} \times \left(b_{i,m,n} - B_{i,m,n}\right) +$$
$$\sum \mu_{4,i,m,n,k} \times \left(\beta_{i,m,n,k} - \beta'_{i,m,n,k}\right) \tag{5-35b}$$

$$\mu_{1,i,m,n} = q_{i,m,n} \times \hat{S}_{i,m,n} \tag{5-36}$$

$$\mu_{2,i,m,n,k} = q_{i,m,n,k} \times \hat{S}_{i,m,n} \tag{5-37}$$

$$\mu_{3,i,m,n} = q_{i,m,n} \times \frac{N_{i,n}-1}{N_{i,n}} \hat{S}_{i,m,n} \tag{5-38}$$

$$\mu_{4,i,m,n,k} = q_{i,m,n,k} \times \frac{N_{i,n}-1}{N_{i,n}} \hat{S}_{i,m,n} \tag{5-39}$$

Where, $\mu_{z,i,m,n}$ are the weighting factors based on traffic volumes from $\boldsymbol{m}$ to $\boldsymbol{n}$ on link i.

In summary, the proposed models with all above formulations can concurrently provide maximized progression for all selected paths along an arterial and connect them between adjacent links without the need of OD information and under the constraint of the limited left-turn bay length.

Chapter 6
Conclusions and Recommendations

6.1 Conclusions - from local ramp metering to integrated corridor traffic control

This project produced four traffic models for highway agencies to overcome various constraints in practice. Depending on the congestion patterns and their spatial evolution over the target freeway segment, responsible traffic control centers can apply these models individually or collectively to effectively implement congestion management strategies, ranging from local ramp metering to coordinated freeway control or eventual integrated corridor management.

The first model (i.e., AF-ramp) is for executing an arterial-friendly local ramp metering control, focusing on mitigation of freeway local bottlenecks by high on-ramp merging volume and coordination with neighboring intersection signals to prevent the ramp queues from spilling back to local streets—one major concern often raised by local traffic agencies. Different from all existing ramp metering controls in the literature, the proposed RF-ramp has the control objective of maximizing the total throughput for not only the target freeway segment but also all arterial links within the impact area of the interchange. To ensure that both the ramp queues and the turning volumes form intersections to the on-ramp will not overflow and cause a gridlock, the set of control variables produced from the RF-ramp model includes not only the optimal cycle length and green splits for all intersections within the control area, but also their offsets and phase sequences to progress arteria traffic flows and coordinate with the ramp metering signal.

Conceivably, traffic patterns on congested freeways, especially those for daily commute, are likely to incur multiple local bottlenecks on those segments in the vicinity of interchanges, and may thus justify the implementation of a series of local ramp metering controls. Since both exiting-to-off-ramp weaving and on-ramp merging maneuvers will inevitably cause the freeway mainline to experience shock waves and consequently propagate the resulting congestion patterns to upstream freeway segments, it is imperative that all neighboring ramps be coordinated properly under such congested traffic scenarios so as to best smooth the traffic conditions from the perspective of the entire freeway segment, rather than from individual ramps.

A well-established practice to perform a coordinated freeway ramp control typically consists of local ramp metering and a macroscopic freeway module for replicating and projecting the mainline traffic conditions between neighboring ramps. Depending on the needs for time-of-day or real-time operations, the traffic control community has developed a large body of models and software over the past decades for both modules, but mostly implemented such control only at the project demonstration level.

Certainly, there are various technical and implementation issues that contribute to the lack of adopting the coordinated ramp control in practice, despite the ever-increasing congestion on most commuting freeways. Among those, insufficiently accounting for the on-ramp weaving impacts in the freeway module and neglecting the potential lane-blockage by off-ramp queue spillback are two primary technical issues to be addressed by the traffic researchers. Note that the former often results in an underestimate of the available freeway capacity to receive the on-ramp flows, thus incurring excessive on-ramp queues or a local freeway bottleneck due to mass weavings of high on-ramp volume. The congestion impacts on the freeway mainline by the latter, caused primarily by inadequate green time allocated for the approach accommodating the exiting flows at the off-ramp signal, can be very pronounced during peak periods, especially   at those interchanges neighboring major trip destinations, such as center business areas or industrial parks.

To ensure the effectiveness of coordinated ramp-metering controls, if justified to implement, this study has developed two models to tackle those two vital but inadequately-addressed technical issues: reflecting the impacts of on-ramp weavings and off-ramp queue spillback on the freeway mainline segment's traffic conditions, so that two neighboring ramps and their common connected mainline segment can be properly captured to constitute a coordinated system in the control mode.

As for the integrated corridor control, such a system typically includes a freeway segment and its parallel arterials, operated with the common objective of minimizing the total system-wide delay or maximizing the total throughput. Theoretically, all key control modules responsible for regulating either freeway or arterial flows can be constructed and operated in the same control platform with either a time-of-day or real-time control mode. Despite being conceptually appealing, to do so with insufficient data precision and reliability to establish the complex temporal and spatial relations between all traffic state variables, the integrated control often cannot yield the currently optimal state for both the freeway and arterials, and likely to demand that system operators perform ad hoc manual-adjustment, especially under highly fluctuating traffic conditions, to prevent any performance conflict (e. g., on- and off-ramp queue spillbacks).

An alternative for the corridor-wide control in practice to avoid all potential data and operations-related issues is to operate the freeway coordinated ramp metering independently from the arterial progression, supplementing their operations with the following two modules: an optimized off-ramp signal design to prevent the ramp-exiting flows from spilling back onto the freeway, and an arterial-friendly local ramp metering to ensure no overflows to arterial links. In

addition and also most importantly, the arterial to facilitate the corridor-wide control must be designed with the advanced multi-path progression system, as proposed in this study, that functions to coordinate not only the intersection phase for the arterial-to-ramp flows with the ramp metering signal, but also to provide dual progression bands to both the through traffic flows and the large-volume of turning flows from the off-ramp to the arterial.

6.2 Recommendations for future studies

Additional field demonstration and evaluation tasks discussed below should be considered:

- Field demonstration of the arterial-friendly local ramp metering system

The primary purpose for conducting such a field test is to assess the interactions between the on-ramp flows, freeway traffic, and arterial volume level. Most importantly, with the actual time-of-day traffic patterns on both the freeway and arterials, the field tests will provide some key data essential for selecting the best set of model parameters, including: the data interval (e.g., 5 or 15 minutes) for time-of-day off-line control, maximal signal turning ratios for moving-to-ramp flows, the cycle length constraints for arterial and ramp signals, and threshold for activating and deactivating the local metering control.

With the set of best calibrated model parameters, one can then conduct the local ramp control during the peak hours over the entire week and observe the following key MOEs:

- freeway speeds and flow rates before and after the weavings by on-ramp metering flows;
- the evolution of on-ramp queue length with and without the control during the observation periods;
- the queue length evolution at those neighboring intersections feeding flows to the freeway ramp;
- the intersection delay before-and-after the local ramp control for arterial flows not turning to the freeway ramp.

The results from the above MOEs and the identified model parameters can serve as the basis for assessing the needs to extend the time-of-day to real-time operations.

- *Deployment and evaluation of the off-ramp signal optimization model to prevent potential queue spillback to the freeway mainline*

This demonstration task is to be conducted at interchanges suffering from queue spillback due to high existing volume and insufficient green duration provided by the off-ramp signal. Deployment of such control not only can eliminate the freeway bottlenecks due to lane-blockage

impacts by excessive off-ramp queues, but also can provide a better estimate of the mainline flow rate for the local ramp control to compute the remaining freeway capacity for receiving the on-ramp flows.

Note that this is a relatively straightforward demonstration task, despite the complexity of the control module's embedded mathematical formulations and a large number of behavioral parameters. The effectiveness of such a control, however, lies in the potential institutional barriers between local traffic agencies responsible for operating the arterial signals and highway departments focusing mainly on the freeway's efficiency.

- *Design and demonstrate coordinated ramp metering control that accounts for the impacts on the freeway's traffic conditions by both the on-ramp weavings and off-ramp queues*

Coordinated ramp control is deployed typically on the freeway segment where each pair of its neighboring ramps is justified to activate local ramp control and the resulting weaving impacts, by the downstream on-ramp flows, have sustainably propagated to the upstream ramp and mainline segment. Conducting such a demonstration, however, is a more complex task, and must proceed first with integration of key freeway control models for different focused applications into a seamless operation platform.

Extensive laboratory experiments and evaluation with a real-world freeway system can then be conducted to assess the interactions between traffic conditions on the mainline segment and at on- and off-ramp weaving areas under the impacts of each individual control module and also collective impacts of all control strategies. Upon completing the laboratory simulation evaluation with the developed operating platform and identifying all key parameters based on the behaviors of target driving populations, one can then proceed the field deployment of   coordinated control and collect the same MOEs used in the laboratory experiments.

- *Exploring the potential of operating the corridor-wide integrated control with coordinated ramp metering and multi-path arterial progression*

To alieviate concerns that effective coordinated freeway ramp controls may be at the expenses of local arterials, likely plagued by the same level of congestion as for freeway during the peak hours, the system for integrated corridor control shall be capable of relieving the congestion incurred by the excessive on-ramp queues and also by the impedance to the arterial traffic progression due to the large turn-in off-ramp volume. Hence, one of the most critical and innovative tasks for effective corridor control is to incorporate the multi-path signal progression model, developed in this study, into the operating platform for coordinated ramp-metering control. By providing the progression bands not only for the arterial's through flows but also the

turning flows existing from the off-ramp and moving to the on-ramp from different arterial links, the integrated corridor control, if operated seamlessly, can effectively accommodate the impacts of turning flows, getting off or onto the freeway, on the local traffic under the deployed freeway coordinated controls.

Note that due to the large number of control modules and key parameters, it is desirable that some reliable sensors be placed at critical locations for system performance monitoring during project demonstration. The real-time detected data along with the computed MOEs will enable the responsible highway agency to develop criteria of guidelines for resolving the following imperative issues:

- the best interval length for time-of-day control for different control periods over different days of a week;
- the optimal length of control interval for the freeway coordinated ramp metering and for arterial progression operations; and
- the criteria and procedures to activate the local system adjustments of all control parameters with available data from various sources in response to unexpected incidents or surges in traffic volumes and distributions.

References

[1] Agarwal, S., Kachroo, P., Contreras, S., and Sastry, S. 2015. "Feedback-coordinated ramp control of consecutive on-ramps using distributed modeling and Godunov-based satisfiable allocation." *IEEE Transactions on Intelligent Transportation Systems*, 16(5), 2384-2392.

[2] Aboudolas, K. and Geroliminis, N. 2013. "Perimeter and boundary flow control in multi-reservoir heterogeneous networks." *Transportation Research Part B: Methodological*, 55, 265-281.

[3] Ahn, S., Bertini, R. L., Auffray, B., Ross, J. H., and Eshel, O. 2007. "Evaluating benefits of systemwide adaptive ramp-metering strategy in Portland, Oregon." *Transportation Research Record*, 2012(1), 47-56.

[4] Banks, J. H. 1991. "Two-capacity phenomenon at freeway bottlenecks: a basis for ramp metering?" *Transportation Research Record*, 1320, 83-90.

[5] Bertini, R. L. and Malik, S. 2004. "Observed dynamic traffic features on freeway section with merges and diverges." *Transportation Research Record*, 1867(1), 25-35.

[6] Carlson, R. C., Papamichail, I., and Papageorgiou, M. 2014. "Integrated feedback ramp metering and mainstream traffic flow control on motorways using variable speed limits." *Transportation Research Part C: Emerging Technologies*, 46, 209-221.

[7] Carlson, R. C., Papamichail, I., Papageorgiou, M., and Messmer, A. 2010. "Optimal motorway traffic flow control involving variable speed limits and ramp metering." *Transportation Science*, 44(2), 238-253.

[8] Cassidy, M. J., Anani, S. B., and Haigwood, J. M. 2002. "Study of freeway traffic near an off-ramp." *Transportation Research Part A: Policy and Practice*, 36(6), 563-572.

[9] Cassidy, M. J. and Bertini, R. L. 1999. "Some traffic features at freeway bottlenecks." *Transportation Research Part B: Methodological*, 33(1), 25-42.

[10] Cassidy, M. J. and Rudjanakanoknad, J. 2005. "Increasing the capacity of an isolated merge by metering its on-ramp." *Transportation Research Part B: Methodological*, 39(10), 896-913.

[11] Chang, E. C., Cohen, S. L., Liu, C., Chaudhary, N. A., & Messer, C. 1988. "MAXBAND-86: program for optimizing left-turn phase sequence in multiarterial closed networks." *Transportation Research Record*, 1181, 40-46.

[12] Chang, G. L. and Kao, Y. M. 1991. "An empirical investigation of macroscopic lane-changing characteristics on uncongested multilane freeways." *Transportation Research Part A: General*, 25(6), 375-389.

[13] Chang, G. L., Park, S. Y., and Paracha, J. 2011. "Intelligent transportation system field demonstration: integration of variable speed limit control and travel time estimation for a recurrently congested highway." *Transportation Research Record*, 2243(1), 55-66.

[14] Chaudhary, N.A., Kovvali, V.G., C.-L., Chu, Kim, J., and Alam, S.M. 2002. *Software for timing signalized arterials*. Report FHWA/TX-03/4020-1, Texas Transportation Institute, the Texas A&M University System, College Station, Texas.

[15] Chen, Y. H., Cheng, Y., and Chang, G. L. 2019. "Concurrent progression of through and turning movements for arterials experiencing heavy turning flows and bay-length constraints." *Transportation Research Record*, 2673(9), 525-537.

[16] Chen, Y. H., Cheng, Y., and Chang, G. L., 2020. "Design of multi-path traffic progression for congested arterials with connected local progression bands." Presented at *Transportation Research Board 99th Annual Meeting*.

[17] Chen, Y. Y. and Chang, G. L., 2013. "A macroscopic signal optimization model for arterials under heavy mixed traffic flows." *IEEE Transactions on Intelligent Transportation Systems*, 15(2), 805-817.

[18] Cheng, Y., Chang, G. L., and Rahwanji, S. 2018. "Concurrent optimization of signal progression and crossover spacing for diverging diamond interchanges." *Journal of Transportation Engineering Part A: Systems*, 144(3), 04018001.

[19] Chow, A. H. and Li, Y. 2014. "Robust optimization of dynamic motorway traffic via ramp metering." *IEEE Transactions on Intelligent Transportation Systems*, 15(3), 1374-1380.

[20] Christofa, E., Ampountolas, K., and Skabardonis, A. 2016. "Arterial traffic signal optimization: a person-based approach." *Transportation Research Part C: Emerging Technologies*, 66, 27-47.

[21] Chung, K., Rudjanakanoknad, J., and Cassidy, M. J. 2007. "Relation between traffic density and capacity drop at three freeway bottlenecks." *Transportation Research Part B: Methodological*, 41(1), 82-95.

[22] Coifman, B. 2003. "Estimating density and lane inflow on a freeway segment." *Transportation Research Part A: Policy and Practice*, 37(8), 689-701.

[23] Daganzo, C.F. 1994. "The cell transmission model: a dynamic representation of highway traffic consistent with the hydrodynamic theory." *Transportation Research Part B: Methodology*, 28(4), 269–287.

[24] Daganzo, C. F. 2002. "A behavioral theory of multi-lane traffic flow part II: merges and the onset of congestion." *Transportation Research Part B: Methodological*, 36(2), 159-169.

[25] Daganzo, C. F., Cassidy, M. J., and Bertini, R. L. 1999. "Possible explanations of phase transitions in highway traffic." *Transportation Research Part A: Policy and Practice*, 33(5), 365-379.

[26] Frejo, J. R. D. and Camacho, E. F. 2012. "Global versus local MPC algorithms in freeway traffic control with ramp metering and variable speed limits." *IEEE Transactions on Intelligent Transportation Systems*, 13(4), 1556-1565.

[27] Gartner, N.H., Assman, S.F., Lasaga, F., and Hou, D.L. 1991. "A multi-band approach to arterial traffic signal optimization." *Transportation Research Part B: Methodological*, 25(1), 55-74.

[28] Gartner, N. H. and Stamatiadis, C. 2002. "Arterial-based control of traffic flow in urban grid networks." *Mathematical and Computer Modelling*, 35(5-6), 657-671.

[29] Gartner, N. H. and Stamatiadis, C. 2004. "Progression optimization featuring arterial-and route-based priority signal networks." *Journal of Intelligent Transportation Systems*, 8(2), 77-86.

[30] Gazis, D. C., Herman, R., and Weiss, G. H. 1962. "Density oscillations between lanes of a multilane highway." *Operations Research*, 10(5), 658-667.

[31] Geroliminis, N., Srivastava, A., and Michalopoulos, P. 2010. "A Coordinated ramp metering algorithm for Minnesota's freeways based on density." In *Proc., 13th International IEEE Conference on Intelligent Transportation Systems*, 1456-1461.

[32] Geroliminis, N., Srivastava, A., and Michalopoulos, P. 2011. "A dynamic-zone-based coordinated ramp-metering algorithm with queue constraints for Minnesota's freeways." *IEEE Transactions on Intelligent Transportation Systems*, 12(4), 1576-1586.

[33] Ghods, A. H., Fu, L., and Rahimi-Kian, A. 2010. "An efficient optimization approach to real-time coordinated and integrated freeway traffic control." *IEEE Transactions on Intelligent Transportation Systems*, 11(4), 873-884.

[34] Gipps, P. G. 1986. "A model for the structure of lane-changing decisions." *Transportation Research Part B: Methodological*, 20(5), 403-414.

[35] Gomes, G. and Horowitz, R. 2006. "Optimal freeway ramp metering using the asymmetric cell transmission model." *Transportation Research Part C: Emerging Technologies*, 14(4), 244-262.

[36] Gregurić, M., Ivanjko, E., and Mandžuka, S. 2016. "The use of cooperative approach in ramp metering." *Promet-Traffic & Transportation*, 28(1), 11-22.

[37] Grewal, M. S. and Payne, H. J. 1976. "Identification of parameters in a freeway traffic model." *IEEE Transactions on Systems, Man, and Cybernetics*, 3, 176-185.

[38] Hall, F. L. and Agyemang-Duah, K. 1991. "Freeway capacity drop and the definition of capacity." *Transportation Research Record*, 1320, 91-98.

[39] Hasan, M., Jha, M., and Ben-Akiva, M. 2002. "Evaluation of ramp control algorithms using microscopic traffic simulation." *Transportation Research Part C: Emerging Technologies*, 10(3), 229-256.

[40] Hegyi, A., De Schutter, B., and Hellendoorn, H. 2005. "Model predictive control for optimal coordination of ramp metering and variable speed limits." *Transportation Research Part C: Emerging Technologies*, 13(3), 185-209.

[41] Holland, E. N. and Woods, A. W. 1997. "A continuum model for the dispersion of traffic on two-lane roads." *Transportation Research Part B: Methodological*, 31(6), 473-485.

[42] Kashani, H. R. and Saridis, G. N. 1983. "Intelligent control for urban traffic systems." *Automatica*, 19(2), 191-197.

[43] Kerner, B. S. 2005. "Control of spatiotemporal congested traffic patterns at highway bottlenecks." *Physica A: Statistical Mechanics and Its Applications*, 355(2-4), 565-601.

[44] Keyvan-Ekbatani, M., Kouvelas, A., Papamichail, I., and Papageorgiou, M. 2012. "Exploiting the fundamental diagram of urban networks for feedback-based gating." *Transportation Research Part B: Methodological*, 46(10), 1393-1403.

[45] Keyvan-Ekbatani, M., Papageorgiou, M., and Papamichail, I. 2013. "Urban congestion gating control based on reduced operational network fundamental diagrams." *Transportation Research Part C: Emerging Technologies*, 33, 74-87.

[46] Kotsialos, A., Papageorgiou, M., Mangeas, M., and Haj-Salem, H. 2002. "Coordinated and integrated control of motorway networks via non-linear optimal control." *Transportation Research Part C: Emerging Technologies*, 10(1), 65-84.

[47] Koutsoyiannis, A., 1973. *Theory of econometrics: an introductory exposition of econometric methods*. London: McMillan Press.

[48] Kwon, E., 1999. *Estimation of the capacity in freeway weaving areas for traffic management and operations*. Minnesota Department of Transportation.

[49] Lertworawanich, P. and Elefteriadou, L., 2001. "Capacity estimations for type B weaving areas based on gap acceptance." *Transportation Research Record*, 1776(1), 24-34.

[50] Lertworawanich, P. and Elefteriadou, L., 2003. "A methodology for estimating capacity at ramp weaves based on gap acceptance and linear optimization." *Transportation Research Part B: Methodological*, 37(5), 459-483.

[51] Li, J. Q. 2013. "Bandwidth synchronization under progression time uncertainty." *IEEE Transactions on Intelligent Transportation Systems*, 15(2), 749-759.

[52] Li, Z., Chang, G. L., and Natarajan, S. 2009. "An integrated off-ramp control model for freeway traffic management." Presented at *15th World Congress on Intelligent Transportation Systems*, New York.

[53] Li, Z., Liu, P., Xu, C., Duan, H., and Wang, W. 2017. "Reinforcement learning-based variable speed limit control strategy to reduce traffic congestion at freeway recurrent bottlenecks." *IEEE Transactions on Intelligent Transportation Systems*, 18(11), 3204-3217.

[54] Lighthill, M. J. and Whitham, G. B. 1955. "On kinematic waves II. A theory of traffic flow on long crowded roads." In *Proc., the Royal Society of London. Series A. Mathematical and Physical Sciences*, 229(1178), 317-345.

[55] Lim, K., Kim, J. H., Shin, E., and Kim, D. G. 2011. "A signal control model integrating arterial intersections and freeway off-ramps." *KSCE Journal of Civil Engineering*, 15(2), 385-394.

[56] Little, J. D. C. 1966. "The synchronization of traffic signals by mixed-integer linear programming." *Operations Research*, 14(4), 568-594.

[57] Little, J. D. C., Kelson, M.D. and Gartner, N. H., 1981. "MAXBAND: a program for setting signals on arteries and triangular networks." *Transportation Research Record*, 795, 40-46.

[58] Liu, Y. and Chang, G. L. 2011. "An arterial signal optimization model for intersections experiencing queue spillback and lane blockage." *Transportation Research Part C: Emerging Technologies*, 19(1), 130-144.

[59] Lo, H. K., Chang, E., and Chan, Y. C. 2001. "Dynamic network traffic control." *Transportation Research Part A: Policy and Practice*, 35(8), 721-744.

[60] Maryland State Highway Administration. *Traffic signal timing guidelines and training manual*, undated.

[61] Messer, C. J., Whitson, R. H., Dudek, C. L., and Romano, E. J. 1973. "A variable-sequence multiphase progression optimization program." *Highway Research Record*, 445(1973), 24-33.

[62] Messner, A. and Papageorgiou, M., 1990. "METANET: a macroscopic simulation program for motorway networks." *Traffic Engineering and Control*, 31(8), 466-470.

[63] Michalopoulos, P. G., Beskos, D. E., and Yamauchi, Y. 1984. "Multilane traffic flow dynamics: some macroscopic considerations." *Transportation Research Part B: Methodological*, 18(4-5), 377-395.

[64] Morgan, J. T. and Little, J. D. C. 1964. "Synchronizing traffic signals for maximal bandwidth." *Operations Research*, 12(6), 896-912.

[65] Munjal, P. K. and Hsu, Y. S. 1973. "Experimental validation of lane-changing hypotheses from aerial data." *Highway Research Record*, 456, 5-11.

[66] Munjal, P. K. and Pipes, L. A. 1971a. "Propagation of on-ramp density perturbations on unidirectional two-and three-lane freeways." *Transportation Research*, 5(4), 241-255.

[67] Munjal, P. K. and Pipes, L. A. 1971b. "Propagation of on-ramp density waves on uniform unidirectional multilane freeways." *Transportation Science*, 5(4), 390-402.

[68] Munoz, J. C. and Daganzo, C. F. 2002. "The bottleneck mechanism of a freeway diverge." *Transportation Research Part A: Policy and Practice*, 36(6), 483-505.

[69] Oliver, R. M. and Lam, T. 1965. *Statistical experiments with a two-lane flow model*. California University Berkeley Operations Research Center.

[70] Pahl, J., 1972. "Lane-change frequencies in freeway traffic flow." *Highway Research Record*, 409, 17-33.

[71] Papageorgiou, M., Hadj-Salem, H., and Blosseville, J. M. 1991. "ALINEA: a local feedback control law for on-ramp metering." *Transportation Research Record*, 1320(1), 58-67.

[72] Papageorgiou, M. and Kotsialos, A. 2002. "Freeway ramp metering: An overview." *IEEE Transactions on Intelligent Transportation Systems*, 3(4), 271-281.

[73] Papamichail, I., Kotsialos, A., Margonis, I., and Papageorgiou, M. 2010a. "Coordinated ramp metering for freeway networks–a model-predictive hierarchical control approach." *Transportation Research Part C: Emerging Technologies*, 18(3), 311-331.

[74] Papamichail, I., Papageorgiou, M., Vong, V., and Gaffney, J. 2010b. "Heuristic ramp-metering coordination strategy implemented at Monash freeway, Australia." *Transportation Research Record*, 2178(1), 10-20.

[75] Papola, N. 1992. "Bandwidth maximization: split and unsplit solutions." *Transportation Research Part B: Methodological*, 26(5), 341-356.

[76] Persaud, B., Yagar, S., and Brownlee, R. 1998. "Exploration of the breakdown phenomenon in freeway traffic." *Transportation Research Record*, 1634(1), 64-69.

[77] Rakha, H. and Zhang, Y., 2006. "Analytical procedures for estimating capacity of freeway weaving, merge, and diverge sections." *Journal of Transportation Engineering*, 132(8), 618-628.

[78] Richards, P. I. 1956. "Shock waves on the highway." *Operations Research*, 4(1), 42-51.

[79] Robertson, D.I. 1969. *TRANSYT: a traffic network study tool*. TRRL Report LR 253, Road Research Laboratory, England.

[80] Roess, R. P. and Ulerio, J. M., 2009. "Capacity of freeway weaving segments." *Transportation Research Record*, 2130(1), 34-41.

[81] Smaragdis, E. and Papageorgiou, M. 2003. "Series of new local ramp metering strategies: emmanouil smaragdis and markos papageorgiou." *Transportation Research Record*, 1856(1), 74-86.

[82] Smaragdis, E., Papageorgiou, M., and Kosmatopoulos, E. 2004. "A flow-maximizing adaptive local ramp metering strategy." *Transportation Research Part B: Methodological*, 38(3), 251-270.

[83] Spiliopoulou, A., Kontorinaki, M., Papageorgiou, M., and Kopelias, P. 2014. "Macroscopic traffic flow model validation at congested freeway off-ramp areas." *Transportation Research Part C: Emerging Technologies*, 41, 18-29.

[84] Spiliopoulou, A. D., Manolis, D., Papamichail, I., Papageorgiou, M., Wu, J., and Jin, X. 2010. "Queue management techniques for metered freeway on-ramps." *Transportation Research Record*, 2178(1), 40-48.

[85] Srivastava, A. and Geroliminis, N. 2013. "Empirical observations of capacity drop in freeway

merges with ramp control and integration in a first-order model." *Transportation Research Part C: Emerging Technologies*, 30, 161-177.

[86] Stevanovic, A., Martin, P. T., and Stevanovic, J. 2007. "VisSim-based genetic algorithm optimization of signal timings." *Transportation Research Record*, 2035(1), 59-68.

[87] Tian, Z. and Urbanik, T. 2007. "System partition technique to improve signal coordination and traffic progression." *Journal of Transportation Engineering*, 133(2), 119-128.

[88] Toledo, T., Koutsopoulos, H. N., and Ben-Akiva, M. 2007. "Integrated driving behavior modeling." *Transportation Research Part C: Emerging Technologies*, 15(2), 96-112.

[89] van Beinum, A., Farah, H., Wegman, F. and Hoogendoorn, S., 2018. "Driving behaviour at motorway ramps and weaving segments based on empirical trajectory data." *Transportation Research Part C: Emerging Technologies*, 92, 426-441.

[90] Wallace, C. E. and Courage, K. G. 1982. "Arterial progression-New design approach." *Transporation Research Record*, 881, 53-59.

[91] Wallace, C.E., Courage, K.G., Reaves, D.P., Shoene, G.W., Euler, G.W., and Wilbur, A. 1988. *TRANSYT-7F user's manual: technical report*. University of Florida, Gainesville, FL.

[92] Wang, Y. and Papageorgiou, M. 2006. "Local ramp metering in the case of distant downstream bottlenecks." In *Proc., the IEEE Intelligent Transportation Systems Conference*, 426-431.

[93] Wattleworth, J. A. 1967. "Peak period analysis and control of a freeway system/with discussion." *Highway Research Record*, 157.

[94] Wiedemann, R. and Reiter, U. 1992. *Microscopic traffic simulation: the simulation system MISSION, background and actual state.* Project ICARUS (V1052) Final Report, 2, 1-53.

[95] Yang, Q. and Koutsopoulos, H. N. 1996. "A microscopic traffic simulator for evaluation of dynamic traffic management systems." *Transportation Research Part C: Emerging Technologies*, 4(3), 113-129.

[96] Yang, X., Chang, G. L., and Rahwanji, S. 2014. "Development of a signal optimization model for diverging diamond interchange." *Journal of Transportation Engineering*, 140(5), 04014010.

[97] Yang, X., Cheng, Y., and Chang, G. L. 2015. "A multi-path progression model for synchronization of arterial traffic signals." *Transportation Research Part C: Emerging Technologies*, 53, 93-111.

[98] Yang, X., Cheng, Y., and Chang, G. L. 2016. "Operational analysis and signal design for asymmetric two-leg continuous-flow intersection." *Transportation Research Record*, 2553(1), 72-81.

[99] Yang, X., Cheng, Y., and Chang, G. L. 2018. "Integration of adaptive signal control and freeway off-ramp priority control for commuting corridors." *Transportation Research Part C: Emerging Technologies*, 86, 328-345.

[100] Yang, X., Lu, Y., and Chang, G. L. 2014. "Dynamic signal priority control strategy to mitigate off-ramp queue spillback to freeway mainline segment." *Transportation Research Record*, 2438(1), 1-11.

[101] Yang, X., Lu, Y., and Chang, G. L. 2015. "Exploratory analysis of an optimal variable speed control system for a recurrently congested freeway bottleneck." *Journal of Advanced Transportation*, 49(2), 195-209.

[102] Yuan, K., Knoop, V. L., and Hoogendoorn, S. P. 2015. "Capacity drop: relationship between speed in congestion and the queue discharge rate." *Transportation Research Record*, 2491(1), 72-80.

[103] Yun, I. 2006. "Application of stochastic optimization method for an urban corridor." In *Proc., the Winter Simulation Conference*, 1493-1499.

[104] Zhang, C., Xie, Y., Gartner, N. H., Stamatiadis, C., and Arsava, T. 2015. "AM-band: an asymmetrical multi-band model for arterial traffic signal coordination." *Transportation Research Part C: Emerging Technologies*, 58, 515-531.

[105] Zhang, H. M. and Ritchie, S. G. 1997. "Freeway ramp metering using artificial neural networks." *Transportation Research Part C: Emerging Technologies*, 5(5), 273-286.

[106] Zhao, D., Bai, X., Wang, F. Y., Xu, J., and Yu, W. 2011. "DHP method for ramp metering of freeway traffic." *IEEE Transactions on Intelligent Transportation Systems*, 12(4), 990-999.

[107] Zheng, Z., Ahn, S., Chen, D. and Laval, J., 2011. "Freeway traffic oscillations: microscopic analysis of formations and propagations using wavelet transform." *Procedia-Social and Behavioral Sciences*, 17, 702-716.

[108] Zheng, Z., Ahn, S., Chen, D. and Laval, J., 2013. "The effects of lane-changing on the immediate follower: anticipation, relaxation, and change in driver characteristics." *Transportation Research Part C: Emerging Technologies*, 26, 367-379.